Masterthesis

Determination of Optimal Expansion Strategies for Biogas-to-Liquid and Biogas-CHP Units for Flexible Biogas Plants

Tobias Jandt

Fakultät Life Sciences
Department Umwelttechnik

Faculty of Life Sciences
Department of Environmental Engineering

To my father,
whose unwavering pride in me
gave me the confidence to follow the right path,
and whose presence I feel with every step.

Tobias Jandt

Matrikelnummer: [redacted]

Determination of Optimal Expansion Strategies for Biogas-to-Liquid and Biogas-CHP Units for Flexible Biogas Plants

Masterarbeit eingereicht im Rahmen der Masterprüfung
im Studiengang Renewable Energy Systems
am Department Umwelttechnik und Verfahrenstechnik
der Fakultät Life Sciences
der Hochschule für Angewandte Wissenschaften Hamburg

Erstprüfer: Prof. Dr.-Ing. Torsten Birth-Reichert
Zweitprüfer: Hendrik Zachhariassen, M. Sc.

Betreuende (HAW): Jan-Malte Kapust

Eingereicht am: 21.07.2025

Title of the Master Thesis

Determination of Optimal Expansion Strategies for Biogas-to-Liquid and Biogas-CHP Units for Flexible Biogas Plants

Keywords

Biogas-to-Liquid, Plasmacracking Technology, Fischer-Tropsch Synthesis, Combined Heat and Power, Flexible Biogas Plants, Linear Programming, Unit Commitment Problem, Arbitrage Model, Simulation

Abstract

This thesis investigates the technical and economic feasibility of a flexible biogas plant system that combines a Biogas-to-Liquid (BGtL) plant—using a novel low-temperature microwave plasmacracking plant for syngas production and Fischer-Tropsch synthesis (FTS) for FT-syncrude production—with a Combined Heat-and-Power Unit (CHPU), considering different expansion strategies. Using a Mixed-Integer Linear Programming (MILP) model and real German electricity price data from 2023, various operating scenarios were simulated based on the arbitrage and unit commitment problem. Results show that, under current market conditions, separate operation of BGtL and CHPU is more profitable than combined operation, mainly due to higher specific investment costs and limited spot market volatility. While flexible CHPU benefits from overbuilding and flexibility bonuses, BGtL achieves better returns when run steadily. However, simulated large BGtL plants can already produce FT-syncrude at competitive costs, and combined flexible operation may become attractive as electricity markets evolve and investment costs decrease. The presented model and results provide a basis for future optimization and techno-economic assessment of hybrid biogas systems.

Table of Contents

List of Figures

List of Tables

List of Acronyms

AI	Artificial Intelligence
ASF	Anderson–Schulz–Flory
ATR	Autothermal Reforming
BGS	Biogas Storage
BtL	Biomass-to-Liquid
BG	Biogas
BGtL	Biogas-to-Liquid
CAPEX	Capital Expenditure
CC4E	Competence Center für Erneuerbare Energien und EnergieEffizienz
CCS	Carbon Capture and Sequestration
CHP	Combined Heat and Power
CHPU	Combined Heat and Power Unit
ChatGPT	Chat Generative Pre-trained Transformer
CPLEX	IBM ILOG CPLEX Optimizer
CR	Consumption Ratio
DAC	Direct Air Capture
DMR	Dry Methane Reforming
DSM	Demand Side Management
EEG	Erneuerbare-Energien-Gesetz
EEX	European Energy Exchange AG
EPEX SPOT SE	European Power Exchange Spot Societas Europaea
FLH	Full Load Hours
FM	Fresh Mass
FOAK	First-Of-A-Kind
FT	Fischer-Tropsch
FTS	Fischer-Tropsch Synthesis

LHV	Lower Heating Value
LR	Learning Rate
MILP	Mixed-Integer Linear Programming
OPEX	Operational Expenditure
OS	Organic Solids
oTS	Organic Total Solids
PC	Plasmacracking
PCU	Plasmacracking Unit
POX	Partial Oxidation
PQ	Power Quotient
PtL	Power-to-Liquid
PV	Photovoltaic
ROI	Return on Investment
SAF	Sustainable Aviation Fuel
SG	Syngas
SGS	Syngas Storage
SMR	Steam Methane Reforming
SFO	Smart Force Optimization
TS	Total Solids
UCP	Unit Commitment Problem
VAT	Value Added Taxes
WGS	Water–Gas Shift

List of Symbols

$\Delta H_{\mathrm{R}}^{0}$	Standard enthalpy of reaction	kJ/mol
C	Total cost	€
C_{Capital}	Capital costs	€
C_{var}	Variable costs	€
C_0	Initial investment cost	€
C_r	Reference plant cost	€
C_Q	Production cost for cumulative quantity Q	€
C_1	Production cost for the first plant	€
L	Salvage value	€
N	Asset lifetime	years
i	Interest rate	–
f	Scale factor	–
Q	Cumulative number of plants	–
b	Experience curve parameter	–
LR	Learning rate	%
ACE	Average capital employed	€
Π	Profit	€
R_{rev}	Total revenues	€
ROI	Return on investment	%
$C_0(S)$	Scaled investment cost at plant size S	€
P	Rated power	kW
$P_{\mathrm{rated},i}$	Rated power of unit i	kW
$P_{\mathrm{rated,\,biogas}}$	Biogas plant design output	kW
$\dot{V}_{\mathrm{biogas},\,i}$	Biogas flow into unit i	m^3/h
$\dot{V}_{\mathrm{production}}$	Total biogas production rate	m^3/h
PQ_i	CHP overbuilding factor for unit i	–
V	Rated biogas capacity	$1000\ \mathrm{m}^3$
p_t	Electricity price at time t	€/kWh
S_0^{BG}	Initial biogas storage	m^3
S_0^{SG}	Initial syngas storage	m^3
R_{min}	Minimum runtime	periods
D_{min}	Minimum downtime	periods
$P_{\mathrm{CHP}}^{\mathrm{max}}$	Maximum CHP electrical output	kW
$P_{\mathrm{CHP}}^{\mathrm{min}}$	Minimum CHP electrical output	kW
$P_{\mathrm{PC}}^{\mathrm{max}}$	Maximum PC power	kW
$P_{\mathrm{PC}}^{\mathrm{min}}$	Minimum PC power	kW
$\eta_{\mathrm{CHP}}^{\mathrm{el}}$	CHP electrical efficiency	–
$\eta_{\mathrm{CHP}}^{\mathrm{th}}$	CHP thermal efficiency	–
LHV_{BG}	Lower heating value of biogas	$\mathrm{kWh}/\mathrm{m}^3$
$F_{\mathrm{BG,\,PC}}$	Biogas consumption factor PC	$\mathrm{m}^3/\mathrm{kWh}$

$F_{\mathrm{SG,\,PC}}$	Syngas production factor PC	$\mathrm{m^3/kWh}$
$F_{\mathrm{power,\,PC}}$	Power scaling factor PC	kW/kW
$V_{\mathrm{BG}}^{\max}$	Max. biogas storage	$\mathrm{m^3}$
$V_{\mathrm{SG}}^{\max}$	Max. syngas storage	$\mathrm{m^3}$
$V_{\mathrm{production}}^{\mathrm{BG}}$	Biogas production	$\mathrm{m^3}$
θ	Threshold price for CHP operation	€/kWh
P_t^{CHP}	CHP electrical output at t	kWh
P_t^{PC}	Plasma cracker power at t	kWh
S_t^{BG}	Biogas storage level at t	$\mathrm{m^3}$
S_t^{SG}	Syngas storage level at t	$\mathrm{m^3}$
$f_{t,u}^{\mathrm{BG}}$	Biogas flow to unit u at t	$\mathrm{m^3}$
y_t^{SG}	Syngas sent to FTS at t	$\mathrm{m^3}$
u_t^{CHP}	CHP on/off at t	–
u_t^{PC}	PC on/off at t	–
σ_t^{CHP}	CHP start indicator at t	–
σ_t^{PC}	PC start indicator at t	–
δ_t^{CHP}	CHP stop indicator at t	–
δ_t^{PC}	PC stop indicator at t	–
z_t	Revenue contribution at time t	€
$Biogas_{CR}$	Biogas Consumption Ratio	–

1 Introduction

Aviation relies on highly energy-dense fuels because of the long distances involved and the limited on-board volume available for energy storage. To date, batteries and non-carbon-based fuels such as hydrogen or ammonia cannot meet these stringent requirements [1] (see Figure 1.1). Conventional jet fuel consists of long-chain hydrocarbons; the presence of carbon is essential for

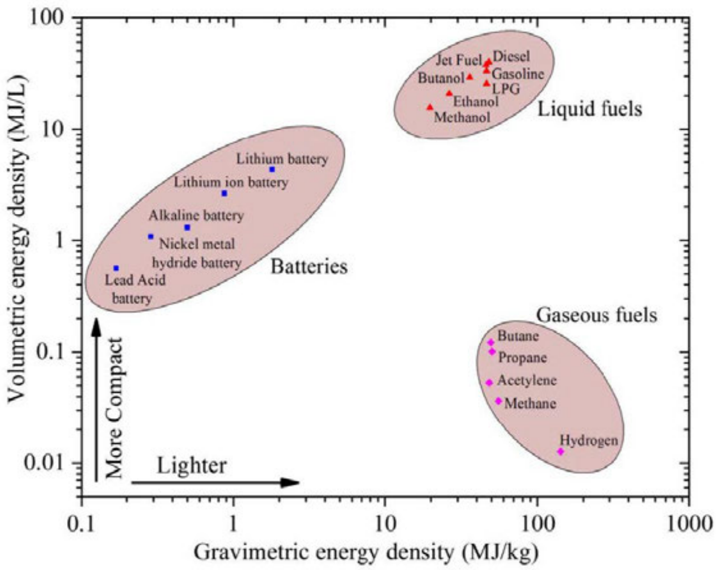

Figure 1.1: Comparison of volumetric and gravimetric energy densities for various storage technologies and materials [2].

achieving the required energy density. Consequently, the production of Sustainable Aviation Fuel (SAF) requires a sustainable carbon source. In this study, biogas—primarily composed of methane (CH_4) and carbon dioxide (CO_2)—is employed as that source. The carbon contained in biogas has been sequestered from the atmosphere, so its combustion closes the carbon loop and avoids net CO_2 emissions. To convert biogas into SAF, Power-to-Liquid (PtL) or, when the feedstock is of biogenic origin, Biomass-to-Liquid (BtL) technologies are required. These processes use renewable-electricity-driven synthesis steps to transform biogas into liquid hydrocarbons. A recent innovation is Plasmacracking (PC) reforming (plasmalysis), which cracks biogas and steam into synthesis gas (a mixture of H_2 and CO) suitable for downstream Fischer-Tropsch Synthesis (FTS). The Fischer-Tropsch (FT) reactor produces syncrude that can be upgraded to SAF. The PC step, powered by renewable electricity, dissociates both CH_4 and CO_2, thereby utilising the carbon in the CO_2 fraction as well as that in CH_4. By contrast, conventional CHPUs combust biogas directly for electricity generation, and the CO_2 is usually removed during biomethane upgrading [3]. Biogas-fuelled Combined Heat and Power (CHP) plants are widespread in Germany. A key feature of these systems is their flexibility: operators intentionally oversize the CHPU relative to average biogas production, store unused biogas when electricity prices are low—typically during periods of surplus renewable generation—and dispatch the CHPU when prices peak, thus relieving the grid and capturing higher revenues. In this way, CHPUs act as a valuable counterbalance to fluctuating wind and photovoltaic output.

Over the past few years, intraday electricity price volatility has risen sharply (see Figure 1.2). This increase is driven not only by the energy crisis triggered by Russia's invasion of Ukraine but also by the continued deployment of fluctuating renewable energy sources (primarily wind turbines and photovoltaik systems). Forecasts indicate that volatility will rise further as additional renewable capacity is installed [4–6].

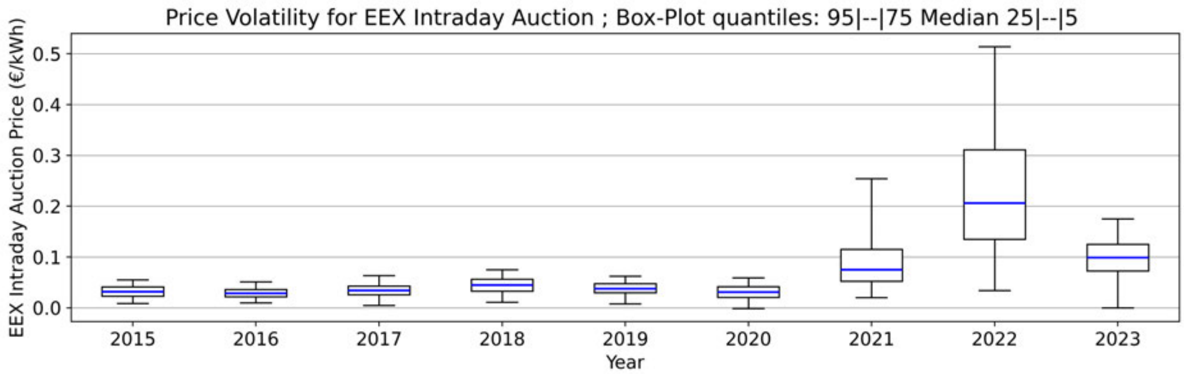

Figure 1.2: Price volatility in the EEX intraday auction market.

The Biogas-to-Liquid (BGtL) plant operates in the opposite way to a conventional biogas CHPU because it consumes electricity to convert biogas into synthetic fuel. Combining both plant types at the same facility would therefore enable complementary operation: the BtL unit could run when electricity is abundant and prices are low or negative, while the CHPU could generate electricity in periods of scarcity and high prices.
Because the BGtL unit and the CHPU behave oppositely with respect to electricity prices, this raises a central research question: is the expansion of a biogas plant with a BGtL unit—comprising a PC reactor, Syngas Storage (SGS), and FTS—economically viable? Moreover, can the combined operation of both units (CHPU and Plasmacracking Unit (PCU)) create operational synergies that enhance overall profitability?
To answer questions like these, this thesis develops a deterministic, multi-period Mixed-Integer Linear Programming (MILP) model that optimises the combined operation (or single operation) of the CHPU and BGtL unit for the year 2023, taking into account technical constraints and the intraday electrcity auction prices for the year 2023 to maximise total revenue. Additionally, capital and operating costs are calculated for each simulation run to determine annual profit and Return on Investment (ROI), allowing simple comparison of scenarios and rapid identification of the most and least attractive parameter configurations. To explore the economic impact of different expansion strategies, four key parameters are varied: total plant capacity, degree of overbuilding for CHPU and BGtL unit, and the biogas consumption ratio between CHPU and BGtL unit.

The thesis is divided into the following chapters:

Chapter 1 provides the introduction to this thesis. Chapter 2 addresses the current state of the art and is divided into three main sections: Integration of BtL technologies, Flexibilization of biogas CHPUs in Germany, and Optimization approaches for flexible plant operation. Chapter 3 lays the theoretical foundation: it outlines biogas production and utilization in Germany, reviews the fundamentals of BGtL, PC technology, and FTS, details the configuration of the reference plant, and gives an overview of the formulas used for the cost calculation.

Chapter 4 introduces the methodology, describing the methodological approach that briefly explains the process of this thesis from idea to results. In Chapter 5, the simulation parameters and assumptions are presented. Organized according to the six subplants of the reference plant, this chapter specifies all technical and economic parameters used in the simulations, the variable parameters, as well as the electricity spot market data applied.

Chapter 6 forms the core of the methodology. It introduces the Unit Commitment Problem (UCP) and the arbitrage model as guiding concepts, then describes in detail the MILP formulation—including decision variables, objective function, and constraints. Furthermore, the function of the program code is explained, as well as the simulation procedure and what happens in the code during a simulation.

Chapter 7 covers the implementation of the simulations. Here, the variable simulation parameters are introduced. In addition, the simulation setups are described.

In Chapter 8, the results of the simulations are presented. Chapter 9 discusses the findings in the context of existing literature and practical applications.

Finally, Chapter 10 concludes the thesis with a summary of the key insights and provides an outlook on future research directions for flexible biogas plant expansions integrating BGtL units and CHPUs.

2 State of the Art

This chapter provides an overview of established and emerging approaches for the conversion of biogas into synthetic fuels, with particular attention to the technological diversity and the challenges associated with syngas production and utilization. Furthermore, it summarizes current practices and developments in the flexible operation of biogas CHPUs, which play a key role in stabilizing electricity systems with high shares of renewables. Finally, mathematical optimization approaches for the scheduling and economic assessment of flexible energy systems are reviewed, with a focus on models relevant to multi-unit plant configurations.

By consolidating the findings from these areas, the chapter aims to identify knowledge gaps and research needs, thus providing the foundation for the subsequent methodological development and the focus of this thesis.

Integration of BtL technologies

For BtL technology, two steps are essential: syngas production via a reforming process and liquid fuel synthesis from the produced syngas. FTS is predominantly used for the latter, which requires a H_2/CO ratio of approximately 2—ideally slightly above 2.

There are various technological approaches for syngas production from biogas (BGtL) or biomethane (BtL), including established processes such as Steam Methane Reforming (SMR) [7], Partial Oxidation (POX) [8, 9], and Autothermal Reforming (ATR) [10], as well as more recent technologies such as Dry Methane Reforming (DMR)[11–13].

SMR is widely used but highly energy-intensive, producing a syngas with a suboptimal hydrogen content ($H_2/CO \approx 3$), which necessitates additional process steps such as the Water–Gas Shift (WGS) and results in CO_2 emissions that can only be avoided through Carbon Capture and Sequestration (CCS) [12, 14].

POX is exothermic and more energy efficient, but also only utilizes methane, leaving the CO_2 fraction of biogas unexploited. ATR combines SMR and POX, enabling better temperature management, but still fails to utilize CO_2 and increases overall process complexity. [12]

DMR directly uses the entire biogas stream (CH_4 and CO_2), but is strongly endothermic, requires high temperatures, and produces a low H_2/CO ratio (≈ 1), necessitating further steps such as WGS or partial oxidation to reach the ratio required for FTS [15, 16].

Tri-reforming integrates steam reforming, dry reforming, and partial oxidation in a single process, which can reduce the required temperature and slightly improve efficiency compared to purely endothermic processes. However, the operating temperature remains high, and the process itself is complex [17, 18].

Current projects also combine carbon capture technologies and electrolysis for syngas production [19, 20]. These utilize industrial CO_2 streams, but this approach is energy-intensive and requires multiple units. Another setup combines Direct Air Capture (DAC) with a PC reactor to generate

CO from CO_2, which is then converted with water via WGS into syngas; however, a portion of the CO is converted back to CO_2, which needs to be recycled [21].

Additionally, there are already BtL plants operating at biogas plant sites, which combine the CO_2 generated during biogas upgrading with hydrogen from electrolysis to produce syngas. The CH_4 is still used for electricity generation or gas grid injection [22, 23]. This approach makes use of previously unused CO_2, but still requires an electrolyser, resulting in additional costs and energy demand.

In summary, the various synthesis gas production processes exhibit significant differences in terms of energy efficiency, complexity, and utilization of available biogas components. Established methods often leave either methane or CO_2 unused or require additional energy-intensive steps to achieve an appropriate H_2/CO ratio for FTS. This is exactly where research into low-temperature microwave PC technology, such as that currently pursued in the Plasma2X project, becomes relevant. This innovative technology, which is still in the planning phase and has not yet been commissioned, enables the direct conversion of raw biogas (CH_4, CO_2, and H_2O) into synthesis gas in a single process step without relying on strongly endothermic processes such as the WGS reaction. Additionally, current research investigates the adjustment of the H_2/CO ratio through variations in the H_2O feed, potentially allowing the desired ratio to always be realized directly in the syngas. The process operates at comparatively low temperatures due to the microwave plasma technology, reducing energy demand and enhancing process efficiency. The resulting synthesis gas can then be directly converted into FT-Syncrude or methanol [24].

The production costs of sustainable FT-syncrude vary greatly depending on the technology, ranging from 1.4 to 5.8 $€/kg_{\mathrm{Syncrude}}$ [25–27].

Flexibilization of biogas CHPUs in Germany

In Germany, most biogas plants use CHPUs to convert biogas into electricity and heat. A major advantage of CHPUs is their ability to operate flexibly: unlike other renewable sources, they can quickly adjust output to match market demand and thus play a unique role in stabilizing the electricity grid, which is increasingly dominated by fluctuating wind and solar generation [28].

This flexibility is enabled by oversizing the CHPU—sometimes by a factor of five compared to the average gas production rate—and expanding Biogas Storage (BGS), so that biogas can be accumulated during low-price periods and used for full-load generation during peak-price hours [29].

In practice, small-scale biogas plants typically meet the on-site electricity and heat demand of farms, while larger installations can supply several hundred households with heat and feed most of their electricity into the public grid. By operating flexibly, these larger units not only provide renewable heat and power, but also contribute significantly to grid stability, especially during demand peaks [30, 31].

Despite these benefits, conventional flexible operation is still limited to electricity and heat production, and the potential of biogas for advanced synthetic fuel production remains largely untapped.

Optimization approaches for flexible plant operation

The increasing complexity of modern energy systems, especially with the integration of flexible synthetic fuel production, requires advanced scheduling methods to ensure both economic efficiency and technical feasibility. In this context, mathematical optimization models have become an essential tool for determining optimal operating strategies for systems with multiple flexible units.

A typical application is the use of synthetic fuel plants as Demand Side Management (DSM) options: by operating PtL plants primarily during periods of low electricity prices or surplus renewable generation, the overall grid can be stabilized and the cost-effectiveness of such plants can be increased [32]. When these plants are integrated with other units (e.g., CHPUs, electrolysers, storage), the optimal coordination becomes a challenging scheduling problem, commonly addressed with mathematical programming.

Various optimization approaches have been proposed in recent literature: For example, Taslimi et al. developed a MILP-based optimization model for a large-scale green methanol plant in Denmark, integrating Photovoltaic (PV), grid, electrolyser, methanol synthesis, and district heating. Their model minimizes annual net costs while considering detailed technical and contractual constraints, and decides hourly whether to prioritize hydrogen production or direct electricity sales, depending on market prices [33, 34].

Dotzauer analyzed different component configurations of flexible biogas plants in Germany by varying parameters such as CHPU overbuilding factor (Power Quotient (PQ))and storage sizes, using a hybrid optimization approach. The study highlights how investment decisions and technical restrictions interact, and introduces an efficient search method (Smart Force Optimization (SFO)) for profitable operating schedules. The models consider dynamic electricity prices, regulatory frameworks, and detailed cost structures [35].

Güsewell et al. implemented an MILP framework to optimize the hour-by-hour operation of flexible biogas plants, accounting for binary start/stop decisions, substrate allocation, gas and heat storage management, and market price signals. Their results demonstrate the importance of flexible scheduling for economic viability, but also underline the increasing computational complexity with system size and additional plant combinations [36].

While these approaches demonstrate the state of the art in flexible energy system operation, several limitations remain. Most models either focus on a single plant type or on relatively simple system combinations. A model that combines a BGtL system with CHPU does not yet exist.

Summary and Research Gap

In summary, the reviewed literature demonstrates that a broad spectrum of technological pathways exists for converting biogas into valuable products, ranging from established syngas production methods (SMR, POX, ATR, DMR, tri-reforming) to novel low-temperature plasma processes. The recent innovation low-temperature PC technology promise significant gains in process integration and energy efficiency, potentially enabling the direct, single-step conversion of raw biogas into a syngas with an optimal H_2/CO ratio for FTS. However, these technology remain at the experimental stage, and the operational performance and integration into real energy systems are not yet addressed.

In parallel, the flexible operation of biogas CHPUs has been widely adopted in Germany and proven to deliver important benefits for grid stability and renewable integration. Yet, the vast majority of flexible biogas plants are still limited to electricity and heat production; the potential for producing synthetic liquid fuels, especially in combination with flexible BGtL technologies, remains unexploited.

While advanced optimization models have been developed for various flexible energy systems, the existing literature predominantly focuses either on single operating plants or relatively simple combinations. Integrated operational optimization and economic assessment of biogas plants that combine both flexible CHPU and BGtL units, especially using the novel PC technology, has not yet been addressed.

Thus, there is a clear research gap regarding the optimal dimensioning and operation of hybrid biogas systems that combine flexible electricity generation with advanced synthetic fuel production, particularly leveraging the novel PC technology. The question of how such integrated systems can be designed and scheduled to maximize both economic performance and system flexibility under real market conditions, remains open and forms the focus of this thesis.

3 Fundamentals

In this chapter, the fundamentals are covered. First, an overview of the current biogas production, utilization, and market integration is provided. This is followed by a brief introduction to the BGtL technology and the two technologies used in the reference plant of this work: PCU and FTS. Next, the structure of the reference system is presented, with a detailed discussion of the BGtL plant. Finally, the economic evaluation methods used in the cost model are introduced.

3.1 Biogas in Germany: Production, Utilization, and Market Integration

Biogas utilization in Germany

In Germany, around 8,500 biogas plants were operated in 2022 for electricity production, with a total capacity of 6.5 GW [28]. Approximately 1,500 plants had an installed capacity of up to 75 kWp, 5,000 plants ranged between 75 and 500 kWp, and about 2,000 biogas plants exceeded 500 kWp. The majority of biogas production takes place in agricultural biogas plants (roughly 8,250 sites), where manure, slurry, and renewable raw materials are used for fermentation. Additionally, 124 waste digestion plants are in operation—over 90% of their substrate input consists of organic waste—and around 120 co-fermentation plants use a mixture of renewable raw materials, manure, and organic residues as substrates. In 2021, the total input for on-site biogas production amounted to approximately 65 million t Fresh Mass (FM) of manure and around 61 million t FM of renewable raw materials. Furthermore, 2–3 million t FM of municipal organic waste and an additional 3–4 million t FM of other organic residues were used for fermentation [28].

The technical potential of solid manure and slurry in Germany lies between 153 and 187 million t FM per year [38], meaning that nearly two-thirds remain unused, indicating a significant untapped resource.

The composition of biogas depends strongly on the feedstock and the type of fermentation [39, 40]. Agricultural biogas typically contains 55–75 vol.% methane, sewage gas 55–65 vol.%, and landfill gas 40–45 vol.%. The remainder is mainly carbon dioxide, with smaller amounts of water, oxygen, nitrogen, ammonia, hydrogen, and hydrogen sulfide [41].

The different gas compositions are also reflected in the mass- and energy-related use of substrates. Figure 3.1 shows the relationship between mass-based and energy-based substrate utilization in German biogas plants for 2023. By mass, farm manure/slurry accounted for the largest share at 50 wt %, followed by renewable raw materials at 41 wt %. Biowaste and residual materials contributed only 4 wt % and 5 wt %. In terms of energy share, renewable raw materials were highest with 68% of the total biomass-derived energy, owing to their high methane content of the produced biogass and thus increased energy density. The energy share of farm manure/slurry drops to 19% due to its lower methane content. Biowaste remains at 4% energy share, and residual materials contribute 9%. This clearly demonstrates that the energy density of renewable raw materials is higher than that of farm manure dew to the higher methane content of the

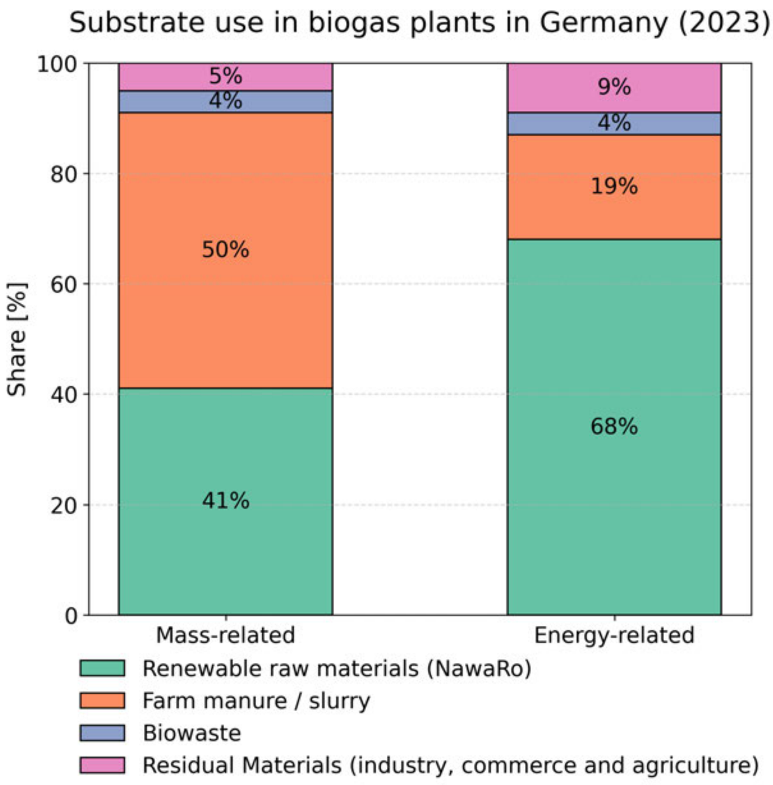

Figure 3.1: Substrate use in biogas plants (Germany 2023) (own illustration, based on [37]).

produced biogas. [37]

Flexibilization of Biogas plants

Older biogas CHPU are typically operated for approximately 8,500 hours per year, thereby providing baseload power. In this mode of operation, neither demand nor market electricity prices are considered. To make the operation of biogas plants more grid-supportive and economically attractive, various strategies can be employed. These include the flexibilization and direct marketing of electricity. [42]

The flexibilization of biogas plants aims to adapt to the supply of weather-dependent renewable energies. CHPUs are controllable generators and can thus be easily adjusted to meet demand. However, biogas production in a biogas plant cannot be regulated, necessitating the storage of biogas during periods when the CHPU is not in operation. This storage can be managed on a small scale by the biogas fermenter and post-digestion tanks. Consequently, flexibilization allows the operation of the CHPU to be adjusted according to the demand in the power grid. Typically, the electricity demand correlates with the market prices. As a result, through direct marketing and flexibility, a higher price for the fed-in electricity can be achieved compared to the average price that would be paid with a regular feed-in tariff. Annually, approximately 5 GW of electricity from biogas plants is fed into the grid. Flexibilization would enable the achievement of around 10 to 15 GW of flexible peak power, thereby alleviating the power grid during periods of high residual load. Thus, the flexibilization of biogas plants can play a crucial role in the future energy system [43]. [42]

Direct Marketing

Since January 1, 2016, all new renewable energy systems with a rated output of at least 100 kW are required to sell their electricity directly on the electricity market. Remote control by the distribution grid operator is also mandatory. The major advantage of direct marketing of the produced electricity is that higher prices than the monthly average market price can be achieved through flexibility. Thus, higher profits can be obtained compared to the traditional Erneuerbare-Energien-Gesetz (EEG) remuneration. This makes direct marketing profitable even for existing plants. [42]

Fundemantals of Biogas CHPUs

In phases where spot-market electricity prices are high, the model dispatches biogas to generate electricity that can be sold at high electricity prices at the spotmarket. This conversion takes place in a CHPU. Modern biogas CHP installations predominantly employ spark-ignition (Otto) engines; approximately two out of three new plants are of this type. [44]

A CHPU simultaneously produces electrical and thermal energy in a single process. The biogas is combusted in an internal combustion engine, yielding mechanical work and waste heat. The mechanical energy drives an electrical generator, while the thermal energy is recovered in a heat exchanger. Thanks to this utilization of waste heat, overall efficiencies of up to 90 % can be achieved. [44]

Biogas CHPUs are inherently dispatchable: they can start up or shut down and modulate output to match demand. Historically, most plants operated at baseload. However, in an increasingly volatile power system, flexibility measures become critical. Enabling rapid load changes typically requires engine oversizing, additional gas and heat storage, and advanced control systems. In many regulatory frameworks, operators receive a “flexibility bonus” for each kilowatt of dispatchable capacity. This incentive offsets the investment costs associated with oversizing the engine and installing storage, and encourages the flexible operation required to integrate variable renewable generation. [29, 44]

3.2 Introduction to the Biogas-to-Liquid technology

BGtL is part of the Power-to-X technologies. Power-to-X refers to processes that make renewable electrical energy storable in other forms. In BGtL, the biogas is converted into syngas via a gasification process powered by renewable electricity. This syngas is then transformed into liquid fuels in a synthesis step (for example, FTS or methanol synthesis).

Figure 3.2 shows an overview of a BGtL plant, using the reference plant described in this work as an example. The produced biogas is converted into syngas in a PC process driven by renewable electricity. The syngas is then fed into the FTS unit and converted into FT-syncrude. In the reference plant for this thesis, the process ends here. But to make the syncrude suitable for aviation, however, it must undergo an additional upgrading process to yield the final SAF.

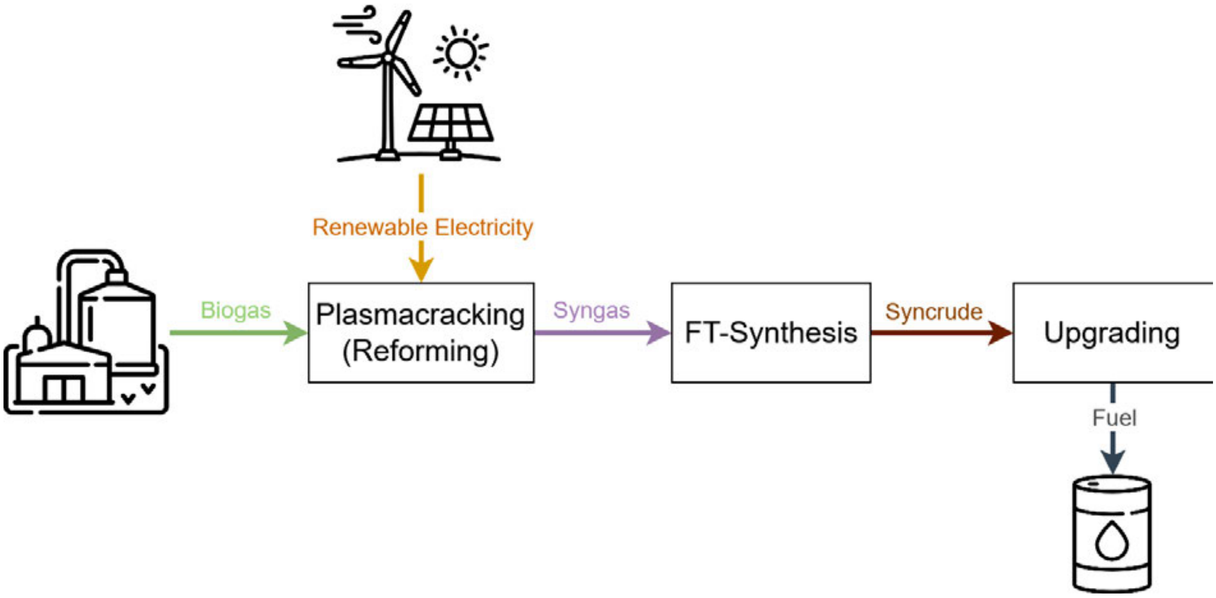

Figure 3.2: Biogas-to-Liquid Concept Diagram (own illustration).

3.3 Basics of the Plasmacracking Process

Plasma is defined as an ionized gas. PC, therefore, describes the process in which a gas is transformed into an ionized gas, creating plasma. The state of plasma cannot be clearly assigned to the three known states of matter (solid, liquid, and gaseous), which is why plasma is often referred to as the fourth state of matter (see Figure 3.3). For a gas to become plasma, an input of energy is required. This energy input causes the atoms and molecules of the gas to ionize, forming plasma. [45]

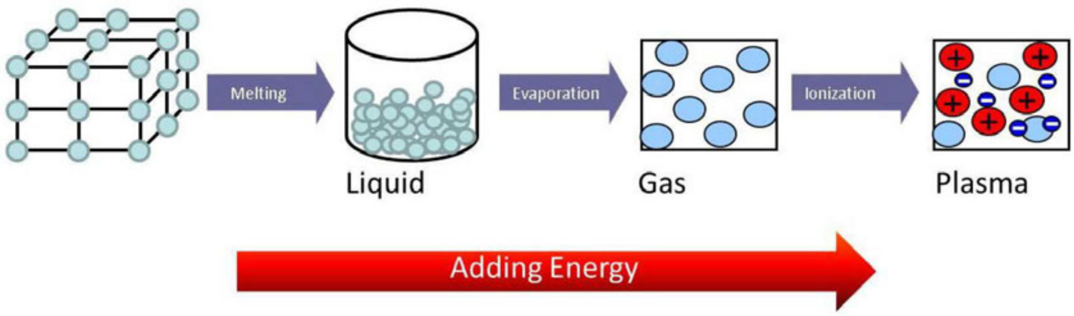

Figure 3.3: The four aggregate states [46].

The required energy can be thermal, electrical, or electromagnetic. The energy excites the electrons, causing them to move towards and collide with the neutral particles of the gas. These collisions can be elastic or inelastic. In an elastic collision, there is no change in the charge of the neutral particles, but their kinetic energy is increased. In inelastic collisions, which occur at sufficiently high electron energy, the electron structure of the impacted, previously neutral particle

is altered to form ions, changing the internal energy of the molecule. Electrical plasmolysis can be distinguished by the wavelength and frequency used, with common methods utilizing low-frequency waves, radio waves, and microwaves. [45, 47]
In the reference model, PC is implemented using microwaves. The gas mixture of CO2, CH4, and water, along with a support gas (e.g. argon or nitrogen), is subjected to plasmolysis. Through plasmolysis, the bonds within the gases are cracked and new bonds are formed. It is expected that carbon monoxide, carbon dioxide, and hydrogen will be produced.

$$\mathrm{CO_2} + \mathrm{H_2} + \mathrm{H_2O} + \mathrm{CO} + \mathrm{CH_4} + \ldots \rightarrow x\,\mathrm{CO} + y\,\mathrm{H_2} + z\,\mathrm{CO_2} \tag{3.1}$$

By adjusting the reactants, the ratio of the reaction products can be altered, which can influence the resulting synthesis gas. [45]

3.4 Basics of the Fischer-Tropsch Synthesis

During a synthesis, several starting materials are combined and, under specific temperatures and pressures that trigger reactions, a new starting material or materials are formed. For instance, using carbon monoxide and hydrogen as syngas, various hydrocarbon compounds, described as syncrude, can be produced, which can serve as a basis for fuels.In this work, the FTS is applied, which is therefore described in more detail.

The FTS takes its name from Franz Fischer and Hans Tropsch, who developed the concept in the 1920s [48]. The process is now widely applied, with numerous commercial plants operating on syngas derived from coal or biomass feedstocks [49]. It is a polymerization process in which predominantly gaseous, liquid, and solid hydrocarbons of different chain lengths are obtained from synthesis gas. This results in gaseous hydrocarbons (C1–C4), gasoline (C5–C10), diesel (C11–C18), and waxes (C19+), which are also desribed as FT-syncrude. The basic equation of the FT process is shown in Equation 2. [48]

$$\mathrm{CO} + 2\mathrm{H_2} \leftrightarrow [-\mathrm{CH_2}-] + \mathrm{H_2O}; \quad \Delta H_\mathrm{R}^0 = -165\frac{\mathrm{kJ}}{\mathrm{mol}} \tag{3.2}$$

In reality, the reaction is much more complex, as various reactions occur depending on a multitude of parameters. For precise calculations, the Anderson–Schulz–Flory (ASF) distribution can be utilized. The ASF distribution is a probability function that describes the formation of n-chain hydrocarbons based on the chain growth probability α. Figure 3.4 shows the product distribution as a function of the chain growth probability α. [45, 48]

Cobalt or iron are used as catalysts in industrial applications [50]. The product distribution is specific to the catalyst used, the gas composition and reaction conditions such as temperature and pressure [51].

It is important to note that a CO_2-based FTS process exists [53], but it is not utilized in this thesis and will therefore not be discussed further.

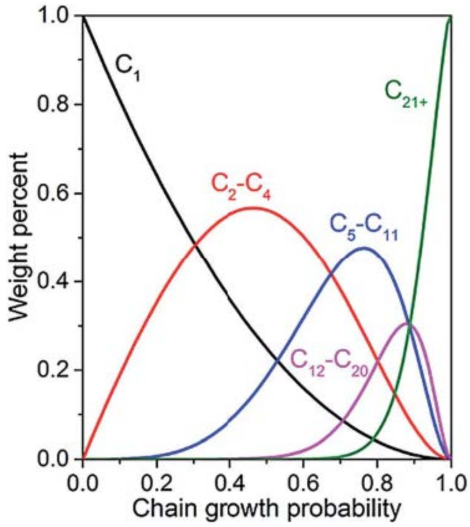

Figure 3.4: Product distribution of an FTS process according to the ASF model [52].

3.5 Structure of the reference system consisting of BGtL and CHP units

In this chapter, the reference plant for which the simulations were performed is introduced, and the BGtL plant is described in detail.

The reference plant is a hypothetical model consisting of six main components. Biogas is produced in a biogas plant equipped with a BGS unit that allows storing of the biogas. There are two possible utilization routes for the biogas. The first route is the electricity generation in a CHPU; in this process, waste heat is also produced, which is likewise utilized and marketed within the system. The second route leads to the BGtL plant. Here, in the first step, the biogas is converted into synthesis gas in a PCU. This synthesis gas can be stored in a SGS tank and then converted into FT-syncrude in an FTS plant. The flexible units in the system are the CHPU and the PCU: in an overbuild scenario, they can be operated flexibly, whereas the biogas plant and the FTS operate at constant rated capacity. The structure of the reference plant is shown in Figure 3.5.

Presentation of the BtL system in Detail

The configuration of the BGtL plant is based on the planned pilot plant of the Plasma2X project.

In the Plasma2X project, a BGtL pilot plant will be developed and constructed with the help of research and industry partners. This plant will chemically decompose raw biogas through a PC process, allowing the elemental components to be recombined to produce CO_2-neutral liquid fuels (for aviation or maritime use) via synthesis. A key component, in addition to PC, is a membrane separation. By cleverly combining membranes with different selectivities, unreacted feedstocks or by-products can be recirculated, and synthesis gas can be concentrated. This intermediate product will then react in either a FTS or methanol synthesis to produce liquid fuels. In this thesis, however, only the FTS is used as the synthesis unit. [54]

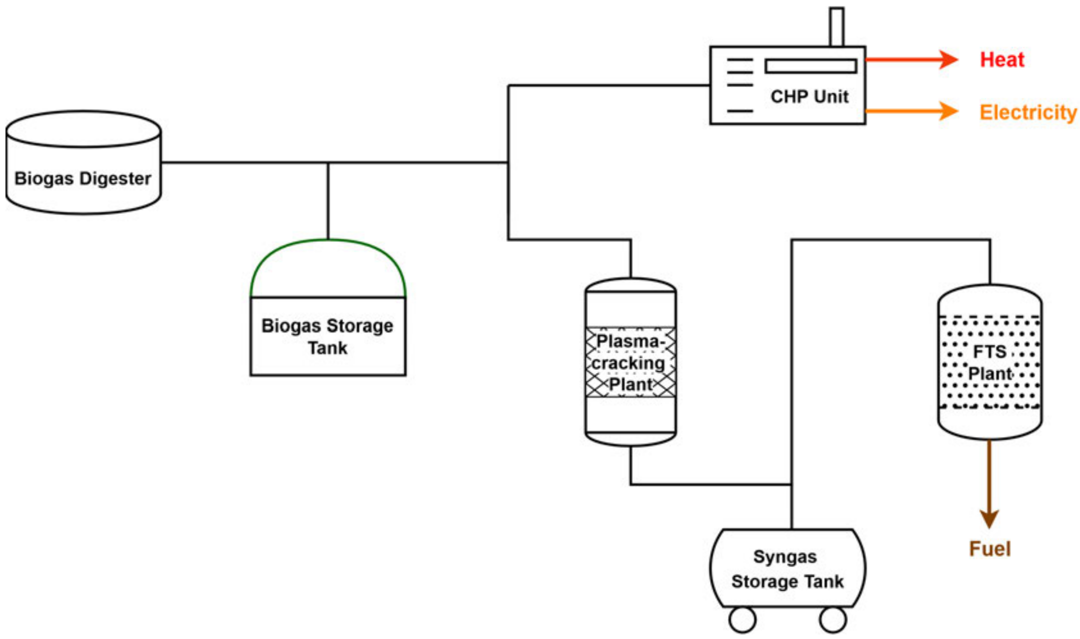

Figure 3.5: Structure of the BGtL system in combination with the CHPU.

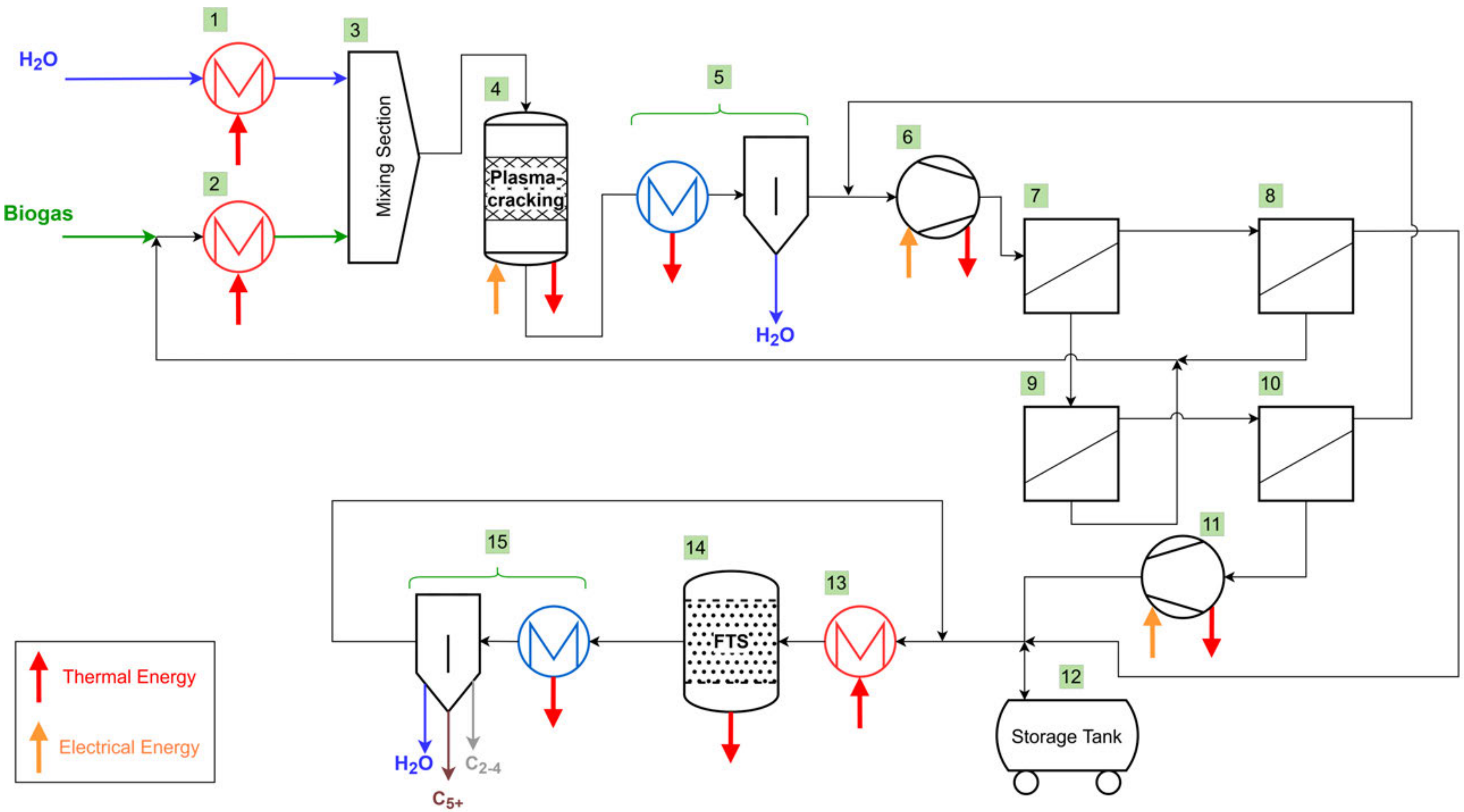

Components of the BtL Plant					
1.	Water Heater	6.	Compressor Gasmixture	11.	Compressor H_2
2.	Biogas Heater	7.	H_2/CO-Membrane Seperation	12.	Syngas Storage Tank
3.	Mixing Section	8.	CO/CH_4-Membrane Seperation	13.	Heater Syngas
4.	PC Reactor	9.	H_2/CO_2-Membrane Seperation	14.	FTS Reactor
5.	Water Seperator	10.	H_2/Residual-Membrane Seperation	15.	Seperator Hydrocarbons and Water

Figure 3.6: BGtL plant process flow diagram (above) with legend of numbered components (below).

Detailed Description of the Plasma-to-X System Components

This section describes the functions of the individual components of the BGtL plant. Figure 3.6 shows a flow diagram with a table containing all components of the BGtL process. The detailed thermodynamic calculations for each component and the material streams are provided in the Appendix.

Water Heater (1)
The Water Heater not only raises the feed water temperature to approximately 105 °C, but also fully vaporizes it to produce steam.

Biogas Heater (2)
Analogous to the Water Heater, the Biogas Heater heats both the fresh biogas feed and the recycled gas from the membrane separation to 105 °C. These recycled gases are those that were not cracked in the PC processes. To increase overall efficiency, they are returned to the PC step for a second pass.

Mixing Section (3)
In the Mixing Section, the steam, fresh biogas and recycled gas streams are combined at ambient pressure and at roughly 105 °C, ensuring a uniform feed to the PC reactor.

Plasmacracking Reactor (4)
Inside the PC Reactor, a microwave generator ignites and sustains a plasma. This plasma cracks the incoming gas molecules—methane, carbon dioxide and water vapor—into their constituent fragments, primarily CO and H_2, which serve as syngas for the subsequent FTS. An inert gas (e.g. argon or nitrogen) is also injected. In this model, only 20 % of the feed gas is cracked on each pass; the remaining 80 % bypasses the plasma and is recycled back into the biogas feed after the membrane seperation.

Water Separator (5)
To protect the membranes from liquid, uncracked steam is condensed out in a Water Separator. This cools the gas mixture to about 25 °C and removes liquid water.

Compressor Gasmixture (6)
The dry gas mixture is then compressed from ambient pressure up to 30 bar, the operating pressure required for the membrane separation trains and the FTS Process.

Membrane Separation Section (7–10)
After compression to 30 bar, the mixed gas enters the first membrane unit. Here it is roughly split into two streams:

- a retentate stream rich in carbon monoxide and methane, and
- a permeate stream rich in hydrogen (with some residual gases).

The hydrogen-rich permeate is sent to a second membrane, where carbon dioxide is removed and returned to the Biogas Feed. It then passes a third membrane to filter high-purity hydrogen; any residual gas left over is recycled back between the Water Separator (5) and the Gas Mixture Compressor (6).

Meanwhile, the CO/CH_4 retentate from the first membrane is directed to a fourth membrane module. There carbon monoxide is separated out as a pure syngas stream, and the methane that passes through is recycled into the biogas feed.

Syngas Compressor (11)

Because the H_2 stream drops below 30 bar during membrane separation, it must be recompressed to 30 bar before blending with the CO stream. The two high-pressure streams are then merged to form the final syngas.

SGS Tank (12)

In flexible operation scenarios the PC reactor is oversized to respond to electricity market signals, while the FT plant remains at nominal capacity. Thus, excess syngas must be temporarily stored. A buffer tank holds the syngas until the FT reactor can process it.

Syngas Heater (13)

Syngas from either the SGS or directly from the membranes is preheated to 250 °C in a heat exchanger ahead of the FTS reactor.

FTS Reactor (14)

The FTS reactor converts syngas into long-chain hydrocarbons, also called FT-syncrude which consists of: gasoline, diesel, kerosene, waxes and water. This reaction is strongly exothermic; in this thesis the released heat is recovered to drive the three heat exchangers (Water Heater, Biogas Heater and Syngas Heater).

Hydrocarbons & Water Separator (15)

Finally, the FTS product stream (hydrocarbons plus water) is sent to a separator. In industrial practice multiple stages are used, but here we assume a single unit for simplicity. Unconverted syngas are not separated but recycled back into the syngas feed upstream of the Syngas Heater.

3.6 Economic Evaluation Methods

In this chapter the formulas used for the cost calculations are presented. These are structured into the Cost Comparison Calculation, Profit Calculation and ROI (based on [55]).

Cost Comparison Calculation

The calculation of total costs C combines the capital costs C_{Capital} and the variable costs C_{var}. The capital costs consist of the linear depreciation—calculated as the difference between the initial investment cost C_0 and the salvage value L (in this thesis assumed to be zero for all assets at end-of-life) divided by the asset lifetime N—and the interest on the tied-up capital, computed as the average of C_0 and L divided by two and multiplied by the interest rate i:

$$C = C_{\text{Capital}} + C_{\text{var}} = \frac{C_0 - L}{N} + \frac{C_0 + L}{2} \cdot i + C_{\text{var}} \tag{3.3}$$

Profit Calculation

The profit Π is calculated as revenues R_{rev} minus total costs C.

$$\Pi = R_{rev} - C \tag{3.4}$$

Return on Investment (ROI) Calculation

The ROI is defined as profit Π divided by the ACE, expressed here as half the initial investment $C_0/2$, and multiplied by 100 to yield a percentage:

$$ROI = \frac{\Pi}{ACE} \cdot 100 = \frac{\Pi}{\frac{C_0}{2}} \cdot 100 \tag{3.5}$$

4 Methodological Approach

This chapter describes the methodology applied in this thesis.

4.1 Conceptual Framework and Model Workflow

The basis of the referenced BGtL unit of this thesis was the BGtL plant planned in the Plasma2X project and the question of how this plant, with its novel low-temperature microwave PC technology for syngas production followed by FTS, could be integrated into the existing Biogas plant market. Because the BGtL plant consumes electricity to convert biogas into syngas, while the most widespread way of utilising biogas is to generate electricity in a CHPU, a market concept emerged: combine the two plant types and operate them in response to electricity market signals. When electricity prices are high, the CHPU converts biogas into electricity; when prices are low, the electrically driven PCU converts the biogas into syngas. Thus, the CHPU acts as an intelligent electricity producer, and the PCU as an intelligent electricity consumer.

To simulate this plant combination, it was clear from the beginning that an optimisation model would be required to generate an electricity-price-driven operating schedule. The work therefore began with model development. A literature review provided an overview of existing projects with comparable optimisation models. Although a number of projects were identified, they were only partly comparable with the reference plant, so a completely new model was written. The optimisation logic of existing models was consulted, but the modelling Framework (objective function, constraints and parameter sets) was developed primarily from the literature and at the beginning a rudimentary model was created, in which the model parameters were supplemented by placeholders and the constraints had to be further elaborated.

Once a basic model structure had been defined, the next step was to program the model. The task required a structured, easily understood codebase and a method of visualising the optimisation results. Python was chosen because it requires no licence, offers many libraries and is easy to understand, making the code reusable, adaptable and suitable for further research.

After setting the modelling environment and creating the theoretical model, it had to be transferred into program code. Among other resources, OpenAI's ChatGPT was used to convert the model into Python quickly; the specific role of ChatGPT is explained separately in Chapter 4.2.

In this phase, an optimisation script and a main script were produced. The main script handled the initialisation of simulation parameters - still placeholders at this stage - and all data handling. It transferred the simulation parameters and the optimisation window with electricity market data to the optimisation script (which contained the model) and received the optimised plant schedule and parameters in return.

To test the model for errors, a visualisation of the optimisation window was implemented simultaneously, allowing the optimisation behaviour to be inspected and adjusted visually. Meanwhile, research on the individual simulation parameters started so that placeholders could be replaced with real values. To make the model as realistic as possible, the simulation parameters were derived from extensive literature research; in the case of the novel PC technology, comprehensive thermodynamic calculations were carried out to evaluate the operating parameters.

Once the parameters had been fixed, the program code had to be extended with cost calculations. A separate script now receives the cost and revenue parameters of the simulation and calculates total costs, profit and ROI. It was decided to use the ROI as the final output parameter so that simulation results could be compared.

Because one of the main objectives - and the thesis title itself - was the determination of optimal expansion strategies for BGtL plants and Biogas-CHPUs in flexible biogas facilities, various expansion scenarios had to be developed and simulated. Therefore variable simulation parameters representing these different expansions were defined and embedded in the main script.

Finally, the code was extended with a function that visualises all results in a heatmap.

After the main simulations with the various variable parameters had been carried out and evaluated, it became apparent that further simulations - one to determine the optimal syncrude price for the BGtL plant and another to quantify a potential flexibility bonus for the BGtL plant - would complete the thesis. These additional simulations were therefore conducted, and their results were evaluated and discussed.

4.2 Use of AI for Program Code Generation

This section explains clearly when and how OpenAI ChatGPT was used in the present thesis. The system served only as a tool that converted existing ideas into working Python code more quickly; no scientific concepts or interpretations were produced by the Artificial Intelligence (AI) itself.

Implementation of the MILP model in Python

ChatGPT was first employed to translate the MILP optimisation model taken from the literature into a Python implementation that relies on the pyomo library. At the same time, a basic framework for simulation, data handling, and result storage was generated. Because the original conversations were very long, the text below presents a short example prompt that asked ChatGPT to insert the objective function into the Python model. For complex queries of this kind, the `o3` or `o4-mini` models were primarily used; for smaller, straightforward requests, the `GPT-4o` model was chosen to save resources and obtain faster responses.

User Prompt

```
Hello ChatGPT,
could you please add the following objective function to my Python
   model?
I am working with Pyomo and CPLEX, and the model is already structured
   as shown below:
```

```
- Previous Code -

This is the objective function:

- Objective Function -
```

Listing 1: Example: Implementation of the Objective Function in Python (User prompt)

ChatGPT response

```
# -----------------------------------------------
# 1.  Helper coefficients for the objective
# -----------------------------------------------
def chp_coef_init(m, t):
    """Slope for the CHP term:
       p_t          if p_t > θ
       p_t - θ      else (== - (θ - p_t))"""
    p = m.price[t]
    return p if p > m.theta else p - m.theta

m.c_CHP = pyo.Param(m.T, initialize=chp_coef_init, mutable=False)

# Plasma-cracking term is always  -F_power_PC * p_t
m.c_PC  = pyo.Param(m.T,
                    initialize=lambda m, t: -F_power_PC * m.price[t],
                    mutable=False)

# -----------------------------------------------
# 2.  Objective - maximise total revenue
# -----------------------------------------------
def obj_rule(m):
    return sum(
        m.c_CHP[t] * m.P_CHP[t] +    # CHP contribution (possibly
           negative)
        m.c_PC[t]  * m.P_PC[t]       # PC contribution (negative price
           flips sign)
        for t in m.T
    )

m.total_revenue = pyo.Objective(rule=obj_rule, sense=pyo.maximize)
```

Listing 2: Example: Implementation of the Objective Function in Python (ChatGPT response)

The code produced by ChatGPT served as a starting point and was adapted step by step until the final version was obtained. The development process consisted of alternating rounds of manual editing and additional requests to ChatGPT for more complex adjustments.

Tool for Chart Generation

ChatGPT was also used to create several figures for the thesis. Instead of asking for new visual layouts, the desired appearance was described precisely, and ChatGPT delivered an initial code draft in the same style as already existing figures, for example:

User Prompt

```
Hello ChatGPT,
I have the following electricity market data that I would like to
   visualize using Python code. The data is saved in a txt file and
   stored in the same folder as the Python file:
Data:
data.txt

Please make sure that the chart is created in the same style as my
   previous charts:

- Here is the program code for an already created chart -
```

Listing 3: Example: Chart generation (User prompt)

ChatGPT response

```
import pandas as pd, matplotlib.pyplot as plt, matplotlib.dates as
   mdates
from matplotlib.ticker import ScalarFormatter
import numpy as np

plt.rcParams['font.size'] = 13

df = pd.read_csv('data.txt', sep='\t',
                 parse_dates=['Time'], dayfirst=True)
df['Price_kWh'] = df['Price [€/MWh]'] / 1_000

#-------------------------------------------------
# 1) Time-series plot
#-------------------------------------------------
fig, ax = plt.subplots(figsize=(9, 4))
ax.plot(df['Time'], df['Price_kWh'], lw=1, color='k')
ax.set(title='15-min Intraday Auction\nDE-LU 2023',
       xlabel='Month', ylabel='Price (€/kWh)')
ax.xaxis.set_major_locator(mdates.MonthLocator())
ax.xaxis.set_major_formatter(mdates.DateFormatter('%b'))
ax.yaxis.set_major_formatter(ScalarFormatter())
ax.grid(ls='--', alpha=.4)
fig.tight_layout()
fig.savefig('timeseries.png', dpi=350)

#-------------------------------------------------
```

```
# 2) Empirical CDF
#-------------------------------------------------
p = np.sort(df['Price_kWh']);     r = np.arange(1, len(p) + 1)
fig2, ax2 = plt.subplots(figsize=(9, 3.5))
ax2.step(r, p, where='mid', lw=1, color='k')

ax2.axvline((p >= 0).argmax() + 1,  ls='--', c='g')
ax2.axvline((p > 0.18).argmax() + 1, ls='--', c='orange')

ax2.set(title='Empirical CDF 2023',
        xlabel='Interval rank', ylabel='Price (€/kWh)',
        xlim=(20, len(p)), ylim=(-.1, .3))
ax2.yaxis.set_major_formatter(ScalarFormatter())
ax2.grid(ls='--', alpha=.4)
fig2.tight_layout()
fig2.savefig('cdf.png', dpi=350); plt.show()
```

Listing 4: Example: Chart generation (ChatGPT response)

Further refinements were added later, but the draft shortened the overall work time. Without ChatGPT the figures would likely have been more basic, even though producing them still required considerable effort.

Help with Debugging

ChatGPT also supported the debugging of the optimisation model. The extract below shows a representative interaction that helped to identify the reason for an infeasible model.

User Prompt

```
Hello ChatGPT,
can you see, why my model is not feasable? This is the callback:

Problem not solvable: infeasible
Period 0 not solvable. Skipping this period.

And this is my Model, that I changed a little bit and now the error
   occurs:

- Model with Objective Function and Constraints -  (code omitted for
   brevity)

Do you have an idea, why the error occurs now?
```

Listing 5: Example: Debugging (User prompt)

ChatGPT response

```
Why CPLEX declares the model "infeasible"
```

```
----------------------------------------

‘optimize_for_period_PC()‘ now contains two hard equalities that cannot
be satisfied simultaneously for every 15-minute step, once you look at
the units and the "/4" scaling you introduced:

 Step                           Supplies syngas       Mandatory demand
 -------------------------------------------------------------------
 Plasma-cracking output         P_Plasmacracking[t] *
                                PC_Production_Factor
 FTS consumption                                     Syngas_Demand_FTS[t] =
                                                     PC_Production_Factor *
                                                     P_Plasmacracking_max /
                                                     (4 * PQ_PC)

1. Supply is capped four-times lower than before
   P_Plasmacracking[t] ≤ (P_Plasmacracking_max / 4) *
      plasmacracking_on[t]

2. Demand is still based on the full, unscaled P_Plasmacracking_max.
   Unless PQ_PC equals 4 (and the cracker runs at max every step) the
   storage balance

   V_Syngasstorage[t] = V_Syngasstorage[t-1]
                      + P_Plasmacracking[t] * PC_Production_Factor
                      - Syngas_Demand_FTS[t]

   drives V_Syngasstorage negative almost instantly.  Because
   V_Syngasstorage ≥ 0, CPLEX reports

   Problem not solvable: infeasible
```

Listing 6: Example: Debugging (ChatGPT response)

In this case the infeasibility was caused by an unintended four-fold increase in biogas consumption by the PCU. This error drove the biogas storage below zero and violated the capacity limit constraint. After ChatGPT pointed out the inconsistency, the model could be corrected quickly.

Summary

ChatGPT was therefore used as a tool for

- generation of Python code for the MILP model and overall simulations,
- creation of plotting scripts for the figures, and
- location and correction of coding errors during debugging.

All scientific ideas, model logic, and final interpretations were developed by the author; ChatGPT helped with the technical implementation and accelerated the process.

5 Simulation Parameters and Assumptions for the MILP Model

To develop the simulation program code, a literature review and state-of-the-art survey were first conducted for the six main units (Biogas Plant, BGS, CHPU, PCU, SGS, and FTS). This enabled the determination of the necessary simulation parameters. In this chapter, the methodology for evaluating each simulation parameter as well as the simulation parameters themselves are presented.

Since the individual plant components are treated separately below, this section first outlines the assumptions made for the system as a whole. For simplicity, it is assumed that Operational Expenditure (OPEX) and the nominal cost of debt are independent of each plant's size. Furthermore, all plants are assumed to share the same nominal cost of debt of 6% [56].

The thermodynamic calculations for the biogas costs and the BGtL plant can be found in the appendix in chapters A.1.3 and A.1.5.

5.1 Constant Simulation Parameters for the Biogas Plant

This section presents the constant parameters for the biogas plant. These are divided into economic and financial parameters—including specific investment costs, OPEX, lifetime and nominal cost of debt—and biogas production costs, which cover substrate costs and electricity consumption.

Economic and Financial Parameters for the Biogas Plant

Since the rated power varies across scenarios, Capital Expenditure (CAPEX) data for biogas plants of different sizes were compiled and fitted to a power-law function. Table 5.1 summarizes the reference CAPEX values, and Figure 5.1 shows the resulting fit.

Table 5.1: Specific investment costs for a Biogas Plant

Rated Power [kWp]	**Specific Investment Costs [€ $\times 10^3$]**	**Source**
75	560; 548	[44, 57]
150	710; 705	[44, 57]
250	1,100; 1,190; 1,175	[44, 57]
500	1,780; 1,800	[44, 57]
750	2,350; 2,325	[44, 57]
1,000	2,670; 2,750; 2,700	[44, 57]

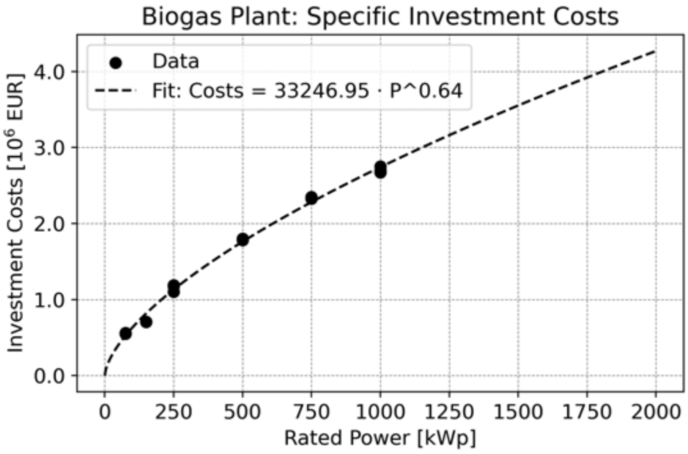

Figure 5.1: Biogas Plant (Consisting of: Substrate storage, Digester, Fermentation residue storage, Planning, Land Cost): Specific Investment Costs (Data from [44, 57]).

The fitted correlation is

$$C_{0,\,\mathrm{Biogas\,Plant}}(P) = 33246.95 \cdot P^{0.64}, \tag{5.1}$$

where P denotes the rated power in kWp.

Furthermore, the OPEX—comprising maintenance and repair costs—are assumed to be 4% of the CAPEX per year [44], and the plant lifetime is set to 20 years [44]. Table 5.2 lists the parameters of the biogas plant.

Table 5.2: Economic parameters of the Biogas Plant.

Parameter	**Value**	**Unit**	**Source**
OPEX	4 (3.5-5.0)	%	[44]
Lifetime	20	years	[44]
Nominal cost of debt	6	%	[56]

Biogas Production Costs

For the simulations, it was also necessary to know the biogas production costs. To this end, the substrate for biogas production was first determined. In order to ensure good comparability, it was decided to base this on the national average in Germany. As shown in Figure 3.1, biogas substrates in Germany consist of 41 wt % renewable raw materials and 50 wt % farm manure [37]. The remaining 9 wt % [37], comprising biowaste and residual materials, were not considered here. Of the farm manure, 69 wt % is cattle slurry [58], and 65 wt % of the renewable raw materials is maize [59]. Therefore, a substrate mixture of 45 wt % maize silage and 55 wt % cattle slurry was used for the simulations.

In the next step, the biogas composition had to be determined. Based on literature values for different substrate types, the following composition was assumed for the simulations: maize silage yields 52–54.5 vol.% CH_4 and 40.5–43 vol.% CO_2 [60, 61], while cattle slurry yields 55–57 vol.%

CH_4 and 40–42 vol.% CO_2 [60, 61]. The residual gases (H_2O, NH_3, H_2S) account for 3–5 vol.% [60, 61]. For the simulations, it was assumed that the biogas contains 54 vol.% CH_4, 41 vol.% CO_2 and 5 vol.% residual gases. Since hydrogen sulfide in the residual gas is harmful to the process and plant components, it is assumed that the residual gas is removed. This results in a biogas composition of 57 vol.% CH_4 and 43 vol.% CO_2.

In the next step, the substrate cost in €/Nm^3 of produced biogas was determined using the biogas yield and the substrate prices. The necessary values for the calculation are listed in Table 5.3. It was assumed that cattle slurry is sourced free of charge from a nearby farm and that maize silage costs 40 €/t Organic Solids (OS) [61]. The detailed calculation is provided in the appendix. This yields substrate costs of 0.158 €/Nm^3 of produced biogas.

Table 5.3: Characteristics of substrates for biogas production [61].

Substrate	**Total Solids (TS) [%]**	**Organic Solids [%]**	**Total (oTS)**	**Biogas Yield [Nm^3/t oTS]**	**Cost [€/t OS]**
Cattle manure	10	80		380	0
Silage maize	35	95		650	40

For the targeted H_2/CO ratio of 2.2, the following stoichiometric equation is obtained:

$$4\,CH_4 + CO_2 + 3\,H_2O \rightarrow 5\,CO + 11\,H_2 \tag{5.2}$$

In the next step, the molar ratio of CH_4 to CO_2 in the produced biogas was compared to the optimal molar ratio for PC (4:1) to determine whether the biogas needed treatment. The produced biogas has a CH_4:CO_2 molar ratio of approximately 4:3, whereas the stoichiometry of the PC process requires 4:1. Therefore, a solution was needed to adjust this ratio.

Essentially, there are three options to address this issue:

1. Use the biogas at 4:3 and remove 2/3 of the CO_2 after PC (which would increase volumetric flow and thus component and energy costs).
2. Co-feed biomethane to raise the ratio to 4:1.
3. Upgrade the biogas before PC by removing 2/3 of the CO_2.

For the simulations, the third option was chosen: reduction of the CO_2 content via a biogas upgrading process.

Using these proportions, the electricity demand for biogas production was then determined. The digester requires 3.8 % of the Lower Heating Value (LHV) of the upgraded biogas, and the upgrading process requires 2.9 % of that LHV [61]. The LHV of the upgraded biogas (80 vol.% CH_4) is 7.96 kWh/m^3 [62], yielding an electrical demand of 0.533 kWh/m^3 of upgraded biogas. It was assumed that the required thermal energy (13 % of the biogas LHV [61]) is supplied via internal recovery.

The biogas production costs are summarized in Table 5.4.

Table 5.4: Biogas production costs.

Parameter	Value	Unit	Source
Substrate cost	0.158	€/Nm^3_{biogas}	[61]
Electricity demand	0.533	kWh/$Nm^3_{upgraded\ biogas}$	[61]

5.2 Constant Simulation Parameters for the CHPU

This section presents the constant parameters for the CHPU. These are divided into investment, operating, and performance parameters—including specific investment costs, OPEX, lifetime, efficiencies, minimum runtime/off-time, minimum part-load, and nominal cost of debt—as well as the electricity sales price, which comprises the remuneration value, service fee, and Value Added Taxes (VAT); the biogas heat remuneration, which comprises the heat tariff and the marketable share; and finally, the flexibility bonus.

Investment, operating, and performance parameters CHPU

For the CHPU, CAPEX data were also collected and a curve-fitting procedure was used to derive a correlation. The collected data are presented in Table 5.5 and the fitted correlation is shown in Figure 5.2.

Table 5.5: Specific investment costs for a CHPU

Rated Power [kWp]	Specific investment costs [€/kWp]	Source
10	4,000	[63]
250	1,300	[64]
500	1,000	[64]
750	900	[64]
1,000	800	[64]
2,000	400	[63]

The fitted correlation is

$$C_{0,\,\mathrm{CHPU}}(P) = 42336.51 \cdot P^{0.40}, \tag{5.3}$$

where P denotes the rated power in kWp.

Furthermore, OPEX were assumed to amount to 3 % of CAPEX per year [65–67]; the electrical efficiency is 40 % [68–71], the thermal efficiency is 45 % [68, 70], and the lifetime was assumed to be 60,000 Full Load Hours (FLH) for units below 1,000 kWp and 80,000 FLH for units above 1,000 kWp [44, 72, 73]. A minimum runtime and offtime of one hour were assumed to reduce wear from highly fluctuating operation and thereby extend equipment life. This value was chosen based on engineering judgment and technical discussion. In addition, a minimum part-load of 70 % of nominal capacity is assumed to maintain both efficiency and durability under turndown conditions [74–76]. Since typical start-up and shutdown times for a CHPU are around 5 and

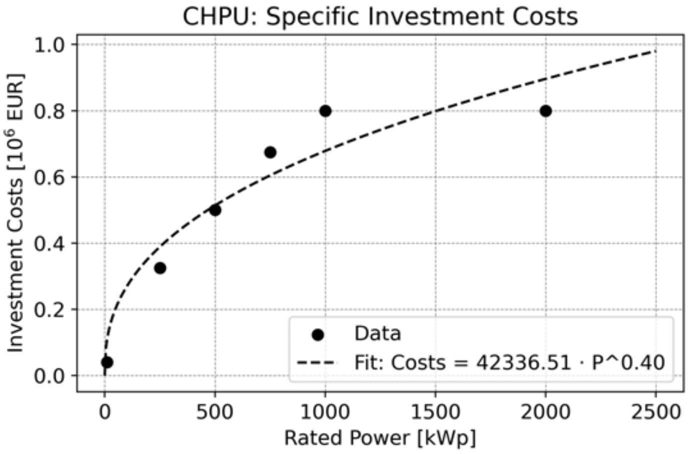

Figure 5.2: CHPU: Specific investment Costs (Data from [63, 64]).

2 minutes, respectively [77], these were neglected to allow faster solution of the optimization problem. Table 5.6 lists the parameters of the CHPU.

Table 5.6: Economic parameters of the CHPU.

Parameter	Value	Unit	Source
OPEX	3 (1–4)	%	[65–67]
Lifetime	60,000; 80,000	FLH	[44, 72, 73]
Electrical efficiency	40 (30–40)	%	[68–71]
Thermal efficiency	45 (40–45)	%	[68, 70]
Nominal cost of debt	6	%	[56]
Minimum runtime/offtime	1	h	–
Minimum part-load	70	%	[74–76]

Electricity Sales Price

The sales price of electricity fed into the grid consists of four components: the spot market price (which changes every 15 minutes), the remuneration value, VAT, and a service fee. In this model, Direct Marketing is applied. Under Direct Marketing, the electricity is marketed via a direct marketer. This allows the plant operator to benefit from flexible operation and fluctuating market prices.

Figure 5.3 illustrates the principle of Direct Marketing. A remuneration value is assigned to the plant, representing the minimum price that the operator will receive for the electricity. If the spot price falls below the remuneration value electricity is fed into the grid, the difference (market premium) is paid by the grid operator. By flexible operation, the operator can nonetheless sell most of the electricity at high spot prices to capture higher revenues. The spot market payment is subject to 19 % VAT [79]. In addition, the direct marketer charges a service fee of 3 % [80]. No tax is applied to the premium paid by the grid operator [81].

The remuneration value is determined by the biogas auction procedure. In biomass auctions, the lowest bids (in cent/kWh) receive awards until the target volume is reached. Under the "pay-as-

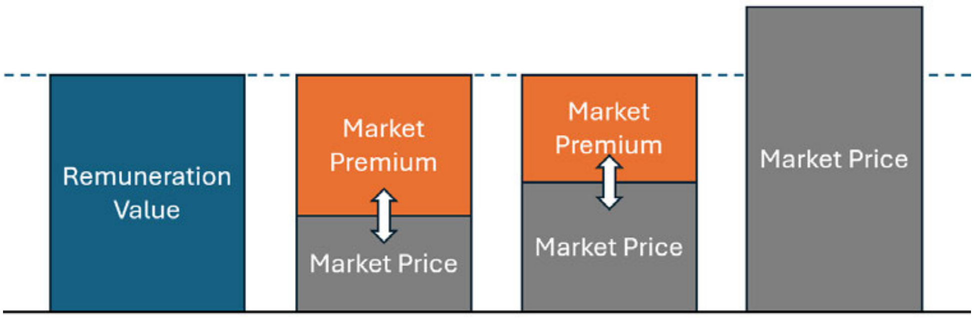

Figure 5.3: Principle of the Direct Marketing (own illustration, based on [78])

bid" principle, each awarded plant is paid its own bid price [82]. To identify a representative remuneration value for the simulations, awarded values from 2019 to 2024 were plotted (see Figure 5.4). The average value has risen over time—from just over 12 cent/kWh in November 2019 to a peak of about 18.5 cent/kWh in April 2023—before settling at approximately 17.5 cent/kWh. Based on these data, a remuneration value of 18 cent/kWh was chosen for the simulations.

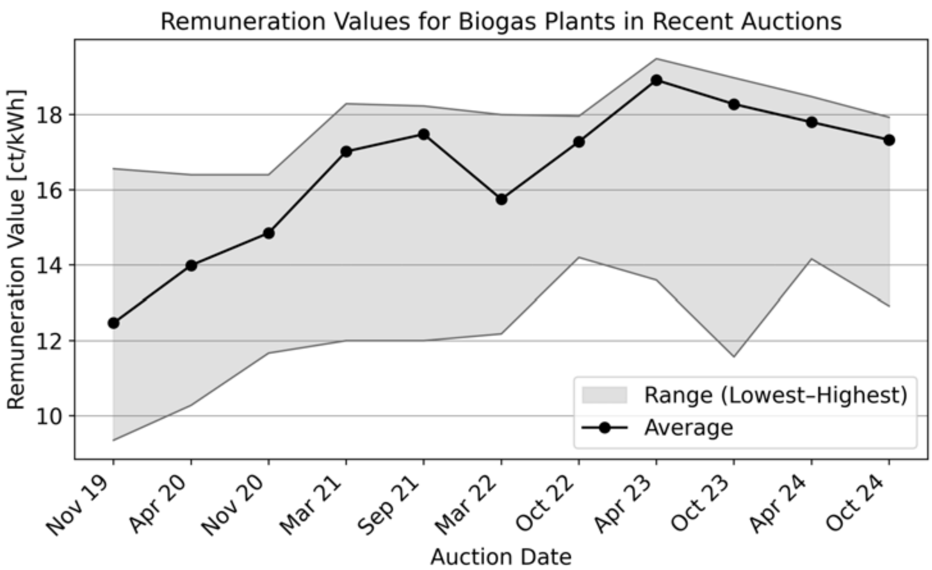

Figure 5.4: Average Remuneration Values from the past years (own illustration, Data from: [83–93])

Table 5.7 lists the parameters for direct marketing.

Biogas Heat Remuneration

To qualify for the electricity feed-in tariff, at least 60% of the heat must be utilized [94]. Of this, 25% [94] is consumed by the digester itself. In practice, marketing the excess heat is challenging, as a local heat off-taker is required and demand varies seasonally (higher in winter than in summer) [94]. Therefore, this study assumes that only 50% of the producible heat can be sold.

Table 5.7: Parameters for Direct Marketing

Parameter	**Value**	**Unit**	**Source**
Remuneration value	18.0	cent/kWh	[83–93]
Service fee	3	%	[80]
VAT	19	%	[79]

Together with the 25% self-consumption for the fermenter, this yields an overall heat utilization rate of 75%.

Biogas heat prices vary widely in practice, ranging from 0 to 9 cent/kWh$_{th}$, with an average of 2.6 cent/kWh$_{th}$ [95]. These fluctuations are driven by the type of heat use, pricing model, and supply level [96]. For the simulations, a heat tariff of 2.6 cent/kWh$_{th}$ is assumed. The parameters for heat utilization are listed in table 5.8.

Table 5.8: Parameters for biogas heat utilization

Parameter	**Value**	**Unit**	**Source**
Heat tariff	2.6 (0–9)	cent/kWh$_{th}$	[44, 95]
Marketable share	50	%	–

Flexibility Bonus

For plants in Germany commissioned after 1st of August 2014, a flexibility bonus can be claimed under § 50a of the EEG 2023 for additional installed CHP capacity if the plant exceeds 100 kW. This bonus amounts to 65 €/kW per year and is paid out over a period of 20 years. The flexibility bonus is also listed again in table 5.9.

Table 5.9: CHPU flexibility bonus

Parameter	**Value**	**Unit**	**Source**
Flexibility bonus	65	€/kW · a	§ 50a EEG 2023

5.3 Constant Simulation Parameters for the PCU

This section presents the constant parameters for the PCU components. These include investment, operating, and performance parameters—such as the specific investment costs, OPEX, lifetime, minimum runtime/off-time, minimum part-load, and nominal cost of debt—as well as the three factors used to determine rated power in the simplified simulation: the power scaling factor, the biogas consumption factor, and the syngas production factor; and, finally, water costs.

Investment, operating, and performance parameters for the PCU

For the planned 10 kW PC pilot plant in the Plasma2X project, the investment cost is approximately 400,000 €. As this is a First-Of-A-Kind (FOAK) system, the costs are very high and there are no comparable values to be found in the literature. Using an experience curve function, the specific production cost C_Q for a cumulative number of plants Q can be forecast. Here, C_1 denotes the cost of the first plant (400,000 €) and b is the experience curve parameter [97]:

$$C_Q = C_1 \cdot Q^b \tag{5.4}$$

The parameter b represents the slope of the experience curve on a double-logarithmic plot. It can be derived from the Learning Rate (LR), which describes the percentage cost reduction when cumulative production doubles. For energy technologies, LR is approximately 20% [97]. This means costs decrease by 20% each time cumulative production doubles.

$$LR = 1 - 2^b \tag{5.5}$$

The resulting experience curve is shown in Figure 5.5.

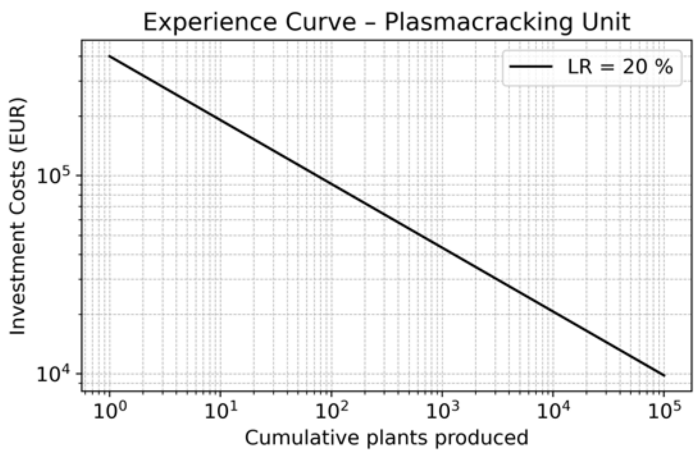

Figure 5.5: Experience Curve Model for the PC Technonoly plant.

It is a matter of interpretation when a technology reaches its break-even point and attains a stable, representative investment cost. In the literature, up to ten units are often assumed to establish this learning plateau [98]. Therefore, in the simulations it was assumed that ten PCUs have already been produced to derive a representative investment cost. Applying the experience curve function then yields an estimated cost of 190,000 € for the tenth PCU.

Next, the impact of plant size on investment cost is determined via the scaling effect, using a power-law relationship (Eq. 5.6). Here, C is the expected cost, S the plant size, C_r the cost of the reference plant (190,000 €), S_r its size (10 kW), and f the scale factor. For chemical process equipment, $f = 0.6$ [99] is commonly assumed:

$$\mathrm{C_0} = \mathrm{C_r} \times \left(\frac{\mathrm{S}}{\mathrm{S_r}}\right)^{\mathrm{f}} \tag{5.6}$$

The resulting Cost Scaling Function is shown in Figure 5.6.

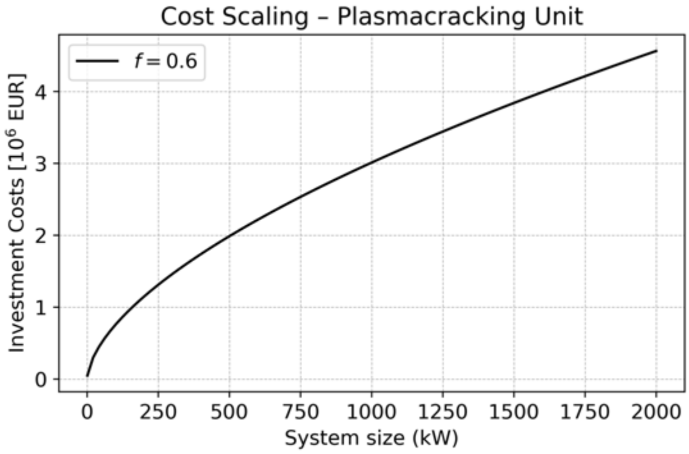

Figure 5.6: Cost Scaling Function for the PC Technonogy plant.

This results in the following formula:

$$C_0(S) = 190,000€ \cdot \left(\frac{\mathrm{S}}{10\mathrm{kW}}\right)^{0.6} \tag{5.7}$$

Since the reference PCU is a pilot installation, no long-term OPEX or lifetime data are yet available. Therefore, assumptions have been aligned with those for the FTS plant and the CHPU. Accordingly, an OPEX of 4 % of CAPEX per year and an expected lifetime of 20 years are adopted for the PC pilot plant. In terms of part-load operation, a minimum load of 70 % of nominal capacity is assumed, following the CHP assumptions. A minimum runtime and offtime of one hour are also imposed to reduce wear from frequent cycling. Startup and shutdown durations are neglected to simplify the optimization model. All parameters are summarized again in table 5.10.

Table 5.10: Economic and operating parameters of the PCU

Parameter	**Value**	**Unit**
OPEX	4	% per year
Lifetime	20	years
Nominal costs of debt	6	% per year
Minimum runtime/offtime	1	h
Minimum part-load	70	%

Electricity Costs

To respond to fluctuating electricity market prices, a dynamic electricity tariff is assumed in the simulations [100]. This tariff comprises the European Energy Exchange AG (EEX) intraday price, grid charges, and taxes and levies. In 2023, taxes and levies for industrial customers amounted to 2.86 cent/kWh [101], and electricity grid charges to 3.30 cent/kWh [102]. The electricity costs are listed in table 5.11.

Table 5.11: Composition of electricity costs for industrial customers

Parameter	Value	Unit	Source
Taxes and levies (2023)	2.86	cent/kWh	[101]
Electricity grid charges (2023)	3.30	cent/kWh	[102]

Rated Power of the PCU Components of the Reference System

To estimate the plant's energy requirements, the nominal power of each component was calculated using thermodynamic balances (see Appendix A.1.3 and the Python script `thermodynamic_calculations.py` in the digital appendices). Table 5.12 lists these rated capacities, separated into thermal and electrical outputs for both the PCU and the FTS Plant. The two systems are distinguished because, in the simulations, the PC Reactor and its auxiliaries are operated flexibly, whereas the FTS Plant runs at steady load.

The net thermal balance of -9.63 $\mathrm{kW_{th}}$ indicates that the process rejects more heat than it consumes. Accordingly, the heat required by the three heaters (Water Heater, Biogas Heater, and Syngas Heater) is assumed to be fully supplied by the combined waste heat of the other components, so no external heating is needed. The total electrical demand of 14.16 $\mathrm{kW_{el}}$ falls entirely on the PC side: 10.00 $\mathrm{kW_{el}}$ for the microwave reactor, about 3.00 $\mathrm{kW_{el}}$ for the gas-mixture compressor, and 1.10 $\mathrm{kW_{el}}$ for the hydrogen compressor; the FTS Plant requires no additional electrical power under the chosen operating conditions.

Table 5.12: Rated power of the PC components of the reference system.

Component	Thermal Power ($\mathrm{kW_{th}}$)	Electrical Power ($\mathrm{kW_{el}}$)
Plasmacracking Plant		
Water Heater	5.68	
Biogas Heater	0.59	
PC Reactor		10.00
PC Reactor (waste heat)	-1.00	
Water Separator (waste heat)	-2.01	
Gas-mixture Compressor		3.06
Gas-mixture Compressor (waste heat)	-3.82	
Hydrogen Compressor		1.10
Hydrogen Compressor (waste heat)	-1.16	
FTS Plant		
Syngas Heater	1.77	
FTS Reactor (waste heat)	-8.14	
Separator Hydrocarbons/Water (waste heat)	-1.54	
Total	-9.63	14.16

The fact that the entire plant has an electrical demand of 14.16 $\mathrm{kW_{el}}$ while the PC reactor itself is 10.00 $\mathrm{kW_{el}}$ allows the scaling of the entire PCU for different reactor sizes. This scaling is essential for the simulations of varying plant sizes. The overall power-scaling factor of the PCU is therefore $1.416\,\mathrm{kW_{PCU,total}}/\mathrm{kW_{PC\text{-}Reactor}}$.

Two further essential factors for the simulations are the biogas consumption factor and the syngas production factor. These indicate how much biogas is consumed per kWh of PC reactor power and how much syngas is produced per kWh. Table 5.13 summarizes the biogas and syngas flows for the reference plant. At an energy input of 10 kWh, 4.108 Nm^3 of biogas is required (0.819 Nm^3 CO_2 and 3.289 Nm^3 CH_4) and 13.144 Nm^3 of syngas is produced (4.124 Nm^3 CO and 9.020 Nm^3 H_2). Thus, the biogas consumption factor is 0.4108 Nm^3/kWh and the syngas production factor is 1.3144 Nm^3/kWh. Here, it is assumed that the plant behaves identically at different scales; in reality, some minor deviations can be expected.

Table 5.13: Scaling factors of the PCU

Parameter	**Value**	**Unit**
Power scaling factor (total/reactor)	1.416	$kW_{PCU,total}/kW_{PC\text{-}Reactor}$
Biogas consumption factor	0.4108	Nm^3/kWh
Syngas production factor	1.3144	Nm^3/kWh

Water Costs

In addition to biogas, water is required for the PC process. The water cost per unit of biogas feed is calculated below. An average water price in Germany is assumed, comprising drinking water and wastewater charges. Total water costs amount to approximately 4.00 €/m^3 [103, 104]. The reference plant consumes 7.960 L/h of water for a biogas feed rate of 4.108 Nm^3/h (see Table A.3). This corresponds to 1.938 L of water per Nm^3 of biogas, resulting in water costs of 0.00775 €/$Nm^3_{\text{Biogas Feed}}$. The water costs are listed in table 5.14.

Table 5.14: Water costs for the PC process.

Cost Component	**Value**	**Unit**	**Source**
Water cost	0.00775	€/$Nm^3_{\text{biogas feed}}$	[103, 104]

5.4 Constant Simulation Parameters for the FTS

This section presents the constant parameters for the FTS. These include investment, operating, and performance parameters—such as the specific investment costs, OPEX, lifetime, LHV of the syncrude, syncrude production factor and nominal cost of debt—as well as the selling price of the Syncrude.

Investment, operating, and performance parameters for the FTS

For the FTS, CAPEX data were also collected and a curve-fitting procedure was used to derive a correlation. However, it must be mentioned that the data researched are from FTS reactors with a rather high capacity. No representative data was found for small plants. The collected data are presented in Table 5.15.

The fitted correlation is shown in Figure 5.7.

Table 5.15: Specific investment costs for FTS reactors

Rated Power [MW_p]	Specific Investment Costs [€/kW]	Source
2	2,955	[105]
5	1,300	[106]
23	808	[105]
50	700	[106]
57	619	[105]
114	503	[105]
200	408	[106]
228	400	[105]

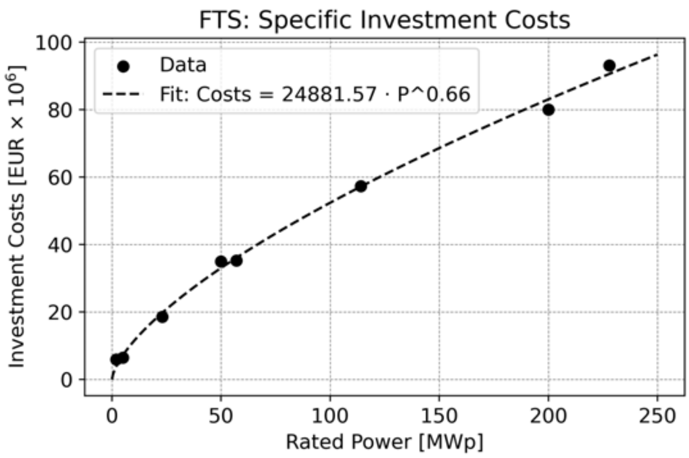

Figure 5.7: FTS: specific investment costs (data from [105, 106]).

The fitted correlation is

$$C_{0,\,\mathrm{FTS}}(P) = 24881.57 \cdot P^{0.66}, \tag{5.8}$$

where P denotes the rated power in MW_p.

OPEX are assumed to be 4 % per year of CAPEX, lifetime is assumed to be 25 years, and the interest rate is 6 % per annum. The lower heating value of the produced syncrude (C_{5+} hydrocarbons) is 44.2 MJ/kg [107–109]. From the syngas produced by the 10 kW PC reactor, 2.326 kg of syncrude are synthesized (C_5+ hydrocarbons; see Table A.3). Thus, per kWh of PC energy, 0.2326 kg of syncrude is produced. The FTS plant matched to a 10 kW_{PC} reactor therefore has an effective capacity of approximately 28.5 kW_p (based on the LHV of the produced syncrude). The parameters are summarized in table 5.16.

Table 5.16: Parameters for the FTS plant

Parameter	Value	Unit	Source
OPEX (% of CAPEX)	4 (2–7)	%	[106, 110–112]
Lifetime	25 (25–30)	years	[106, 110, 113]
Interest rate	6	%	[105]
$LHV_{Syncrude}$	44.2	MJ/kg	[107–109]
Syncrude production factor	0.2326	$kg/kWh_{PC-Reactor}$	–

Selling Price of the Produced FT-Syncrude

For the simulations, a representative FT-Syncrude price was selected based on literature values for the current production costs of renewable FT-Syncrude, as summarized in Table 5.17. Reported prices range from 1.4 to 5.8 €/$kg_{Syncrude}$ [25–27].

Table 5.17: Current production cost ranges for renewable FT-Syncrude

Cost Range	Unit	Source
1.4–4.3	€/$kg_{FT\text{-}Syncrude}$	[25]
2.6–4.8	€/$kg_{FT\text{-}Syncrude}$	[26]
1.6–5.8	€/$kg_{FT\text{-}Syncrude}$	[27]

An average price of 3.5 €/$kg_{Syncrude}$ was assumed for the simulations, reflecting costs for renewable FT-Syncrude (conventional FT-Syncrudes are typically less expensive). In Chapter 8.4, syncrude prices will be varied.

Post-synthesis upgrading of the FT-Syncrude (hydrocracking, isomerization, distillation, desulfurization, etc.) falls outside the scope of this work; therefore, a simplified assumption of 5 % additional cost relative to the production cost is applied [26, 114]. Deducting this upgrade surcharge yields a net selling price of 3.325 €/$kg_{Syncrude}$. The assumed price is shown in table 5.18.

Table 5.18: Assumed net selling price of FT-Syncrude

Parameter	Value	Source
Net selling price	3.325 €/$kg_{Syncrude}$	[25–27]

5.5 Constant Simulation Parameters for the BGS

This section presents the constant parameters for the BGS. These include investment and operating parameters—such as the specific investment costs, OPEX, lifetime, storage capacity and nominal cost of debt.

Investment and Operating Parameters for the BGS

CAPEX data for the BGS were collected for different storage capacities and visualized via curve fitting (see Figure 5.8). Unlike the other assets, where specific investment costs decrease with scale, the BGS exhibits an approximately linear cost–capacity relationship:

$$C_{0,\,\mathrm{BGS}}(V) = 10.11 \cdot V + 15,570.68, \tag{5.9}$$

where V denotes the rated biogas capacity in $10^3\,\mathrm{m}^3$.

OPEX and lifetime for the BGS are assumed to correlate with those of the biogas digester. Table 5.19 summarizes these parameters. According to practical engineering recommendations,

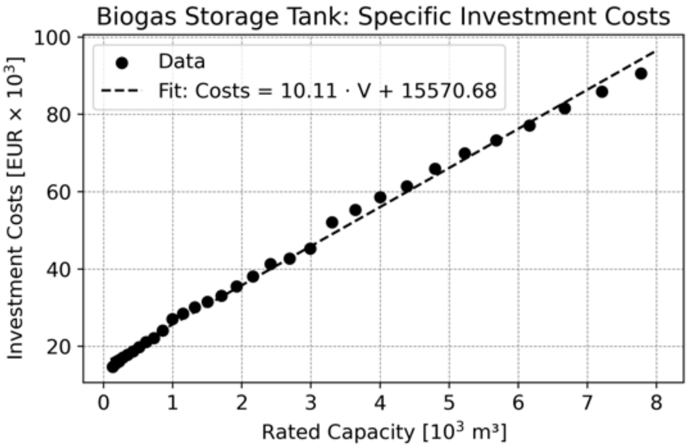

Figure 5.8: BGS: Specific investment costs (data from [64, 115]).

the storage duration should be increased by at least 10 hours for each overbuilding factor [116]. In this study, each overbuilding factor (CHPU and PCU) was assumed to extend the biogas storage by 12 hours (0.5 days). If the overbuilding factor of a unit is less than or equal to 1, or the unit does not exist (PQ = 0), this term does not contribute to the storage requirement (Explanations on overbuilding (PQ value) are provided later in Chapter 7.1). The formula ensures that the storage duration can never become negative:

$$\text{Effective Storage Duration BGS [days]} = [\max(0, PQ_{\text{CHPU}} - 1) + \max(0, PQ_{\text{PCU}} - 1)] \cdot 0.5 \tag{5.10}$$

All parameters are summarized in table 5.10.

Table 5.19: Economic and operating parameters of the BGS

Parameter	Value	Unit	Source
OPEX	7	% of CAPEX	same as biogas digester
Lifetime	20	years	same as biogas digester
Nominal cost of debt	6	%	[56]
Effective Storage Duration BGS	Equation 5.10	days	[116]

5.6 Constant Simulation Parameters for the SGS

Finally, this section presents the constant parameters for the SGS. These include investment and operating parameters—such as the specific investment costs, OPEX, lifetime, storage capacity and nominal cost of debt.

Investment and Operating Parameters for the SGS

Due to limited data on large-capacity SGS tanks, generic hydrogen storage cost data were adopted, assuming that CO and H_2 are mixed and stored together as syngas. This represents a significant simplification, as the specific technical and economic aspects of SGS—such as whether CO and H_2 are stored separately or jointly—are not further considered here. The underlying assumption is that storage costs for syngas are comparable to those for hydrogen, regardless of the exact storage method. This approach was chosen because syngas storage constitutes only a minor aspect of this work, and a detailed investigation of storage technologies would exceed the scope of this thesis. For the purposes of the present analysis, it is therefore simply assumed that syngas can be stored appropriately, irrespective of the precise technical implementation. Reported specific costs range from 20–100 €/$\mathrm{Nm}^3_{\mathrm{H_2}}$ [117], 33–44 €/$\mathrm{Nm}^3_{\mathrm{H_2}}$ [118], 42.3 €/$\mathrm{Nm}^3_{\mathrm{H_2}}$ [119], and 52.8 €/$\mathrm{Nm}^3_{\mathrm{H_2}}$ [120]. The various specific cost parameters are summarized in table 5.20.

Table 5.20: Specific investment costs for SGS

Specific investment costs	**Unit**	**Source**
20–100	€/$\mathrm{Nm}^3_{\mathrm{H_2}}$	[117]
33–44	€/$\mathrm{Nm}^3_{\mathrm{H_2}}$	[118]
42.3	€/$\mathrm{Nm}^3_{\mathrm{H_2}}$	[119]
52.8	€/$\mathrm{Nm}^3_{\mathrm{H_2}}$	[120]

An average cost of 50 €/Nm^3 was assumed and a linear relation applied and is shown in figure 5.9:

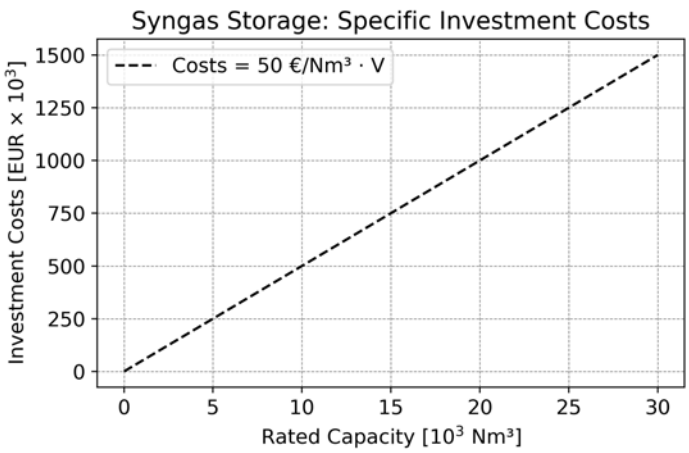

Figure 5.9: SGS: Specific investment costs.

$$C_{0,\,\mathrm{SGS}}(V) = 50\ €/\mathrm{Nm}^3 \ \cdot\ V, \tag{5.11}$$

where V denotes the rated syngas capacity in Nm^3.

OPEX for the SGS are assumed to be 1.5 % of CAPEX per year [60], with a lifetime of 20 years [121, 122] and an interest rate of 6 % per annum [105]. The established sizing principle based on storage days is also applied for the SGS. Since the SGS is exclusively supplied by the PCU, its required storage capacity is determined solely by the overbuilding factor of that unit and is calculated as follows:

$$\text{Effective Storage Duration SGS [days]} = [\max(0, PQ_{\text{PCU}} - 1)] \cdot 0.5 \tag{5.12}$$

These parameters are summarized in Table 5.21.

Table 5.21: Economic and operating parameters of the SGS

Parameter	Value	Unit	Source
OPEX (of CAPEX)	1.5	% per year	[60]
Lifetime	20 (20–25)	years	[121, 122]
Interest rate	6	% per annum	[105]
Effective Storage Duration SGS	Equation 5.12	days	[116]

5.7 Market Data: Intraday Auction Prices

In addition to defining the main plant parameters, appropriate electricity market data were selected to drive the optimization. Fifteen-minute Intraday Auction prices for the Germany–Luxembourg bidding zone in calendar year 2023 were obtained from EPEX SPOT SE. The intraday auction was preferred over the day-ahead market because actual intraday trading prices more accurately reflect short-term adjustments in generation and load. Data retrieval was conducted via an InfluxDB data source in the Competence Center für Erneuerbare Energien und EnergieEffizienz (CC4E) Grafana dashboard. Each timestamp corresponds to the clearing price (€/MWh) of the respective 15-minute call auction. The 15-Minute Intraday Auction Clearing Price data for the year 2023 is shown in the figure 5.10.

To reconcile the availability of day-ahead information with the realism of intraday dynamics, the simulation was initialized at 13:00 p.m. on January 1st, 2023—immediately after EPEX SPOT publishes day-ahead prices for the following delivery day. At this point, perfect foresight of day-ahead prices was assumed; thereafter, the actual 15-minute intraday prices were applied to capture subsequent market imbalances. This procedure ensures that the simulation operates as if driven by known day-ahead prices while still reflecting true intraday price fluctuations in each quarter-hour interval.

Spotmarket Price Threshold for CHPU operation

In the optimization model, a spot market price threshold was introduced to indicate whether operating the CHPU at a given time is economically advantageous or whether it is better to store biogas. This threshold was developed to address an issue with the objective function, which maximizes system revenue over the 140 quarter-hour intervals without distinguishing the magnitude of that revenue. As a result, the biogas storage was routinely emptied even at

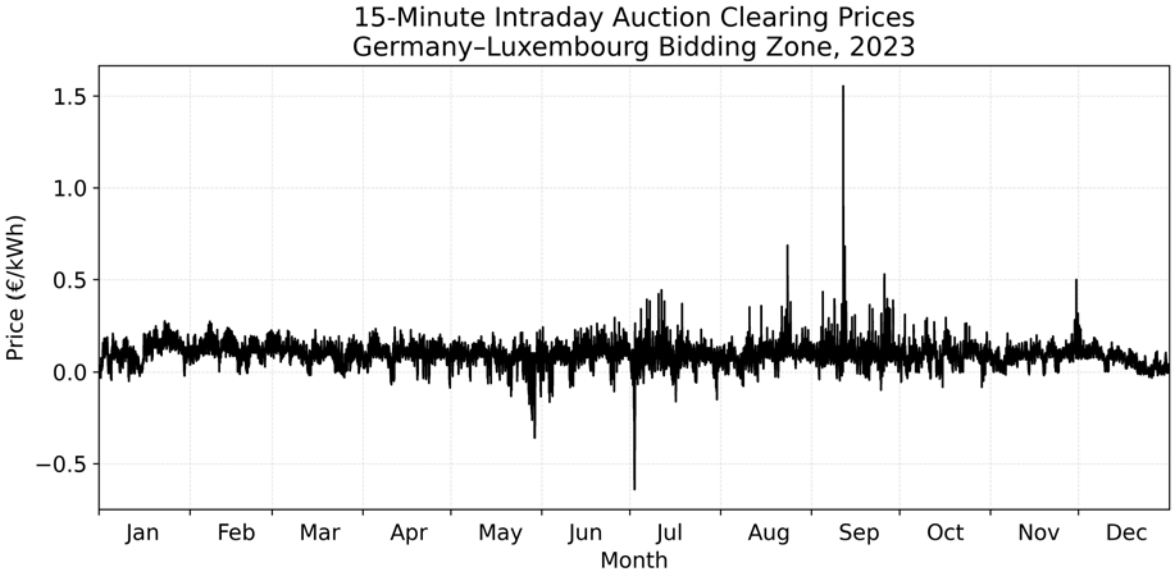

Figure 5.10: 15-Minute Intraday Auction Clearing Prices for the Germany–Luxembourg Bidding Zone, January–December 2023 (own illustration, Data from: [123])

low—but still slightly positive—spot prices, since any incremental increase in revenue, however small, contributed to the objective and was thus favored. The model could not anticipate that significantly higher spot prices might occur later, in which case retaining biogas for future conversion would be more profitable.

To resolve this, the threshold signals when CHPU operation becomes more economical than biogas storage. Because spot prices fluctuate seasonally and the model aims to reflect realistic plant operation, the threshold is recalculated dynamically from historical prices at the start of each optimization run. Specifically, if the spot price exceeds the threshold - corresponding to the cutoff above which the highest 20 % for a double overbuild CHPU, 10 % for a triple overbuild CHPU and for higher overbuilding 5% of spot prices over the past 7 days lie - the CHPU is dispatched. As the CHPU is increasingly overbuilt, its operation should become more selective, responding primarily to high spot market prices. Consequently, its FLH decrease, and the threshold must be adjusted upwards in line with the level of overbuilding. For January 2023, December 2023 prices from the same dataset were used to compute the threshold, as December 2022 prices were artificially elevated by the energy crisis. Figure 5.11 shows the threshold's evolution over the entire simulation period.

No threshold was required for the PCU, since its operation is most profitable at low or even negative spot prices. This does not conflict with the objective function because, for the PC process, the spot price enters as a cost (negative contribution) rather than as revenue (positive contribution), so the model naturally schedules its operation at the lowest available prices.

Figure 5.11: Market Price Thresholds for the Year 2023 in Daily Resolution (own illustration).

6 Development and Structure of the Optimization Model

In this chapter, the structure of the optimization model and the program code is explained. Since the optimization model is the core of the codebase, it is described first, followed by a basic overview of the program's framework.

6.1 Presentation of the MILP model

Optimization modeling is a mathematical approach used to identify the best solution to a problem from a set of possible alternatives, while taking into account specified constraints and objectives. The model is composed of three elements: the objective function, decision variables, and constraints. [124]

The optimization model developed in this thesis is a deterministic, multi-period MILP problem whose aim is to maximize total revenue by deciding, at every quarter-hour interval, whether to operate the CHPU or the PCU. It is deterministic because all inputs - intraday spotmarket prices, initial storage levels, conversion efficiencies, and technical limits - are known and fixed, yielding a uniquely defined objective. It is multi-period in that operational decisions (unit on/off status, start/stop transitions, storage balances, and minimum run - and down-time requirements) are linked across successive time steps. By combining continuous variables (power outputs; flow and storage volumes) with binary variables (unit on/off; start/stop indicators), the model becomes a mixed-integer problem. Finally, it is linear since both the objective function (maximizing revenue via an arbitrage strategy) and all constraints (energy and mass balances; capacity bounds; logical conditions) are expressed as linear relationships, enabling systematic exploration of the solution space to identify the optimal dispatch: when market prices are low, the PCU is run to consume electricity, and when prices are high, the CHPU is run to generate revenue.
The optimization model and its data are implemented and solved in a Python program using the `Pyomo` library and the `CPLEX` solver.
The model builds upon the fundamentals of the unit commitment problem and the arbitrage model; these two concepts are therefore explained in the following sections.

Basic Ideas of the UCP

The UCP is a fundamental challenge in energy management that focuses on the optimal scheduling of power plants. The objective is to determine which generation units should be turned on or off at specific times while considering technical, economic, and environmental constraints. Key factors include minimum run times, startup and shutdown costs, fluctuating energy prices, and load demands. The UCP plays a crucial role in the integration of renewable energy sources, as it enables the efficient utilization of flexibility in conventional and modern power plants to ensure an economical and reliable energy supply. [125–128]

Basics of the Arbitrage Model

Closely related to the UCP is the Arbitrage Model. This model focuses on maximizing profit through the temporal shifting of energy flows. By leveraging price differences in the electricity spotmarket, the Arbitrage Model identifies opportunities to optimize revenue. Typically, energy storage systems are utilized, allowing energy to be stored during periods of low prices and discharged during periods of high prices. In addition to storage systems, flexible electricity producers, such as combined heat and power plants, can adapt their operations to spotmarket price fluctuations. The model considers constraints such as storage capacity, minimum and maximum power output and runtime and operational costs while aligning energy production or consumption with market signals. [129, 130]

Sets Used in the Optimization Model

Table 6.1 lists the sets used in the optimization model. In this model, the only set is the discrete time steps at 15-minute intervals over the optimization horizon.

Set	Description
T	Discrete time steps (e.g. 15-minute intervals over the optimization horizon)

Table 6.1: Index sets

The optimization window comprises 140 time steps, each representing 15 minutes. This choice reflects the fact that quarter-hourly spot market prices for the following day are published daily at 1:00 p.m. Accordingly, a new optimization run begins at 1:00 p.m each day and extends until 11:45 p.m of the next day, totaling 140 quarter-hour intervals. Since the optimization restarts at 1:00 p.m, the period from 1:00 p.m to 11:45 p.m is simulated twice. This overlap allows the model to “look ahead” and smooth the transition between consecutive optimization runs. In other words, the 1:00 p.m to 11:45 p.m interval is re-optimized with the updated price data of the next day, enabling a refined schedule that adapts to the later spot market prices.

Parameters Used in the Optimization Model

In Table 6.2, the parameters of the optimization model are summarized. These parameters are known and remain constant over the optimization horizon.

Parameter	Description	Units
p_t	Electricity price at time t	€/kWh
S_0^{BG}, S_0^{SG}	Initial biogas / syngas storage	m³
$R_{\min}$, $D_{\min}$	Minimum run time / down time for each unit	periods
$P_{\mathrm{CHPU}}^{\max}$, $P_{\mathrm{CHPU}}^{\min}$	Max. / min. electrical output of CHPU	kW
$P_{\mathrm{PCU}}^{\max}$, $P_{\mathrm{PCU}}^{\min}$	Max. / min. power of PC reactor	kW
$\eta_{\mathrm{CHPU}}^{\mathrm{el}}$, $\eta_{\mathrm{CHPU}}^{\mathrm{th}}$	Electrical and thermal efficiency of CHPU	–
LHV_{BG}	LHV of biogas	kWh/m³
$F_{\mathrm{BG,\,PCU}}$	Biogas consumption Factor PCU	m³ /kWh
$F_{\mathrm{SG,\,PCU}}$	Syngas production Factor PC	m³ /kWh
$F_{\mathrm{power,\,PCU}}$	Power Scaling Factor PC	$\mathrm{kW_{total}/kW_{PC\text{-}Reactor}}$
$V_{\mathrm{BG}}^{\max}$, $V_{\mathrm{SG}}^{\max}$	Max. Storage capacity (biogas, syngas)	m³
$V_{\mathrm{production}}^{\mathrm{BG}}$	Biogas production	m³
θ	Threshold price for CHPU operation	€/kWh

Table 6.2: Model parameters

Decision Variables Used in the Optimization Model

Table 6.3 lists the decision variables. Continuous variables describe power, flows and storage levels; binary variables capture unit on/off and start/stop decisions; z_t represents revenue contribution. These parameters change over the optimization horizon.

Variable	Description	Unit	Type
P_t^{CHPU}	Electrical output of CHPU at t	kWh	continuous ≥ 0
P_t^{PCU}	Power of PCU at t	kWh	continuous ≥ 0
S_t^{BG}, S_t^{SG}	Biogas / syngas storage level at t	m³	continuous ≥ 0
$f_{t,u}^{\mathrm{BG}}$	Biogas flow into unit $u \in \{\mathrm{CHPU}, \mathrm{PCU}, \mathrm{Storage}\}$	m³	continuous ≥ 0
y_t^{SG}	Syngas sent to FTS at t	m³	continuous ≥ 0
u_t^{CHPU}, u_t^{PCU}	On/off status of CHPU / PCU at t	-	binary
σ_t^{CHPU}, σ_t^{PCU}	Start indicator for CHPU / PCU at t	-	binary
δ_t^{CHPU}, δ_t^{PCU}	Stop indicator for CHPU / PCU at t	-	binary
z_t	Revenue contribution at time t	€	continuous

Table 6.3: Decision variables

Objective Function Used in the Optimization Model

The objective is to maximize total revenue over all time steps:

$$\max \sum_{t \in T} z_t \tag{6.1}$$

where each z_t is defined piecewise as

$$z_t = \begin{cases} -P_t^{\text{CHPU}}(\theta - p_t) + P_t^{\text{PCU}} F_{\text{power,PCU}}(-p_t), & p_t \le \theta, \\ P_t^{\text{CHPU}} p_t + P_t^{\text{PCU}} F_{\text{power,PCU}}(-p_t), & p_t > \theta. \end{cases}$$

Interpretation

- If $p_t \le \theta$:
  - The term $-P_t^{\text{CHP}}(\theta - p_t)$ penalizes running the CHPU at low prices—larger gaps $\theta - p_t$ yield more negative contribution.
  - The PCU term $P_t^{\text{PCU}} F_{\text{power,PCU}}(-p_t)$ multiplies by the negated spot price, so operation when p_t is negative (i.e. being paid to consume) produces a positive revenue contribution.
- If $p_t > \theta$:
  - The CHPU term $P_t^{\text{CHPU}} p_t$ rewards producing electricity at market price p_t.
  - The PCU term remains $P_t^{\text{PCU}} F_{\text{power,PCU}}(-p_t)$, ensuring that even when p_t is just above zero, consumption revenues from PCU are still captured.

Constraints Used in the Optimization Model

Unit Commitment Logic

The binary on/off status u_t and the start σ_t / stop δ_t indicators enforce consistent transitions:

$$\begin{aligned} &\sigma_t^u \ge u_t - u_{t-1}, \qquad && \sigma_t^u \le u_t, \qquad && \sigma_t^u \le 1 - u_{t-1}, \\ &\delta_t^u \ge u_{t-1} - u_t, && \delta_t^u \le u_{t-1}, && \delta_t^u \le 1 - u_t, \end{aligned}$$

for $u \in \{\text{CHPU}, \text{PCU}\}$ and all t, with u_{-1} initialized to the known off/on state at $t = 0$.

- $u_t = 1$ if the unit is running during period t, and $u_t = 0$ otherwise.
- $\sigma_t^u = 1$ precisely when the unit starts up at t (transition off$\rightarrow$on).
- $\delta_t^u = 1$ precisely when the unit shuts down at t (transition on$\rightarrow$off).

Minimum Run and Down Times

Once a unit starts, it must remain on for at least $R_{\min}$ periods; once it stops, it must remain off for at least $D_{\min}$ periods. For the CHPU:

$$\sum_{k=t}^{t+R_{\min}-1} u_k^{\text{CHPU}} \;\geq\; R_{\min}\,\sigma_t^{\text{CHPU}}, \qquad \sum_{k=t}^{t+D_{\min}-1} \left(1-u_k^{\text{CHPU}}\right) \;\geq\; D_{\min}\,\delta_t^{\text{CHPU}},$$

and analogously for the PCU. These constraints ensure that whenever $\sigma_t^u = 1$ (a start event), the unit stays on for the next $R_{\min}$ time steps, and whenever $\delta_t^u = 1$ (a stop event), the unit remains off for the next $D_{\min}$ time steps.

Energy Balance and Capacity Limits

The energy balance constraints translate biogas flows into electrical power, and the capacity limits enforce technical bounds:

$$P_t^{\text{CHPU}} = \left(f_{t,\text{BGP}\to\text{CHPU}}^{\text{BG}} + f_{t,\text{BGS}\to\text{CHPU}}^{\text{BG}}\right)\eta_{\text{CHPU}}^{\text{el}}\,LHV_{\text{BG}},$$

$$P_t^{\text{PCU}} = \frac{f_{t,\text{BGP}\to\text{PCU}}^{\text{BG}} + f_{t,\text{BGS}\to\text{PCU}}^{\text{BG}}}{F_{\text{BG,PCU}}},$$

$$P_u^{\min}\,u_t^u \;\leq\; P_t^u \;\leq\; P_u^{\max}\,u_t^u, \quad S_t^u \;\leq\; V_u^{\max}, \quad \forall\, u \in \{\text{CHPU}, \text{PCU}\},\; t \in T.$$

- The *CHPU energy balance* computes the electrical output P_t^{CHPU} by summing the biogas flow from the plant ($f_{t,\text{BGP}\to\text{CHPU}}^{\text{BG}}$) and from storage ($f_{t,\text{BGS}\to\text{CHPU}}^{\text{BG}}$), then multiplying by the lower heating value LHV_{BG} and the electrical efficiency $\eta_{\text{CHPU}}^{\text{el}}$.
- The *PCU energy balance* computes the PCU reactor power P_t^{PCU} by taking the biogas flow drawn directly from the plant ($f_{t,\text{BGP}\to\text{PCU}}^{\text{BG}}$) and the flow drawn from storage ($f_{t,\text{BGS}\to\text{PCU}}^{\text{BG}}$), summing them, and dividing by the biogas consumption factor $F_{\text{BG,PCU}}$, which represents the volume of biogas (m^3) required per kWh of PCU output.
- *Unit capacity limits* enforce that each unit's output P_t^u lies between its minimum part-load $P_u^{\min}$ and maximum capacity $P_u^{\max}$, but only when the unit is on ($u_t^u = 1$).
- *Storage capacity limits* ensure that the stored volume S_t^u never exceeds the maximum storage $V_u^{\max}$ (and is implicitly non-negative).

Storage Dynamics

$$S_t^{\text{BGS}} = S_{t-1}^{\text{BGS}} + f_{t,\text{BGP}\to\text{BGS}}^{\text{BG}} - \left(f_{t,\text{BGS}\to\text{CHPU}}^{\text{BG}} + f_{t,\text{BGS}\to\text{PCU}}^{\text{BG}}\right),$$

$$S_t^{\text{SGS}} = S_{t-1}^{\text{SGS}} + P_t^{\text{PCU}}\,F_{\text{SG, PCU}} - y_t^{\text{SG}},$$

previous

- The *biogas storage balance* updates the biogas stock S_t^{BGS} by taking the level S_{t-1}^{BGS}, adding the biogas sent from the biogas plant to storage $f_{t,\text{BGP}\to\text{BGS}}^{\text{BG}}$, and subtracting the biogas withdrawn from storage to feed the CHPU ($f_{t,\text{BGS}\to\text{CHPU}}^{\text{BG}}$) and the PCU ($f_{t,\text{BGS}\to\text{PCU}}^{\text{BG}}$).

- The *syngas storage balance* updates the syngas stock S_t^{SGS} by taking the previous level S_{t-1}^{SGS}, adding the syngas produced by the PCU (the product of P_t^{PCU} and the syngas production factor $F_{\mathrm{SG,PCU}}$), and subtracting the syngas delivered to the FTS y_t^{SG}. Since in the model the FTS is assumed to run continuously at a constant nominal rate, y_t^{SG} is constant.

Biogas Flow Balance

$$f_{t,\mathrm{BGP}\to\mathrm{CHPU}}^{\mathrm{BG}} + f_{t,\mathrm{BGP}\to\mathrm{PCU}}^{\mathrm{BG}} + f_{t,\mathrm{BGP}\to\mathrm{BGS}}^{\mathrm{BG}} = V_{\mathrm{production}}^{\mathrm{BG}}, \quad \forall t \in T.$$

- The biogas flow balance ensures that at each time step t, the total biogas produced $V_{\mathrm{production}}^{\mathrm{BG}}$ is exactly allocated to the three possible outlets—direct feed to the CHPU $f_{t,\mathrm{BGP}\to\mathrm{CHPU}}^{\mathrm{BG}}$, direct feed to the PCU $f_{t,\mathrm{BGP}\to\mathrm{PCU}}^{\mathrm{BG}}$, and storage $f_{t,\mathrm{BGP}\to\mathrm{BGS}}^{\mathrm{BG}}$.

6.2 Code Structure and Simulation process flow

This chapter briefly explains the Python code used for the simulations. The entire Python source code is included in the digital appendix. Figure 6.1 illustrates the flowchart of the program and the process is explained in detail below.

At the beginning, the variable simulation parameters, which are explained in detail in the following chapter 7.1, are initialized. In addition, the text file containing the electricity market data is read. The different scenarios are implemented with nested loops: for every variable simulation parameter there is one loop, so that every parameter combination is simulated. The outermost loop varies the biogas Consumption Ratio (CR), the next loop the Biogas plant size, then the loop for the overbuilding of the CHPU, and the innermost loop the overbuilding of the PCU. In this way, the various overbuilding stages of the variable simulation parameters are varied first.

Once the parameter combination is set, simulation-dependent parameters are calculated - these include the power output and volumetric flow of the biogas produced, the power outputs of CHPU, PCU, and FTS, the storage capacities, and the CHPU threshold. After all parameters have been established, the optimization stage follows. The optimization is embedded in a loop that runs 365 times - once for each day of the one year simulation period. Optimization always starts at 1 p.m. each day. This imitates the electricity market, where day-ahead prices are published daily at 1 p.m. Because the model optimizes from 1 p.m. to 11:45 p.m. of the following day, and one time step equals 15 minutes, the optimization window spans 140 time steps (35 hours). A new optimization is started every 96 time steps (24 hours). Before each optimization run, parameters such as the CHPU threshold and the current storage levels are updated. The threshold is calculated from the spot-market prices of the past seven days, and the storage levels (BGS and SGS) are taken either from the previous optimization result (the 96th value of the prior run) or—during the first run—from initialized default values.

Depending on whether the CHPU is combined with BGtL, running in single operation, or the

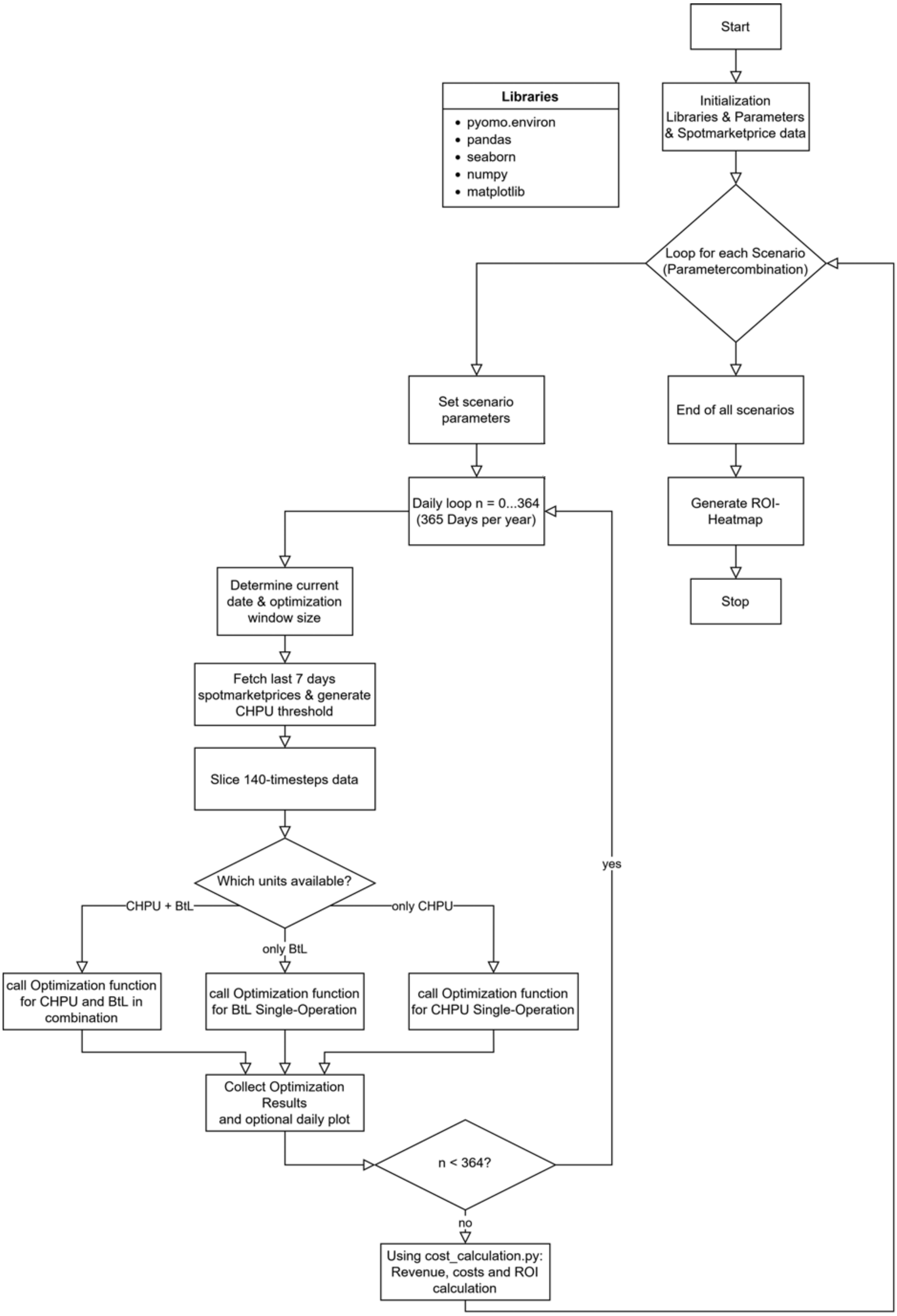

Figure 6.1: Flowchart of the Programcode.

BGtL unit is in single operation, one of three optimization functions is called and all necessary parameters are handed over. The optimization is then solved for the 140 timesteps, respecting the chosen objective function and all constraints, and produces an optimal plant dispatch for that period. Figure 6.2 shows an example optimization horizon; the black line - the spot-market price - makes the individual time steps clearly visible, and the influences of the defined constraints are also evident.

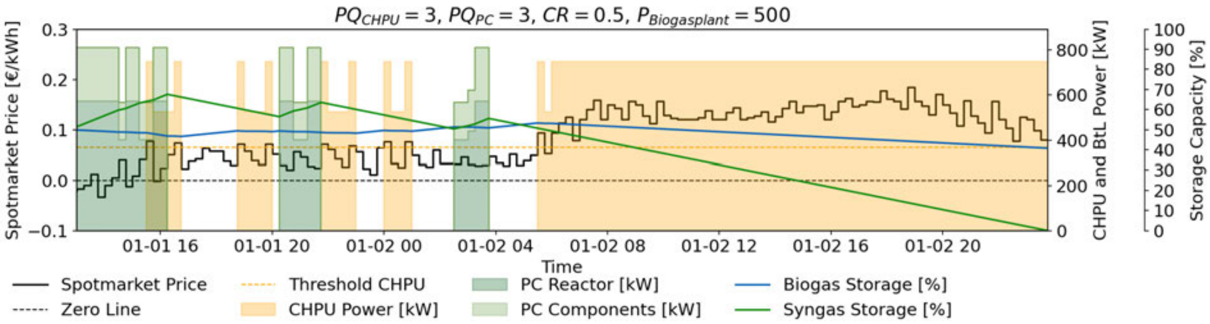

Figure 6.2: Illustration of a optimization window, to explain the MILP model.

After optimization, the revenues per time step - generated electricity, generated heat, and produced syncrude - are calculated, as well as the electricity costs of the PCU. These results, together with other parameters such as storage levels (BGS and SGS) and the power outputs of PCU and CHPU, are stored in separate lists. These lists are returned to the main script as function outputs. There, the optimization step can be visualized if desired, and parameters relevant for later cost calculations are updated. Because only the first 96 time steps actually occur while the remaining 44 will be re-optimized (optimization every 96 steps with a 140-step window), the relevant lists for revenues, electricity costs, and CHPU power must be shorted to the first 96 values. Only the CHPU power list is needed for the subsequent cost calculation, because it is used to compute the FLH and therefore the lifetime; this is unnecessary for the other units, whose lifetime does not depend on FLH. The truncated lists are appended to further lists that grow with each completed optimization. The loop then jumps back to the beginning, and the next day is optimized, continuing until the entire year has been processed.

Once the full year has been simulated, the annual sums of CHPU revenues (electricity and heat), BGtL revenues (syncrude sales), PCU electricity costs, and CHPU power output are formed. All parameters are then passed to a function that determines the ROI. This function in turn calls other functions to compute the individual costs of each component. Every plant type has its own function that calculates investment costs based on rated power or capacity and there specific investment cost functions established in Chapter 5. OPEX and other variable costs are also determined individually. The biogas plant, FTS, and both storage units incur only OPEX as variable costs. The CHPU has OPEX plus biogas substrate costs; the PCU has OPEX, biogas substrate costs, and water costs. The biogas substrate costs are calculated in a separate function, which - based on the biogas CR - splits gas consumption between PCU and CHPU and allocates costs accordingly. PCU water costs are likewise calculated in their own function. Because CHPU lifetime depends on FLH, a dedicated function computes the CHPU lifetime from the total optimized annual output and rated power.

After investment and variable costs are known, a cost calculation (with function 3.6) is performed for each plant. To determine profits separately for CHPU and BGtL, the costs of the biogas plant and BGS are apportioned to both plant types according to the biogas CR. CHPU costs thus comprise CHPU costs plus a share of biogas plant and BGS costs. BGtL costs consist of PCU, FTS, SGS, and the corresponding shares of biogas plant and BGS costs. CHPU revenues are increased by a flexibility bonus calculated in its own function. With the resulting costs and revenues, the profits of the main plants (CHPU and BGtL) and the total system profit are determined (with function 3.6). Finally, using these profits and the previously calculated investment costs, the ROI is computed (with function 3.6). ROI and all additional parameters are returned to the main script.

Back in the main script, the ROI is stored in a list associated with the specific PQ variation. The simulation for this parameter combination then ends and proceeds to the next simulation with a different PQ variation. After all PQ variations for a given biogas CR and biogas plant size have been simulated, a heat map of the collected ROIs is generated and saved, making it possible to compare the different simulations. The program then moves on to the next simulation by changing the biogas plant size, or - if all sizes have been processed - by changing the biogas CR. In this way, the program runs through every simulation, varying all combinations of the variable parameters, and terminates when all parameter combinations have been iterated. Throughout, heatmaps are produced for each biogas CR and biogas plant-size combination, displaying the various overbuilding stages.

7 Implementation of the Simulations

Having introduced the model and program code as well as the general workflow, this chapter now focuses on the simulations that were conducted. First, the variable simulation parameters are presented, followed by a description of the simulation scenarios that were carried out.

7.1 Parameter Variations for the Simulation Scenarios

To determine optimal expansion strategies, it was necessary to define variable simulation parameters whose variation enables the simulation of different expansion scenarios for the biogas plant. Three distinct variable simulation parameters were identified, which will be examined in more detail in this chapter.

Different Biogas Plant Sizes

The first variable parameter is the biogas plant size. Three capacity classes are considered: small (75 kW), medium (500 kW) and large (2,000 kW) biogas plants. These classes reflect the distribution of plant sizes in Germany: approximately 18% of installations are up to 75 kW, about 59% range from 75 kW to 500 kW, and around 23% exceed 500 kW [28]. The chosen capacities therefore cover the full spectrum of typical scales. Table 7.1 summarizes the selected capacities.

Table 7.1: Rated Capacity of the Biogas Plant: Parameter Variations

Rated Capacity	Description
75 kW	Represents a small-scale biogas plant.
500 kW	Represents a medium-scale biogas plant.
2,000 kW	Represents a large-scale biogas plant.

Biogas Consumption Ratio: Distribution Between PCU and CHPU

The Biogas CR (Biogas_{CR}) is used to assess the impact of the biogas distribution between the two systems (CHPU and BGtL) on overall economic performance. For example, it helps determine whether it is advantageous to design both units to consume equal amounts of biogas or if one unit should be sized smaller than the other.

Specifically, the Biogas_{CR} defines the biogas allocation between the CHPU and the BGtL system. A ratio of 0.5 indicates that both units are designed to consume equal amounts of biogas. In a 0.75 ratio, the BGtL consumes 75 vol.% of the produced biogas, while the CHPU uses 25 vol.%. Conversely, a ratio of 0.25 implies that the BGtL receives 25 vol.% of the biogas, with the CHPU consuming the remaining 75 vol.%. Table 7.2 summarizes these three parameter variations.

Table 7.2: Biogas Consumption Ratio: Different Parameter Variations

Parameter	Explanation
0.5	Both units consume equal amounts of biogas.
0.75	The BGtL plant consumes 75 vol.% of the biogas and the CHPU 25 vol.%.
0.25	The BGtL plant consumes 25 vol.% of the biogas and the CHPU 75 vol.%.

Overbuilding Stages of the PCU and the CHPU

"Overbuilding" denotes the ratio between a main unit's rated power and the biogas plant's design capacity. In this work, the PQ formalizes overbuilding as

$$\mathrm{PQ}_i = \frac{P_{\mathrm{rated},i}}{P_{\mathrm{rated,\,biogas}}} \cdot \frac{\dot{V}_{\mathrm{biogas},\,i}}{\dot{V}_{\mathrm{production}}} \tag{7.1}$$

where $P_{\mathrm{rated},i}$ is the rated electric power of unit i, $P_{\mathrm{rated,\,biogas}}$ the biogas plant's design output, $\dot{V}_{\mathrm{biogas},\,i}$ the biogas flow consumed by unit i, and $\dot{V}_{\mathrm{production}}$ the total biogas production rate.

In the model, the CHPU and the PCU are the two flexible units. The FTS runs at constant rated power and is not overbuilt. A higher PQ grants greater flexibility to match volatile electricity prices, at the expense of higher investment costs. Three PQ levels are tested (Table 7.3), plus a zero-PQ case representing single-operation.

Table 7.3: Overbuilding Stages (PQ): Parameter Variations

PQ	Description
0	Only one main unit is installed (single-operation)
1	No overbuilding (continuous operation, 24 h/day)
2	Double overbuilding (on average 12 h/day)
3	Triple overbuilding (on average 8 h/day)

In total, this yields 15 distinct overbuilding scenarios when combining PQ values for both flexible units.

Impact of Overbuilding and Biogas Consumption Ratio

Since the distinction between the PQ and the Biogas_{CR} is not immediately obvious, Figure 7.1 illustrates their combined effect on the optimization model. The figure shows four daily scenarios, plotting biogas consumption (y-axis) against time of day (x-axis) for two plants under each scenario.

In the first scenario ($\mathrm{Biogas}_{CR} = 0.5$, PQ 2:2), both plants run for 12 h and each consumes exactly half of the total biogas over the day. When the PQ parameter is changed to 1:3 (while the Biogas_{CR} remains 0.5), Plant 1 operates continuously for 24 h and Plant 2 for only 8 h. However, because the CR is still 0.5, each plant's total biogas intake over 24 h remains equal.

In the second scenario ($\mathrm{Biogas}_{CR} = 0.25$, PQ 2:2), both plants again run for 12 h, but Plant 1 consumes only 25% of the biogas and Plant 2 consumes 75% over the day. Changing PQ to 1:3 shifts Plant 1's operating time to 24 h and Plant 2's to 8 h, yet the 25/75 split in daily biogas consumption is preserved.

In summary, the PQ parameter governs the distribution of operating hours between plants over a given period, while the Biogas_{CR} fixes each plant's share of total biogas usage.

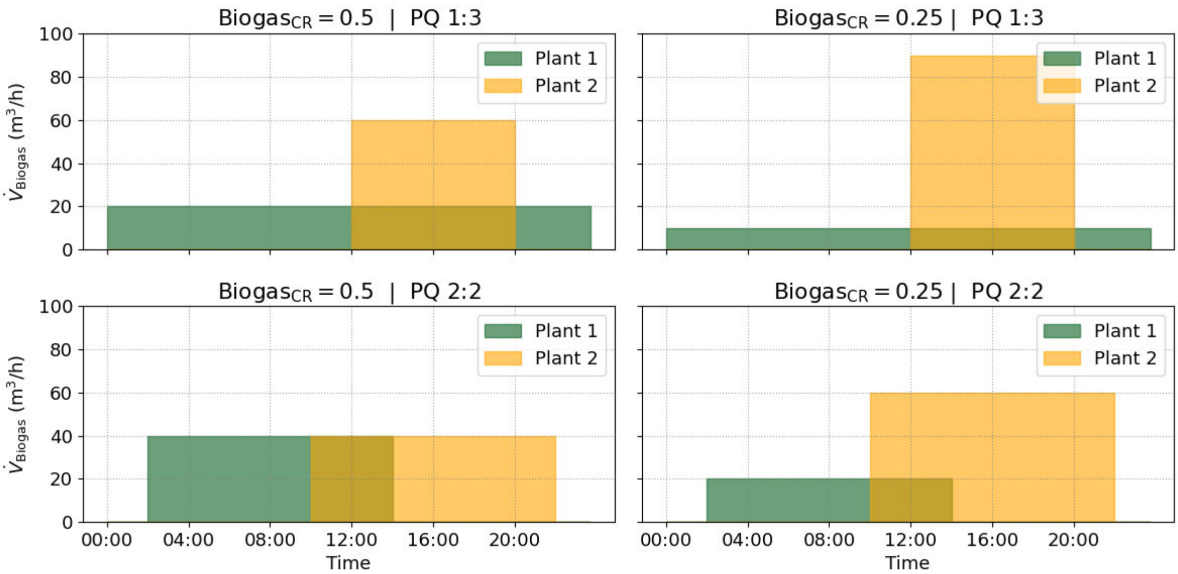

Figure 7.1: Example of the relationship between Overbuilding and Biogas CR.

7.2 Simulation Setups

This section describes the simulations conducted in the context of this thesis. In total, three different simulation runs were performed.

Main Simulation Setup

The first and largest simulation run is referred to in the following as the Main Simulation run. In this simulation run, the constant simulation parameters researched and calculated in section 5 as well as the variable simulation parameters introduced in section 7.1 were initialized in the program code. The constant simulation parameters are summarized again in Table 7.4. Furthermore, the derived equations for the specific investment costs of the respective plants were applied, and the electricity market data introduced in section 5.7 were used.

The variable parameters described previously were also initialized as follows:

$$P_{\text{BiogasPlant}} \in \{75,\ 500,\ 2,000\}\ \text{kW}, \quad PQ_{\text{PCU}} \in \{0,\ 1,\ 2,\ 3\}, \quad PQ_{\text{CHPU}} \in \{0,\ 1,\ 2,\ 3\},$$

$$\text{Biogas}_{\text{CR}} \in \{0.25,\ 0.5,\ 0.75\}.$$

A total of 135 simulations were performed (combinations with both $PQ_{\text{PCU}} = 0$ and $PQ_{\text{CHPU}} = 0$

Table 7.4: Overview of constant simulation parameters.

Parameter	Value
Economic parameters	
Lifetime Biogas plant	20 years
OPEX Biogas plant	4 % of CAPEX per year
Lifetime CHPU	60,000; 80,000 FLH
OPEX CHPU	3 % of CAPEX per year
Lifetime PCU	20 years
OPEX PCU	4 % of CAPEX per year
Lifetime FTS	25 years
OPEX FTS	4 % of CAPEX per year
Lifetime BGS	20 years
OPEX BGS	7 % of CAPEX per year
Lifetime SGS	20 years
OPEX SGS	1.5 % of CAPEX per year
Nominal cost of debt (all plants)	6 % per year
Operational parameters	
Electrical efficiency CHPU	40 %
Thermal efficiency CHPU	45 %
Minimum runtime/offtime (CHPU, PCU)	1 h
Minimum part-load (CHPU, PCU)	70 %
BGS capacity	$(PQ_{\text{CHPU+PCU}}) \cdot 0.5$ days
SGS capacity	$(PQ_{\text{PCU}}) \cdot 0.5$ days
Initial Storage levels	50 %
Financial parameters	
Substrate cost	0.158 €/$\text{Nm}^3_{\text{biogas}}$
Electricity demand biogas upgrading	0.533 kWh/$\text{Nm}^3_{\text{upgraded biogas}}$
Water cost	0.00775 €/$\text{Nm}^3_{\text{upgraded biogas}}$
Remuneration value (Direct marketing)	18.0 cent/kWh
Service fee (Direct marketing)	3 %
VAT	19 %
Heat tariff	2.6 cent/kWh_{th}
Marketable heat share	50 %
Flexibility bonus	65 €/kW · a
Net selling price FT-syncrude	3.325 €/kg
Taxes and levies (2023)	2.86 cent/kWh
Electricity grid charges (2023)	3.30 cent/kWh
Calculation Factors BGtL Plant	
Power scaling factor	1.416 $\text{kW}_{\text{total}}/\text{kW}_{\text{PC-Reactor}}$
Biogas consumption factor	0.4108 Nm^3/kWh
Syngas production factor	1.3144 Nm^3/kWh
Syncrude production factor	0.2326 $\text{kg}_{\text{Syncrude}}/\text{kWh}_{\text{PC}-\text{Reactor}}$

were skipped, as no plant operation exists in these scenarios).

In addition, the Main Simulation was subdivided to analyze the influence of the variable simulation parameters as well as to compare the single-operation of individual units to the combined operation. Selected simulations from the Main Simulation run are presented in more detail in order to improve the understanding of the overall results.

Simulation Setup to Illustrate the Influence of Variable Parameters

First, the single-operation of both plants was examined in detail to allow comparison with the combined operation.

CHPU in Single Operation

For the CHPU in single operation, the following simulation scenarios were analyzed:

$$P_{\text{BiogasPlant}} \in \{75,\ 500,\ 2\,000\}\,\text{kW}, \quad \text{PQ}_{\text{CHPU}} \in \{1,\ 2,\ 3\}.$$

This setup was used to evaluate the effect of both biogas plant size and CHPU overbuilding on costs and revenues. As the biogas CR only makes sense for the combination of the two systems, it is omitted in single-operation.

BGtL in Single Operation

The same approach was applied for the BGtL plant in single operation. Here, the variable simulation parameters are identical, but the overbuilding of the PCU is varied:

$$P_{\text{BiogasPlant}} \in \{75,\ 500,\ 2\,000\}\,\text{kW}, \quad \text{PQ}_{\text{PCU}} \in \{1,\ 2,\ 3\}.$$

CHPU and BGtL in Combination: Influence of Simultaneous Overbuilding

Next, the influence of simultaneously overbuilding both units was evaluated. For this purpose, simulation results for scenarios where both units are overbuilt to the same extent were compared:

$$P_{\text{BiogasPlant}} \in \{75,\ 500,\ 2\,000\}\,\text{kW}, \quad \text{PQ}_{\text{CHPU}} : \text{PQ}_{\text{PCU}} \in \{1:1,\ 2:2,\ 3:3\}, \quad \text{Biogas}_{\text{CR}} = 0.5.$$

Different biogas plant sizes were considered, and a biogas CR of 0.5 was chosen to avoid distortion by this parameter. Only the scenarios with overbuilding stages 1, 2, and 3 were selected for detailed analysis.

CHPU and BGtL in Combination: Influence of Overbuilding a Single Unit

Additionally, the effect of overbuilding only one of the two units (while the other remains at standard capacity) was investigated. The following variable parameter combinations were analyzed:

$$P_{\text{BiogasPlant}} = 500\,\text{kW}, \quad \text{PQ}_{\text{CHPU}} : \text{PQ}_{\text{PCU}} \in \{1:1,\ 1:2,\ 1:3,\ 2:1,\ 3:1\}, \quad \text{Biogas}_{\text{CR}} = 0.5.$$

Here, only simulations with a biogas plant size of 500 kW were considered to keep the analysis manageable. The biogas CR was also fixed at 0.5 in these cases.

CHPU and BGtL in Combination: Influence of the Biogas Consumption Ratio

Finally, the influence of the biogas CR was examined. For this, simulations were selected with a biogas plant size of 500 kW, identical overbuilding stages for both units, and all values of the consumption ratio:

$$P_{\text{BiogasPlant}} = 500\,\text{kW}, \quad \text{PQ}_{\text{CHPU}} : \text{PQ}_{\text{PCU}} \in \{1:1,\ 2:2,\ 3:3\}, \quad \text{Biogas}_{\text{CR}} \in \{0.25,\ 0.5,\ 0.75\}.$$

Simulation Setup for Determination of the Optimal FT–Syncrude Price

In addition to the main simulation, it became apparent during the work that a further analysis of the optimal Syncrude price for different scenarios would be of interest. For this reason, an additional simulation study was carried out to systematically determine the influence of the Syncrude sales price on the economic viability of the BGtL plant.

In this analysis, the BGtL plant was simulated in single-operation. The same constant simulation parameters were used as in the main simulation (see Table 7.4), but with two main modifications: (1) The Syncrude price was varied over a broad range, and (2) the overbuilding stage of the PCU was refined to smaller steps.

The following parameter combinations were considered:

$$P_{\text{BiogasPlant}} \in \{75,\ 500,\ 2\,000\}\ \text{kW}, \quad \text{PQ}_{\text{PCU}} \in \{1.0,\ 1.5,\ 2.0,\ 2.5,\ 3.0\},$$

$$\text{Syncrude Price} \in \{1.0,\ 1.5,\ 2.0,\ 2.5,\ 3.0,\ 3.5,\ 4.0,\ 4.5,\ 5.0\}\ \text{€}/\text{kg}_{\text{Syncrude}}.$$

For each combination, a simulation was performed and the resulting ROI was calculated. The results were first visualized as 3D surface plots for each plant size.

In a further step, a target ROI of 10 % was defined as a minimum requirement for economic viability. This value was selected based on typical discount rates for relevant sectors as given in the EU Reference Scenario 2020 [131]. For each scenario, the minimum Syncrude price needed to achieve this ROI was then determined and displayed in line diagrams.

Simulation Setup for Determination of the Required Flexibility Bonus for the BGtL Plant

After the optimal Syncrude price for economic operation was determined in the previous analysis, a final step was to check if a flexibility bonus—similar to the incentive system used for the CHPU—could also make overbuilding of the BGtL plant profitable. For this reason, one more simulation study was carried out to systematically analyse the influence of a flexibility bonus on the ROI of the BGtL plant operated in single-operation.

In this study, the Syncrude prices that were identified before as the minimum necessary to reach a

10 % ROI for each biogas plant size were used as fixed inputs. These prices were 2.25 €/$kg_{Syncrude}$ for the 2,000 kW biogas plant, 2.76 €/$kg_{Syncrude}$ for the 500 kW plant, and 4.02 €/$kg_{Syncrude}$ for the 75 kW plant.

Again, the overbuilding factor of the PCU (PQ_{PCU}) was varied in steps of 0.5, from 1.0 up to 3.0:

$$P_{\text{BiogasPlant}} \in \{75,\ 500,\ 2\,000\}\ \text{kW}, \quad \text{PQ}_{\text{PCU}} \in \{1.0,\ 1.5,\ 2.0,\ 2.5,\ 3.0\}.$$

For every scenario, a flexibility bonus was assumed, which was paid per kilowatt of the overbuilt PCU capacity. The bonus was calculated in the same way as for the CHPU system. The main simulation outputs for each case were the total investment cost (C_0), annual cost (C), annual revenue (R), and the overbuilt PCU capacity ($P_{\text{PCU, overbuilt}}$).

The flexibility bonus (FB) itself was not fixed in the simulation, but instead was varied in a wide range. For each value of the bonus, the resulting ROI was calculated using the following formula:

$$\text{ROI}(FB) = \frac{(R + P_{\text{PC, overbuilt}} \cdot FB) - C}{C_0/2} \tag{7.2}$$

This procedure was repeated for each plant size and overbuilding factor. In the end, the results were shown as plots of ROI versus flexibility bonus, which allow a direct view of the required bonus values to reach economic viability in the different scenarios.

Simulation Setup for Testing the Application of the Optimal Syncrude Price and BGtL Flexibility Bonus

After the optimal Syncrude prices and flexibility bonus for the BGtL plant were identified in the previous analyses, an additional simulation was performed to investigate if a combination of BGtL and CHP units could become more attractive under adjusted economic conditions. The main aim was to check if the BGtL-CHPU combined operation could compete with BGtL or CHPU single-operation when both systems are compared at the same ROI level.

For this scenario, the biogas plant capacity was fixed at 500 kW, and the overbuilding factors for the PCU (PQ_{PCU}) and the CHPU (PQ_{CHPU}) were each varied from 0 to 3 in steps of 1. The biogas CR was set to 0.5, so that both units received equal shares of the available biogas:

$$P_{\text{BiogasPlant}} = 500\,\text{kW}, \quad \text{PQ}_{\text{PCU}} \in \{0,\ 1,\ 2,\ 3\}, \quad \text{PQ}_{\text{CHPU}} \in \{0,\ 1,\ 2,\ 3\}, \quad \text{Biogas}_{\text{CR}} = 0.5$$

The Syncrude price was set to 2.76 €/$kg_{Syncrude}$, which is the minimum value previously determined to reach a 10 % ROI for the 500 kW plant in single-operation. In addition, a flexibility bonus for the BGtL plant was applied, set at 400 €/$kW_{\text{PC, overbuilt}}$, slightly above the upper end of the required range identified in the flexibility bonus analysis for this plant size.

This setup makes it possible to directly compare the economic performance of combined BGtL-CHPU operation with the single-operation scenarios, under conditions where neither system is advantaged by an artificially high Syncrude price. The main output of the simulation is the ROI for each combination of overbuilding factors, which is presented as a heatmap for the 500 kW case.

8 Results of the Simulations

This chapter presents the results of the simulations introduced earlier. The analysis begins with the evaluation of the single-operation cases for the CHPU and BGtL units, as well as the influence of the main variable simulation parameters. The main simulation results are not shown immediately, but are instead prepared by first discussing the effects of these individual parameters. Afterwards, the overall outcome of the main simulation is visualized and presented using a heatmap (see Figure 8.6). The results of the entire main simulation are therefore presented in chapter 8.3. Following the main simulation, the results of the additional simulations are presented. These include the determination of the optimal Syncrude price and the required flexibility bonus for the BGtL plant. Finally, a dedicated simulation is shown in which these optimized values are applied, in order to assess their impact on overall plant profitability.

8.1 Single Operation of the Plants

Before presenting the combined operation results of the CHPU and BGtL plants, it is instructive to examine each unit's performance when operated in single operation.

8.1.1 CHPU in Single Operation

Figure 8.1 shows the annual costs and revenues for CHPU single-operation for three biogas plant sizes ($P_{\mathrm{BiogasPlant}}$ = 75 kW, 500 kW, 2,000 kW) and three overbuilding stages ($\mathrm{PQ}_{\mathrm{CHPU}} = 1, 2, 3$). The left column displays absolute annual costs and revenues, broken down into their individual components. The right column shows, for each size, the change in annual costs and revenues compared to the standard scenario ($\mathrm{PQ}_{\mathrm{CHPU}} = 1$).

The cost components are divided into CAPEX and OPEX for the biogas plant ($\mathrm{CAPEX}_{\mathrm{BGP}}$, $\mathrm{OPEX}_{\mathrm{BGP}}$), BGS ($\mathrm{CAPEX}_{\mathrm{BGstor}}$, $\mathrm{OPEX}_{\mathrm{BGstor}}$), and the CHPU ($\mathrm{CAPEX}_{\mathrm{CHPU}}$, $\mathrm{OPEX}_{\mathrm{CHPU}}$). In addition, variable costs for biogas production ($C_{\mathrm{biogas,CHPU}}$) are included. Total revenues are composed of electricity sales ($R_{\mathrm{el,CHPU}}$), heat sales ($R_{\mathrm{heat,CHPU}}$), and the flexibility bonus.

Across all plant sizes, both total annual costs and total revenues increase with higher overbuilding factors (PQ). For smaller plants (75 kW), CAPEX and OPEX for the CHPU decrease slightly with increasing PQ, while variable biogas costs remain constant and storage costs are negligible. The revenue components (electricity and heat sales) show little change with increasing PQ, and the flexibility bonus is the main contributor to increasing total revenue.

For the 500 kW and 2,000 kW plants, the share of CAPEX and OPEX in total costs decreases as plant size increases. Biogas production costs become the largest cost component for larger plants. The increase in total annual revenue with higher PQ is more pronounced at these scales, primarily due to the flexibility bonus. For both 500 kW and 2,000 kW, revenues exceed total costs at higher PQ. The right-hand plots illustrate that, the main contributor to the increase in total revenue is the flexibility bonus, while changes in OPEX and CAPEX are small.

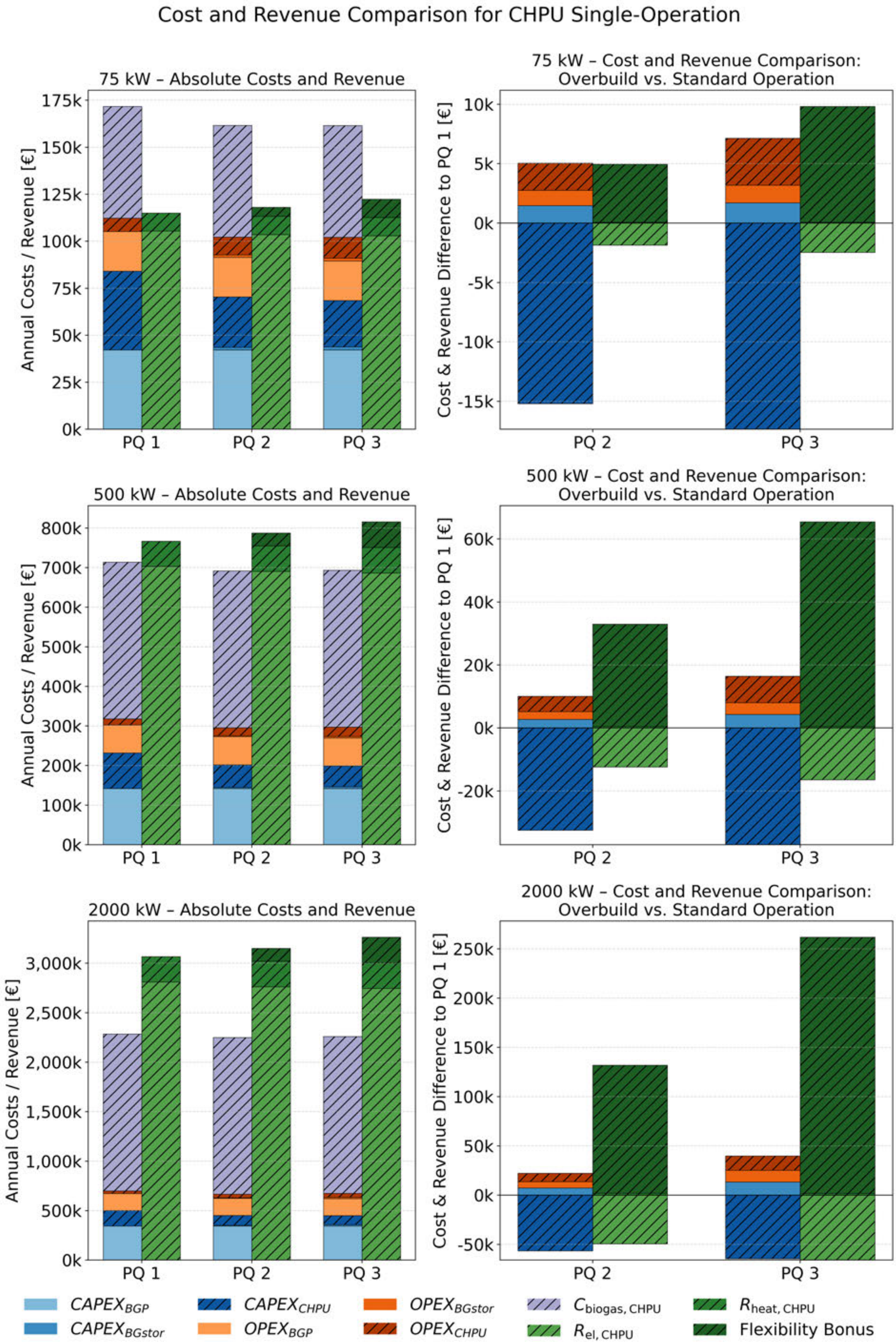

Figure 8.1: Cost and Revenue Comparison for Overbuild of the CHPU in Single-Operation.

8.1.2 BGtL in Single-Operation

Figure 8.2 presents the annual costs and revenues for BGtL single-operation for three different biogas plant sizes ($P_{\text{BiogasPlant}} = 75\,\text{kW},\ 500\,\text{kW},\ 2{,}000\,\text{kW}$) and three overbuilding stages ($\text{PQ}_{\text{PCU}} = 1, 2, 3$). The left column shows the absolute annual costs and revenue, broken down into individual cost components and revenue. The right column displays the difference in costs and revenue for each scenario relative to the base case ($\text{PQ}_{\text{PCU}} = 1$).

The costs are divided into CAPEX and OPEX for the biogas plant ($\text{CAPEX}_{\text{BGP}}$, OPEX_{BGP}),BGS ($\text{CAPEX}_{\text{BGstor}}$, $\text{OPEX}_{\text{BGstor}}$), PCU ($\text{CAPEX}_{\text{PCU}}$, OPEX_{PCU}), FTS unit ($\text{CAPEX}_{\text{FTS}}$, OPEX_{FTS}), and SGS ($\text{CAPEX}_{\text{SGstor}}$, $\text{OPEX}_{\text{SGstor}}$). In addition, variable costs are shown for biogas ($C_{\text{biogas,BGtL}}$), water ($C_{\text{water,BGtL}}$), and electricity ($C_{\text{el,BGtL}}$). Revenue is represented by the sale of FT-Syncrude (R_{Syncrude}).

For all plant sizes, total annual costs increase with higher overbuilding stages (PQ_{PCU}). The breakdown shows that the shares of CAPEX and OPEX for the PCU and SGS increase with increasing PQ_{PCU}, while electricity costs decrease. Revenue remains nearly constant across all overbuilding stages and plant sizes, with slight decreases visible at higher PQ_{PCU} values. For the smallest plant size (75 kW), the difference between costs and revenue becomes negative at higher overbuilding stages, while for larger plant sizes, the difference remains positive or increases. For all plant sizes, the largest single cost component is electricity costs, especially at larger plant sizes. The right-hand panels show that the cost increases between overbuilding stages are greater for the investment-related cost components, while changes in revenue are relatively small.

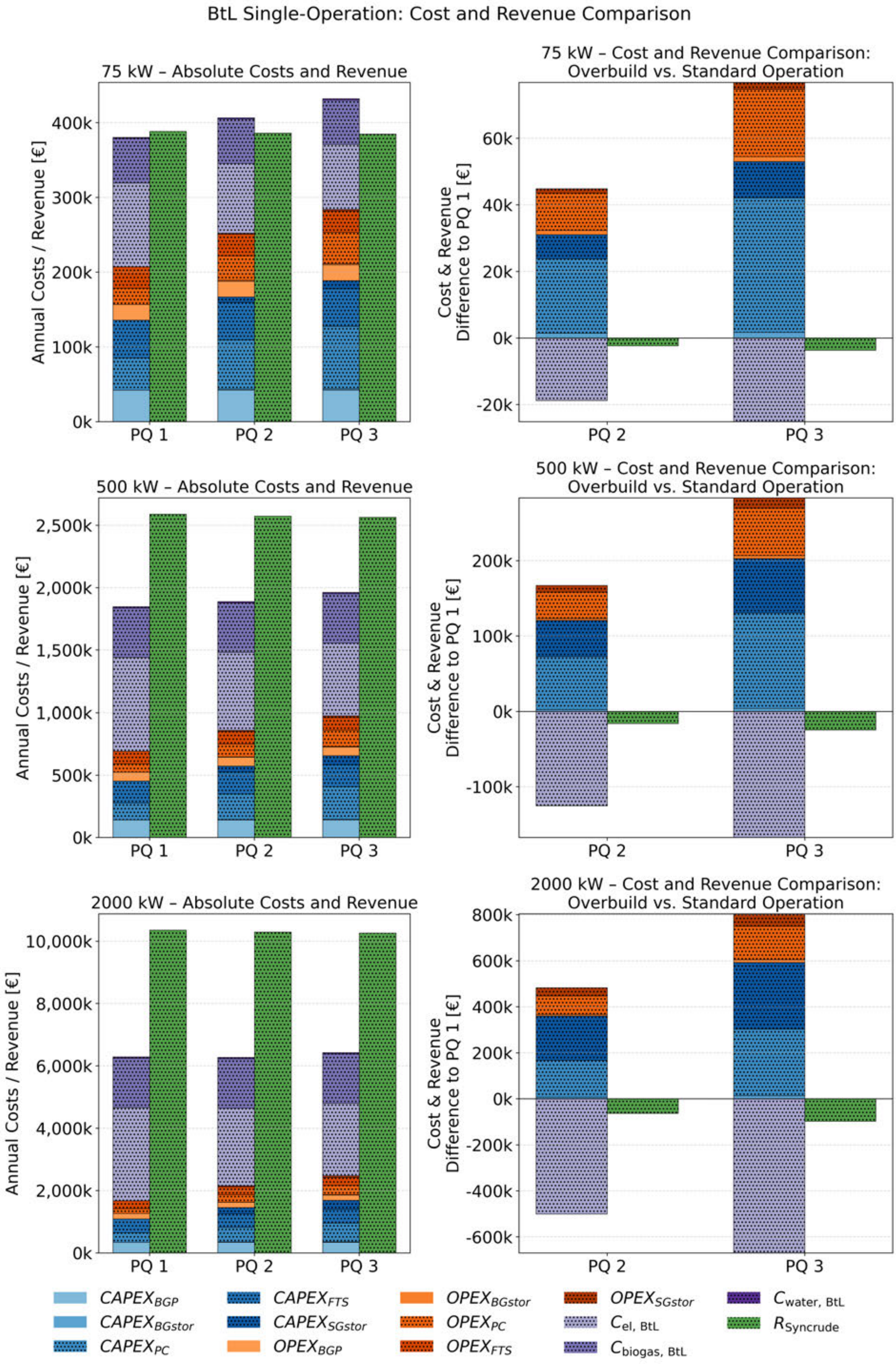

Figure 8.2: Cost and Revenue Comparison for Overbuild of the BGtL Plant in Single-Operation.

8.2 Detailed Visualization and Analysis of the Various Parameter Variations in Combined Operation

After the single-operation results have been presented, the following section describes the outcomes for the combined BGtL and CHPU systems under various parameter variations.

8.2.1 CHPU and BGtL in Combination: Influence of Overbuilding Both Plants to the Same Extent

Figure 8.3 displays the annual costs and revenues for combined operation of CHPU and BGtL plants for three biogas plant sizes ($P_{\mathrm{BiogasPlant}} = 75\,\mathrm{kW}$, $500\,\mathrm{kW}$, $2{,}000\,\mathrm{kW}$) and three matching overbuilding stages ($\mathrm{PQ}_{\mathrm{CHPU}} : \mathrm{PQ}_{\mathrm{PCU}} = 1{:}1$, 2:2, 3:3), with the biogas CR set to $\mathrm{Biogas}_{\mathrm{CR}} = 0.5$.

In the left column of each subplot, the absolute annual costs and revenues are shown for each plant size and overbuilding stage, with costs separated into their individual components (CAPEX and OPEX for all subsystems, as well as variable costs). Revenues are broken down into Syncrude sales (R_{Syncrude}), electricity sales ($R_{\mathrm{el,\,CHPU}}$), heat sales ($R_{\mathrm{heat,\,CHPU}}$), and the flexibility bonus.

The bar charts reveal that for all three biogas plant sizes, the total annual costs and revenues are at their lowest values for the smallest plant (75 kW) and highest for the largest ($2,000\,\mathrm{kW}$). As the overbuilding stage increases (from 1:1 to 3:3), the total costs show an upward trend across all plant sizes, while the total revenues remain nearly constant or show only a slight increase. The CAPEX and OPEX contributions for the PCU, FTS, SGS, and BGS increase with higher overbuilding, while the CAPEX for the CHPU decreases. The variable electricity costs for the BGtL plant decline as overbuilding increases.

Within the revenue breakdown, the Syncrude sales and electricity revenue decrease slightly as overbuilding increases, whereas the flexibility bonus shows an increase. The heat sales show only small changes across the scenarios.

A comparison of the three plant sizes shows that for the 75 kW biogas plant, total annual costs exceed total revenues in all overbuilding stages. For the 500 kW and 2,000 kW plants, total revenues exceed costs in all scenarios, and the difference grows with plant size.

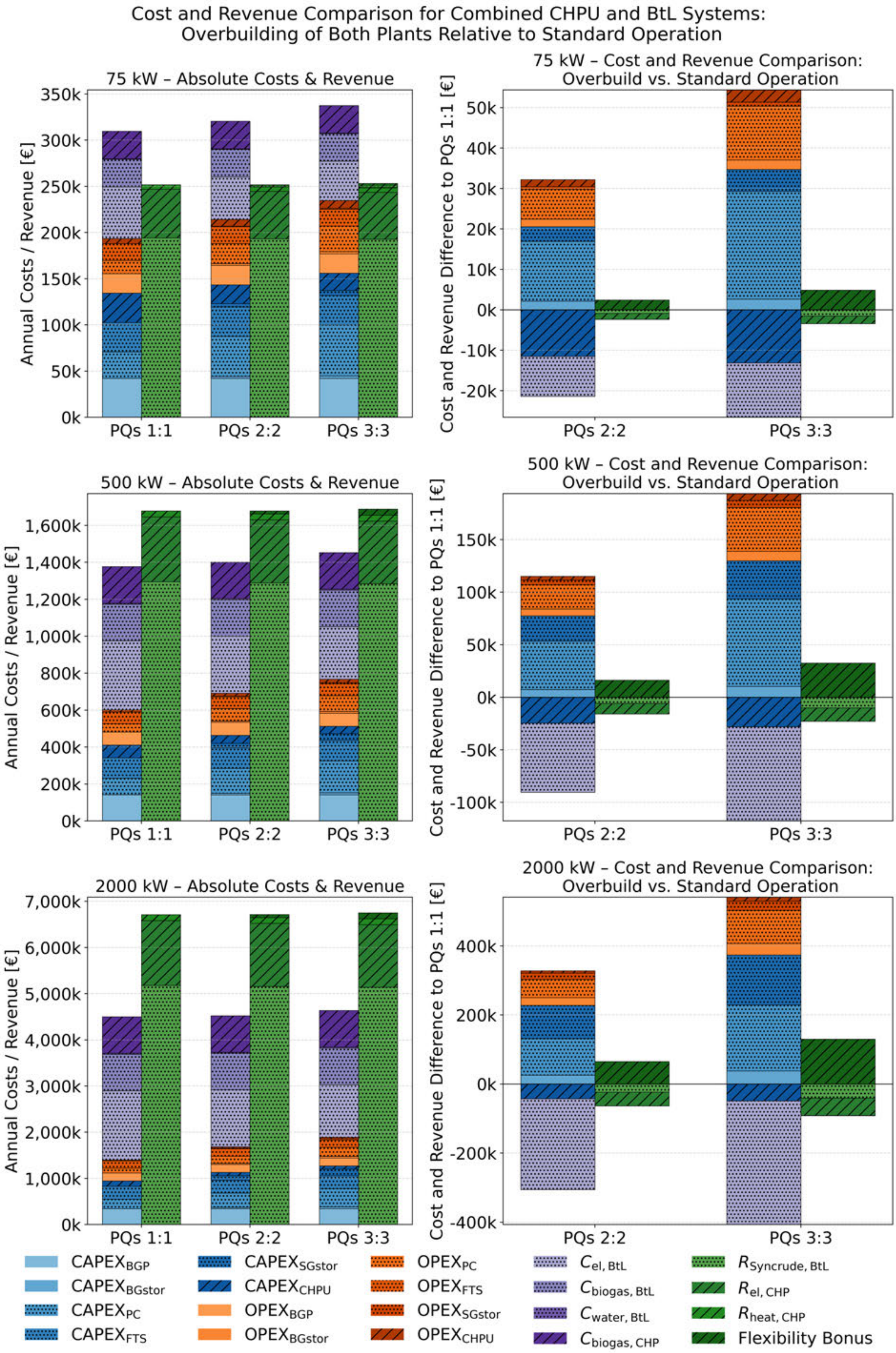

Figure 8.3: Cost and Revenue Comparison for Combined CHPU and BGtL Systems: Overbuilding of Both Plants Relative to Standard. 65

8.2.2 CHPU and BGtL in Combination: Influence of Overbuilding a Single Plant

Figure 8.4 presents the annual costs and revenues for the combined operation of CHPU and BGtL plants, based on a 500 kW biogas plant. The scenarios consider symmetric overbuilding of both plants (1:1, 2:2, 3:3), as well as overbuilding applied only to either the PCU (1:2, 1:3) or the CHPU (2:1, 3:1). For all cases, the biogas CR is set to $\text{Biogas}_{\text{CR}} = 0.5$.

Each row of the figure shows, for one scenario group, the absolute annual costs and revenues (left) and the difference in each cost and revenue component relative to the reference scenario (1:1, right).

In the symmetric overbuilding scenario (top row), both total annual costs and total annual revenues change with increasing overbuilding stage. The breakdown into CAPEX, OPEX, and variable costs for all plant units is visible, as well as the distribution of the different revenue sources. The difference plots (right) show, for 2:2 and 3:3, which components increase or decrease compared to the standard case.

When overbuilding is applied only to the PCU (middle row), the absolute cost bars for 1:2 and 1:3 show an increase in total costs compared to the 1:1 scenario. The breakdown reveals that the CAPEX and OPEX contributions from the PCU and SGS increase with overbuilding. The difference plots display these changes as positive bars for these components, while the electricity cost bar decreases. The total revenue bars for 1:2 and 1:3 are lower than in the 1:1 Scenario.

In the scenario with overbuilding applied only to the CHPU (bottom row), the total annual costs decrease slightly for 2:1 and 3:1 compared to 1:1. The component breakdown shows a reduction in annualized CAPEX for the CHPU, while other costs remain relatively stable. The difference plots (right) show negative bars for $\text{CAPEX}_{\text{CHPU}}$ and small positive bars for $\text{OPEX}_{\text{CHPU}}$, flexibility bonus, and total revenues. The revenues in the 2:1 and 3:1 cases are slightly higher than in 1:1.

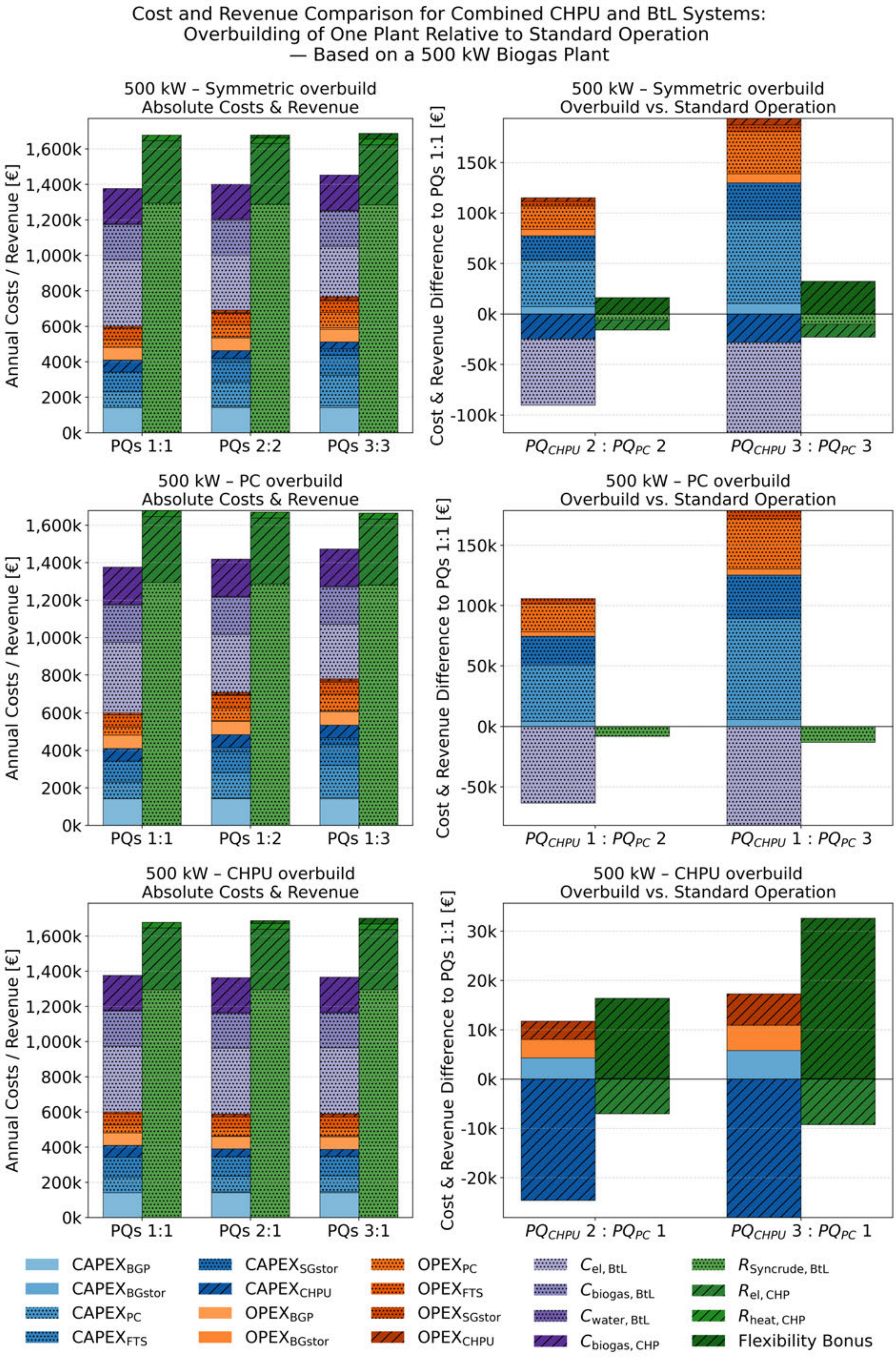

Figure 8.4: Influence of overbuilding only one plant in combination.

8.2.3 CHPU and BGtL in Combination: Influence of Biogas Consumption Ratio

Figure 8.5 shows the absolute annual costs and revenues (left column) and the differences relative to $\text{Biogas}_{\text{CR}} = 0.5$ (right column) for three different biogas CRs ($\text{Biogas}_{\text{CR}} = 0.25$, 0.5, and 0.75) and three overbuilding stages (PQ = 1:1, 2:2, 3:3), with a fixed biogas plant capacity of 500 kW.

In all scenarios, the bars in the left panels indicate that both total annual costs and revenues increase with higher $\text{Biogas}_{\text{CR}}$. The breakdown shows that R_{Syncrude} increases as $\text{Biogas}_{\text{CR}}$ increases, while $R_{\text{el, CHP}}$ decreases correspondingly. The variable costs ($C_{\text{el, BtL}}$, $C_{\text{biogas, BtL}}$, $C_{\text{water, BtL}}$, $C_{\text{biogas, CHP}}$) as well as CAPEX and OPEX components are also higher at larger $\text{Biogas}_{\text{CR}}$.

The right panels visualize the differences in costs and revenues for $\text{Biogas}_{\text{CR}} = 0.25$ and 0.75 compared to the reference case of $\text{Biogas}_{\text{CR}} = 0.5$. The plots show that at $\text{Biogas}_{\text{CR}} = 0.25$, both total costs and revenues are lower than in the reference case, while at $\text{Biogas}_{\text{CR}} = 0.75$, both total costs and revenues are higher. The differences in the individual cost and revenue components are visible for each overbuilding stage.

For all overbuilding stages, the absolute and relative cost and revenue patterns with respect to the biogas CR are similar. The height of the revenue bars for R_{Syncrude} and $R_{\text{el, CHP}}$ changes in proportion to the selected biogas CR, while the flexibility bonus remains almost unchanged.

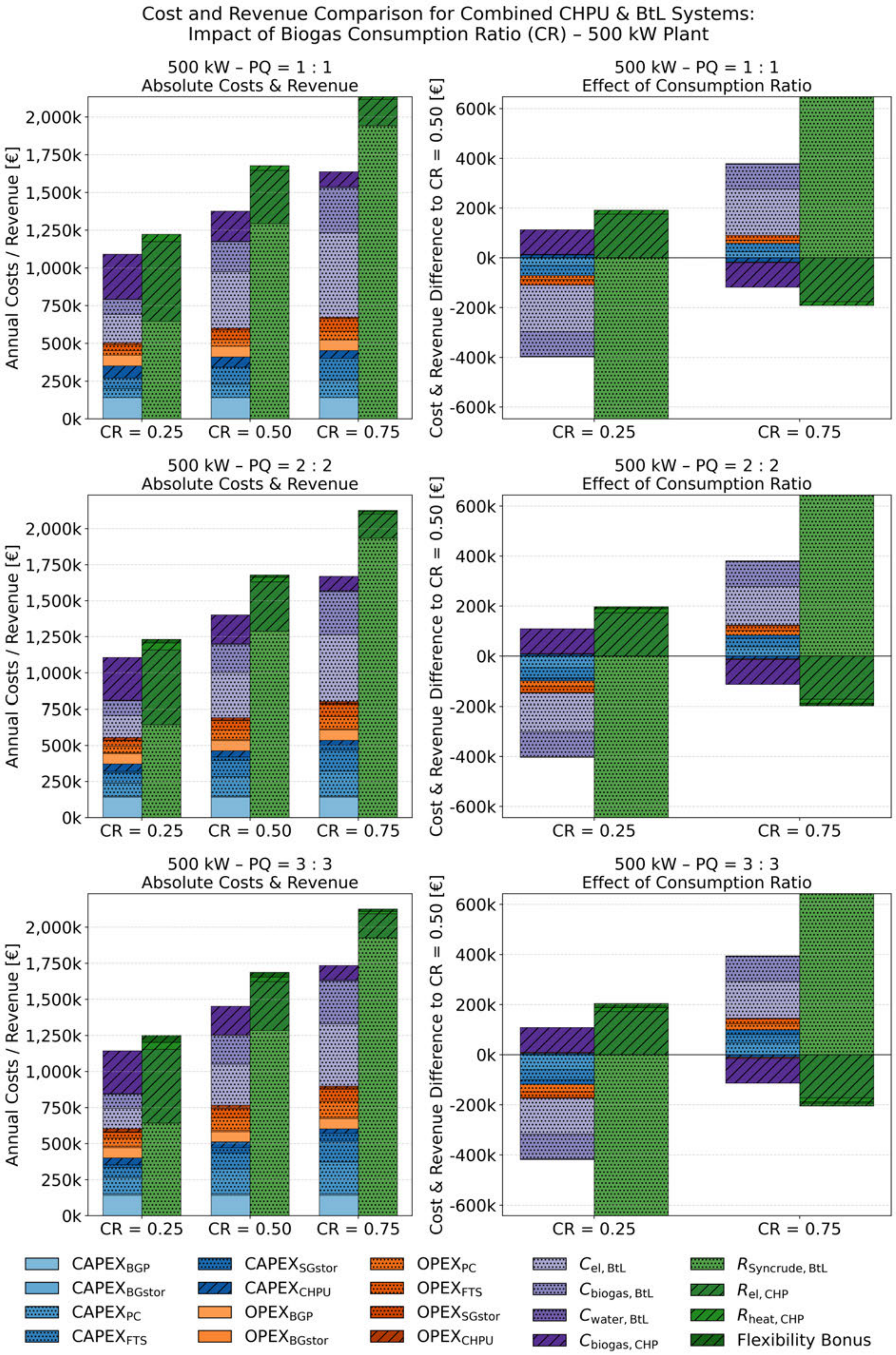

Figure 8.5: Cost and Revenue Comparison for Combined CHPU and BGtL Systems: Impact of Biogas CR - Based on a 500 kW Biogas Plant.[69]

8.3 Results of the Main Simulation

After examining the effects of individual simulation parameters, this section presents the overall outcome across all scenarios. The key performance indicator is the ROI, defined as the ratio of annual profit to invested capital. To illustrate the ROI calculation, the following subsection provides an example calculation, showing the steps from individual costs to the final ROI. Afterwards, the results of all simulations are presented.

Visualization and Description of All Simulation Results

The results of the main simulation are summarized in Figure 8.6 as a composite heatmap.

The heatmap visualizes the calculated ROI (%) for each scenario. Negative ROI values are shaded in gray, while positive values are color-coded from red (lower values) to green (higher values). The figure is arranged as a 3×3 grid of sub-panels: each column corresponds to a different biogas plant size (75 kW, 500 kW, 2,000 kW), and each row to a biogas CR (0.25, 0.5, 0.75).

Within each sub-panel, the horizontal axis indicates the overbuilding stage of the CHPU (PQ_{CHPU}), and the vertical axis shows the overbuilding stage of the PCU (PQ_{PCU}). Each field in the heatmap displays the resulting ROI value for the corresponding parameter combination.

Scenarios in which $PQ = 0$ for one plant correspond to single-operation of the remaining plant; scenarios with both $PQ_{\mathrm{CHPU}} = 0$ and $PQ_{\mathrm{PC}} = 0$ are not shown, as no plant is in operation. In each sub-panel, the effect of both overbuilding stages and biogas CR on ROI can be compared for the selected biogas plant size.

The highest ROI values are found in the lower-right part of the heatmap, corresponding to the largest biogas plant size (2,000 kW) and $\mathrm{Biogas}_{\mathrm{CR}} = 0.75$. In these scenarios, ROI values above 45 % are reached. At the same plant size but with $\mathrm{Biogas}_{\mathrm{CR}} = 0.5$, the maximum ROI is just below 40 %, and for $\mathrm{Biogas}_{\mathrm{CR}} = 0.25$, the highest values are around 34 %.

At the smallest plant size (75 kW), negative ROI values dominate, especially for low biogas CRs and higher overbuilding stages. Only a few scenarios in this size range show slightly positive ROI values, with the highest at 0.9 % for the non-overbuilt PCU ($PQ_{\mathrm{PC}} = 1$) and $PQ_{\mathrm{CHPU}} = 1$.

For the medium plant size (500 kW), ROI values are mostly positive, generally ranging from about 4 % to just over 24 % depending on the parameter combination. In these panels, the ROI increases with increasing $\mathrm{Biogas}_{\mathrm{CR}}$ and tends to decrease with higher overbuilding stages of the PCU.

Within each sub-panel, increasing PQ_{CHPU} at constant PQ_{PC} tends to increase or decrease the ROI depending on the value of $\mathrm{Biogas}_{\mathrm{CR}}$. Overbuilding both units to the same extent ($PQ_{\mathrm{CHPU}} = PQ_{\mathrm{PC}}$) yields ROI values that are generally between the corresponding single-operation results for CHPU and BGtL.

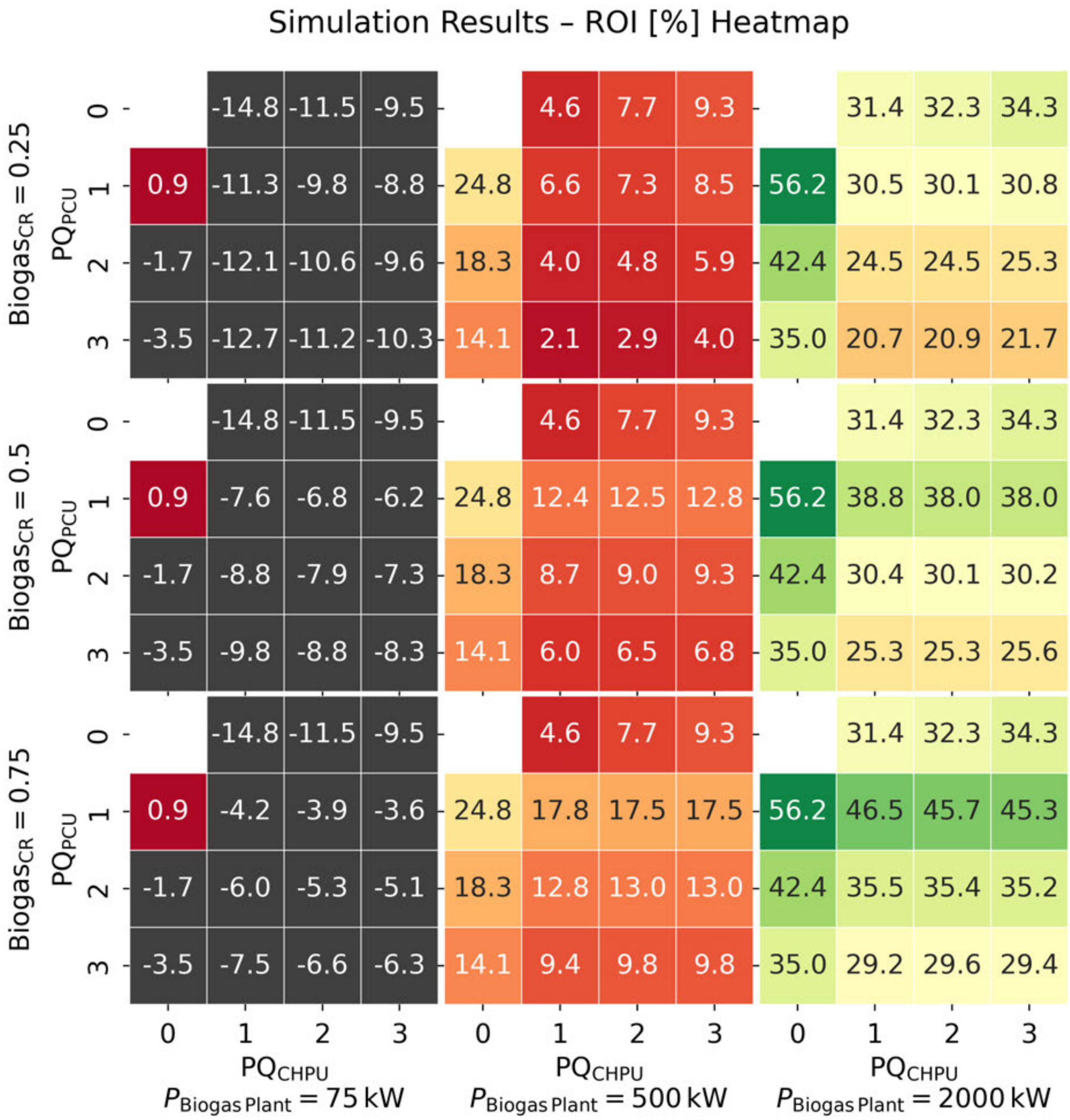

$Biogas_{CR}$	PQ_{PCU}	75 kW: 0	1	2	3	500 kW: 0	1	2	3	2000 kW: 0	1	2	3
0.25	0		-14.8	-11.5	-9.5		4.6	7.7	9.3		31.4	32.3	34.3
0.25	1	0.9	-11.3	-9.8	-8.8	24.8	6.6	7.3	8.5	56.2	30.5	30.1	30.8
0.25	2	-1.7	-12.1	-10.6	-9.6	18.3	4.0	4.8	5.9	42.4	24.5	24.5	25.3
0.25	3	-3.5	-12.7	-11.2	-10.3	14.1	2.1	2.9	4.0	35.0	20.7	20.9	21.7
0.5	0		-14.8	-11.5	-9.5		4.6	7.7	9.3		31.4	32.3	34.3
0.5	1	0.9	-7.6	-6.8	-6.2	24.8	12.4	12.5	12.8	56.2	38.8	38.0	38.0
0.5	2	-1.7	-8.8	-7.9	-7.3	18.3	8.7	9.0	9.3	42.4	30.4	30.1	30.2
0.5	3	-3.5	-9.8	-8.8	-8.3	14.1	6.0	6.5	6.8	35.0	25.3	25.3	25.6
0.75	0		-14.8	-11.5	-9.5		4.6	7.7	9.3		31.4	32.3	34.3
0.75	1	0.9	-4.2	-3.9	-3.6	24.8	17.8	17.5	17.5	56.2	46.5	45.7	45.3
0.75	2	-1.7	-6.0	-5.3	-5.1	18.3	12.8	13.0	13.0	42.4	35.5	35.4	35.2
0.75	3	-3.5	-7.5	-6.6	-6.3	14.1	9.4	9.8	9.8	35.0	29.2	29.6	29.4

Figure 8.6: ROI Heatmap: Overview of all simulated scenarios of the main simulation.

A direct comparison shows that, in all scenarios with combined operation of both plants (i.e., where both $PQ_{\mathrm{CHPU}} > 0$ and $PQ_{\mathrm{PC}} > 0$), the ROI always remains lower than the ROI achieved in the respective BGtL single-operation case (corresponding to $PQ_{\mathrm{CHPU}} = 0$ for the same PQ_{PC} and $\mathrm{Biogas}_{\mathrm{CR}}$).

The lowest ROI observed in all simulations is $-14.8\,\%$ for the 75 kW plant at $\mathrm{Biogas}_{\mathrm{CR}} = 0.25$ and minimal overbuilding, while the maximum value of $56.2\,\%$ is reached at 2,000 kW, $\mathrm{Biogas}_{\mathrm{CR}} = 0.5$, $PQ_{\mathrm{PC}} = 1$, $PQ_{\mathrm{CHPU}} = 1$ (single-operation of the BGtL).

Overall, the heatmap reveals a clear pattern of increasing ROI with increasing plant size and increasing share of biogas allocated to the BGtL plant. The effect of the overbuilding stage varies, with certain combinations leading to lower ROI, particularly for small plant sizes and high overbuilding of the PCU.

8.4 Determination of Optimal FT–Syncrude Prices for Different Biogas Plant Sizes and Overbuilding Stages

Figure 8.7 visualizes the ROI of the BGtL plant in single-operation as a function of Syncrude price and overbuilding stage for each biogas plant size (75 kW, 500 kW, 2,000 kW). On all three surfaces, ROI values are presented for each combination of Syncrude price and overbuilding factor. Across all plant sizes and overbuilding stages, the ROI increases approximately linearly with rising Syncrude price. In the region of low Syncrude prices, the ROI remains negative in all scenarios, but the transition from negative to positive ROI occurs at lower Syncrude prices as the plant size increases. For example, for the 2,000 kW plant, the ROI becomes positive at around 2.00 €/$\mathrm{kg}_{\mathrm{Syncrude}}$, for the 500 kW plant at approximately 2.50 €/$\mathrm{kg}_{\mathrm{Syncrude}}$, and for the 75 kW plant at roughly 3.50 €/$\mathrm{kg}_{\mathrm{Syncrude}}$. With increasing Syncrude price, the ROI surfaces are displaced upward for all plant sizes, while the influence of overbuilding is visible in the shape and position of the surfaces along the PQ-axis.

Figure 8.8 presents the same results as two-dimensional line diagrams, showing ROI versus Syncrude price for all plant sizes and overbuilding factors. Each colored line represents a specific scenario; the dashed horizontal line indicates the target ROI of 10 %. The intersection of each line with the 10 % ROI level shows the minimum Syncrude price required to reach this value. For the 2,000 kW plant, the Syncrude price needed to achieve a 10 % ROI ranges from 2.25 €/$\mathrm{kg}_{\mathrm{Syncrude}}$ (no overbuilding) to 2.44 €/$\mathrm{kg}_{\mathrm{Syncrude}}$ (PQ = 3.0). For the 500 kW plant, the range is 2.76 €/$\mathrm{kg}_{\mathrm{Syncrude}}$ to 3.10 €/$\mathrm{kg}_{\mathrm{Syncrude}}$, and for the 75 kW plant, from 4.02 €/$\mathrm{kg}_{\mathrm{Syncrude}}$ to 4.79 €/$\mathrm{kg}_{\mathrm{Syncrude}}$ as the overbuilding factor increases. For each plant size, curves representing higher overbuilding levels are shifted to the right, so higher Syncrude prices are necessary to reach the target ROI with increasing overbuilding stage.

Overall, both figures provide a comprehensive overview of how Syncrude price, biogas plant size, and overbuilding stage interact to determine the ROI of the BGtL plant in single operation. The graphics illustrate the regions in which the ROI transitions from negative to positive and highlight the minimum Syncrude prices required to achieve the economic target ROI of 10 % for each scenario.

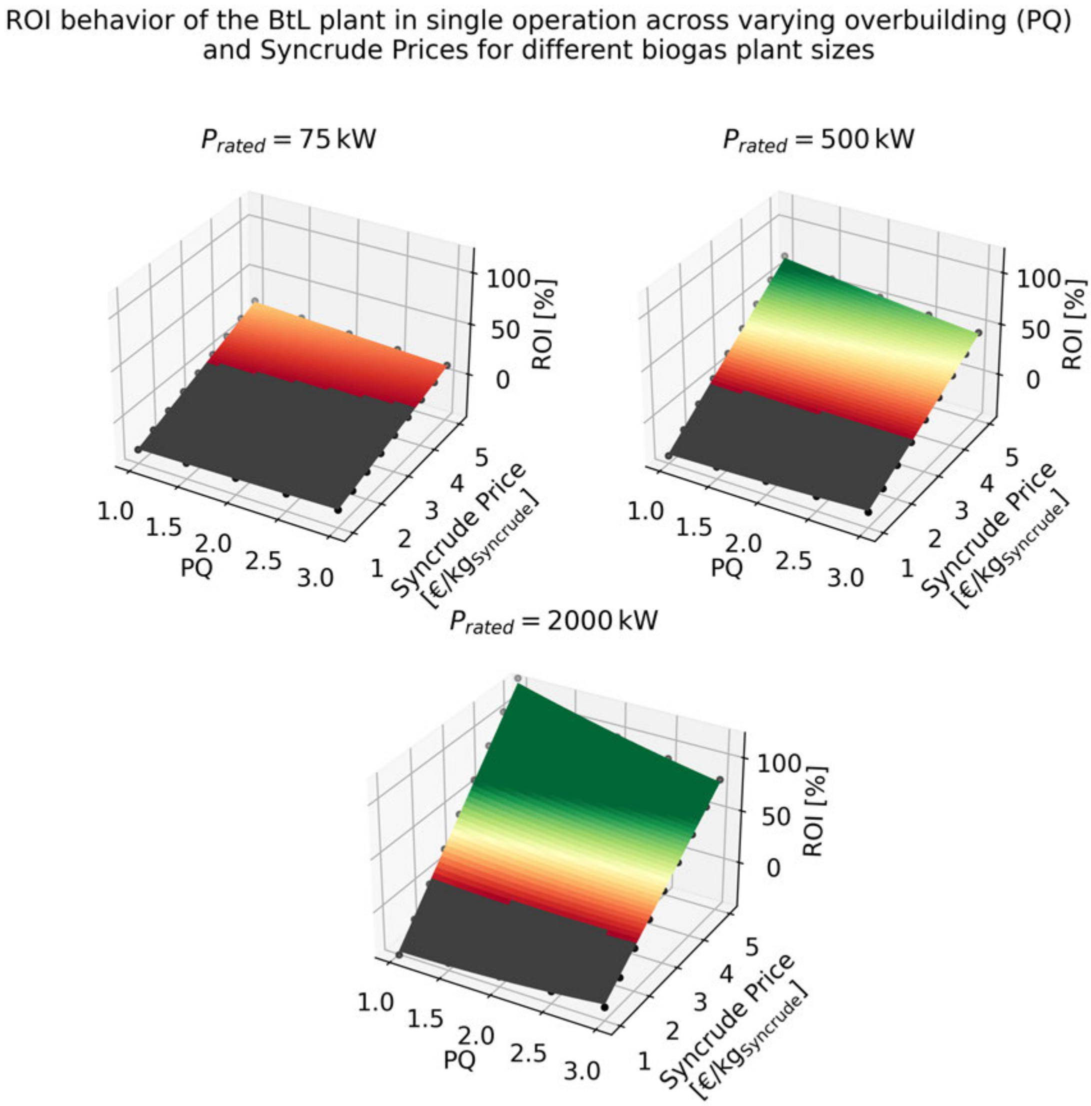

Figure 8.7: ROI behavior of the BGtL plant in single operation across varying overbuilding (PQ) and Syncrude Prices for different biogas plant sizes.

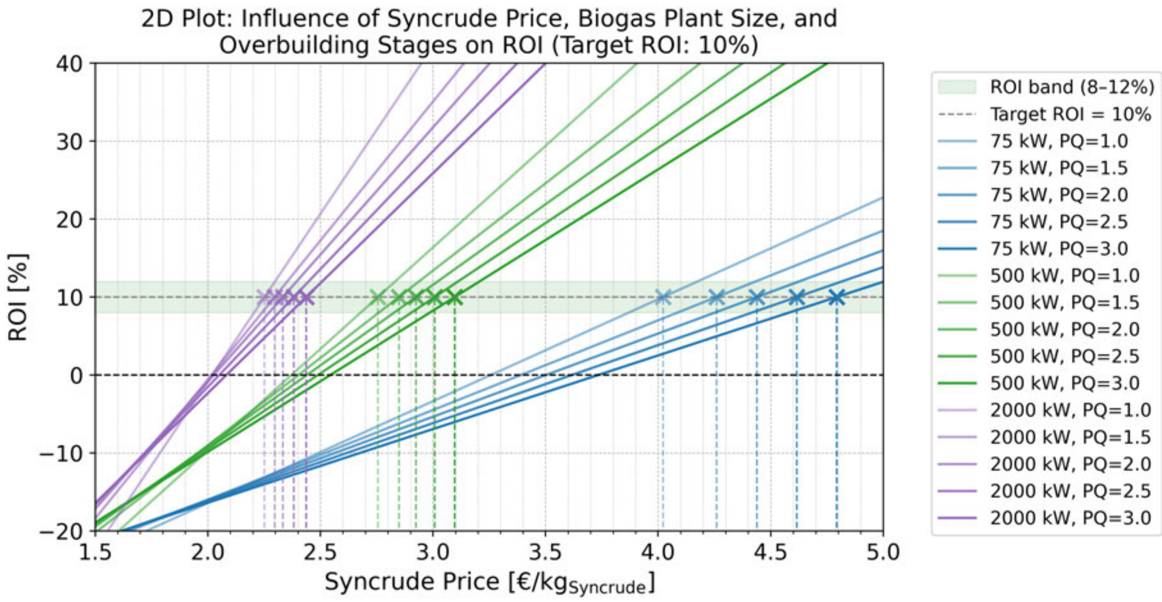

Figure 8.8: Optimal Syncrude price to achieve a 10 % ROI, as a function of biogasplant size and PC overbuilding.

8.5 Determination of the BGtL Plant's Required Flexibility Bonus

Figure 8.9 shows the results of the simulation for the required flexibility bonus to achieve a target ROI of 10 % for the BGtL plant in single-operation. The diagram displays ROI as a function of the flexibility bonus for different plant sizes (75 kW, 500 kW, 2,000 kW) and overbuilding factors (PQ). Each plant size is represented by a group of curves with different colors. For each plant size, several lines are shown, each corresponding to one overbuilding stage between $PQ = 1.0$ and $PQ = 3.0$ in steps of 0.5.

The x-axis represents the flexibility bonus in € per kilowatt of overbuilt PC capacity, and the y-axis shows the resulting ROI in percent. The dashed horizontal line marks the target ROI of 10 %, and the shaded band indicates the ROI range between 8 % and 12 %. For each scenario, the intersection of the curve with the 10 % line defines the minimum flexibility bonus required to reach this target. The intersection points are marked by crosses and vertical dashed lines for each combination of plant size and overbuilding factor.

For the 2,000 kW plant, the required flexibility bonus to reach an ROI of 10 % ranges from approximately 164 to 187 €/ $kW_{PC,\,overbuilt}$, depending on the overbuilding factor. For the 500 kW plant, the necessary flexibility bonus lies between 340 and 379 €/ $kW_{PC,\,overbuilt}$. In the case of the 75 kW plant, the required flexibility bonus ranges from 777 to 963 €/ $kW_{PC,\,overbuilt}$. For each plant size, higher overbuilding factors require a higher flexibility bonus to reach the 10 % ROI threshold.

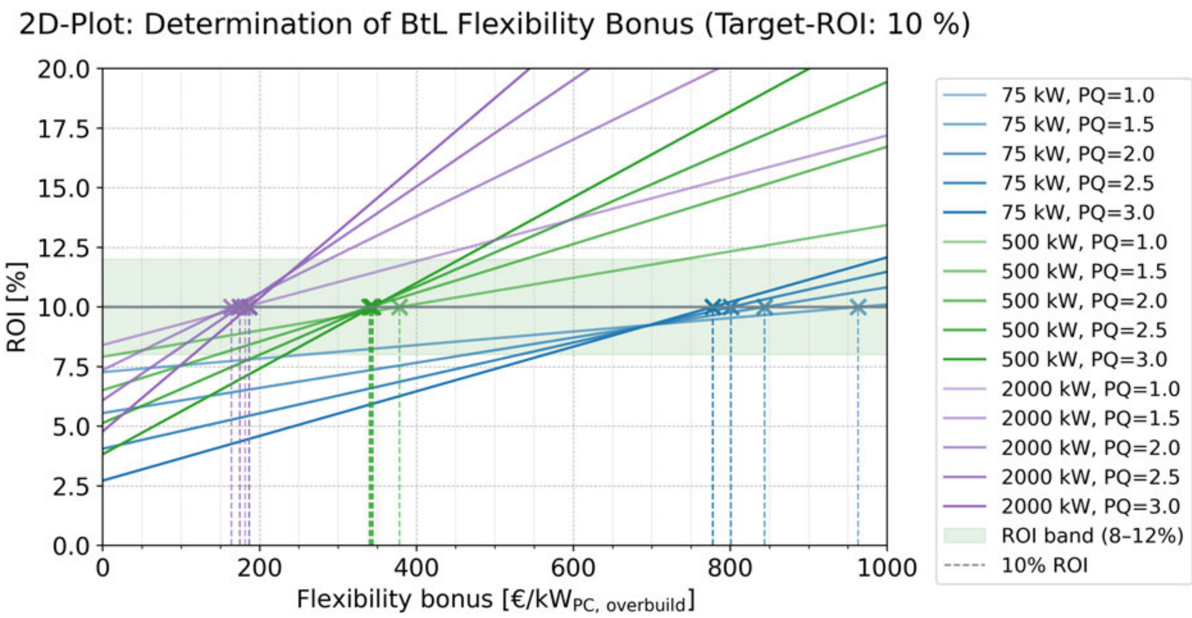

Figure 8.9: Determination of the required flexibility bonus to achieve a 10 % ROI.

8.6 Application of the Evaluated Optimal Syncrude Prices and BGtL Flexibility Bonus

Figure 8.10 displays the results of the simulation for a 500 kW biogas plant with equal biogas distribution between the BGtL and CHPU units ($\text{Biogas}_{\text{CR}} = 0.5$). The overbuilding factors for the PCU (PQ_{PC}) and the CHPU (PQ_{CHPU}) were each varied from 0 to 3 in steps of 1. The Syncrude price was set to 2.76 €/$\text{kg}_{\text{Syncrude}}$, and a flexibility bonus for the BGtL plant of 400 €/$\text{kW}_{\text{PC, overbuilt}}$ was applied.

The figure presents a heatmap of the resulting ROI values (%) for each combination of overbuilding factors. The horizontal axis shows the overbuilding stage of the CHPU (PQ_{CHPU}), while the vertical axis represents the overbuilding stage of the PCU (PQ_{PC}). Each cell of the heatmap contains the corresponding ROI value for that scenario.

Across the different scenarios, ROI values range from 3.3 % to 11.0 %. The ROI increases with rising overbuilding stage of the PCU, while the influence of the CHPU overbuilding stage results in comparatively smaller changes in ROI. The highest ROI of 11.0 % is found at $\text{PQ}_{\text{PC}} = 3$ and $\text{PQ}_{\text{CHPU}} = 0$, and the lowest ROI of 3.3 % appears at $\text{PQ}_{\text{PC}} = 1$ and $\text{PQ}_{\text{CHPU}} = 1$. Additionally, for all combinations where both units are operated together, the ROI values are lower than those achieved in the corresponding single-operation scenarios.

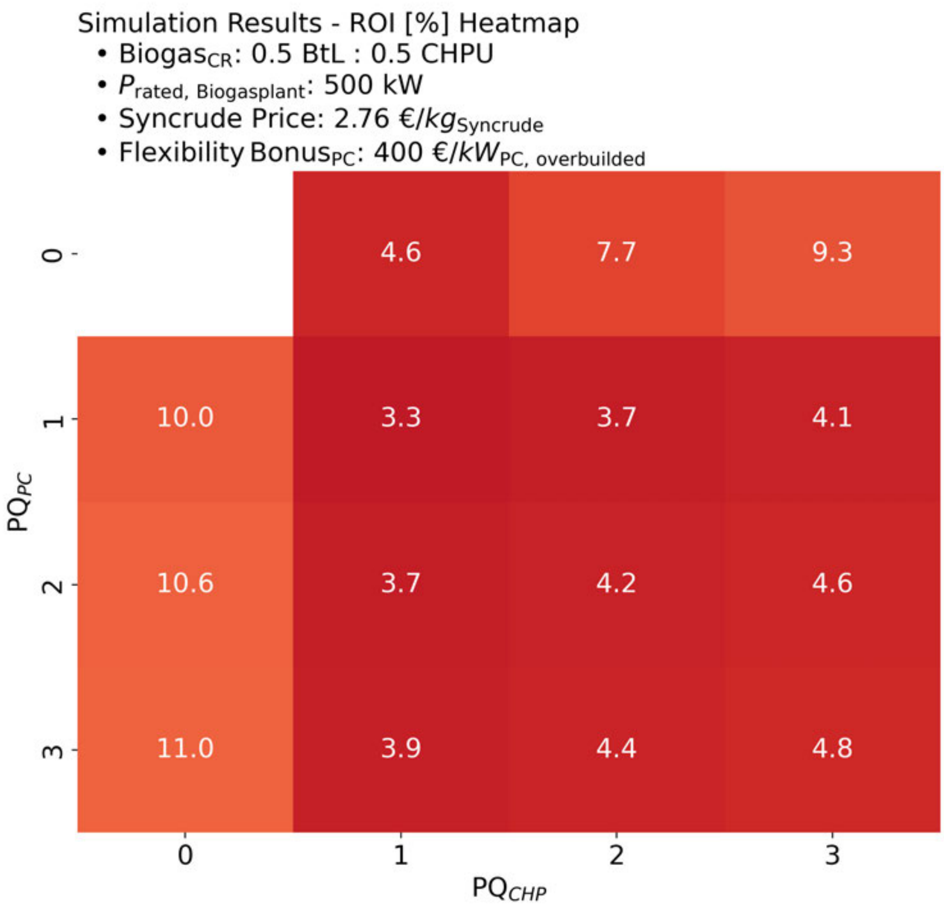

Figure 8.10: Simulation results as ROI [%] with adjusted Syncrude price and BGtL flexibility bonus for a 500 kW biogas plant.

9 Discussion

This chapter provides a critical evaluation and interpretation of the simulation results. The main findings are discussed with a focus on the most important influences on costs, revenues, and profitability for the different plant concepts. Furthermore, the simulation results are compared with values from the literature where possible. Afterwards, the main modeling assumptions are discussed and the limits of the approach are highlighted. Finally, some broader aspects of biogas use for synthetic fuel production are considered, and ideas for future research are presented.

The aim of this discussion is not only to summarize the most relevant outcomes, but also to put them into context with existing knowledge and to identify uncertainties and possible improvements.

9.1 Evaluation of the simulation results

In the first subchapter of the discussion, the results of this thesis are discussed.

CHPU Single-Operation

The analysis shows that with increasing biogas plant capacity ($P_{\mathrm{BiogasPlant}}$) and higher overbuilding stage (PQ), the proportion of total costs attributed to CAPEX and OPEX decreases due to economies of scale. This reflects the typical decline in specific investment costs as capacity grows. For the CHPU, overbuilding results in a reduction of annualized CAPEX—despite higher total investment costs—because the plant's lifetime in the simulation increases as a result of lower FLH due to flexibilization. The OPEX, in turn, increase slightly since they are related to investment costs, which also rise with overbuilding.

The biogas production costs remain constant regardless of overbuilding, and for larger plant sizes, they become the dominant cost component. The effect of storage costs for biogas on total costs is negligible. Overall, these results demonstrate the significance of scale effects in reducing specific capital and operating costs.

On the revenue side, total annual revenue increases linearly with PQ, primarily due to the flexibility bonus, while revenues from direct electricity and heat sales change little with overbuilding. In fact, electricity revenue decreases slightly at higher PQ because, due to the presence of a BGS, some biogas is not converted to electricity by the end of the simulation period. This is confirmed by Figure 9.1, which shows the final optimization window where the BGS remains fully filled. Here, the optimization routine only operates the CHPU when the electricity price exceeds a defined threshold or when the storage would otherwise overflow—resulting in operations being shifted to more profitable periods. However, this also means that some biogas may remain unused at the end of the simulation, thus lowering annual electricity revenues.

Furthermore, the constant or nearly constant CHPU revenue is explained by the high, fixed remuneration rate (18 cent/kWh). As shown in Figure 9.2, this fixed remuneration is only rarely exceeded by the spot market price during the year, meaning spot price fluctuations have little

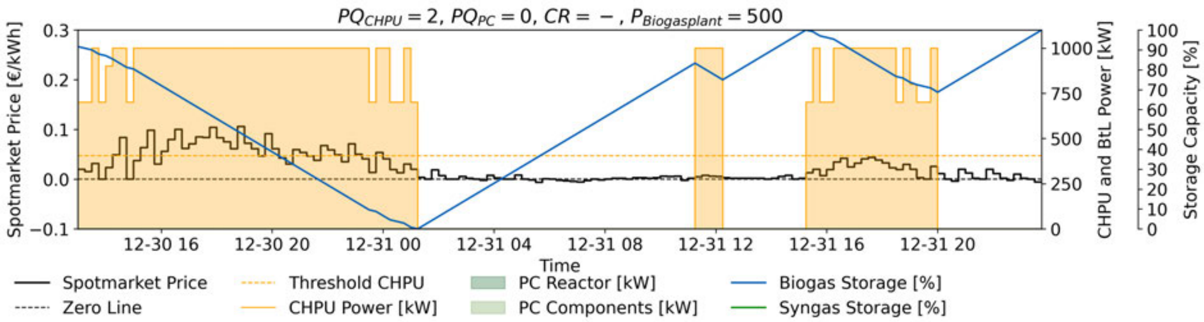

Figure 9.1: Plot of the last optimized day for CHPU in Single-Operation.

effect on overall revenue. The flexibility bonus (€65 per kW and year for each overbuilt kW) is therefore the main driver for increased revenue with higher PQ.

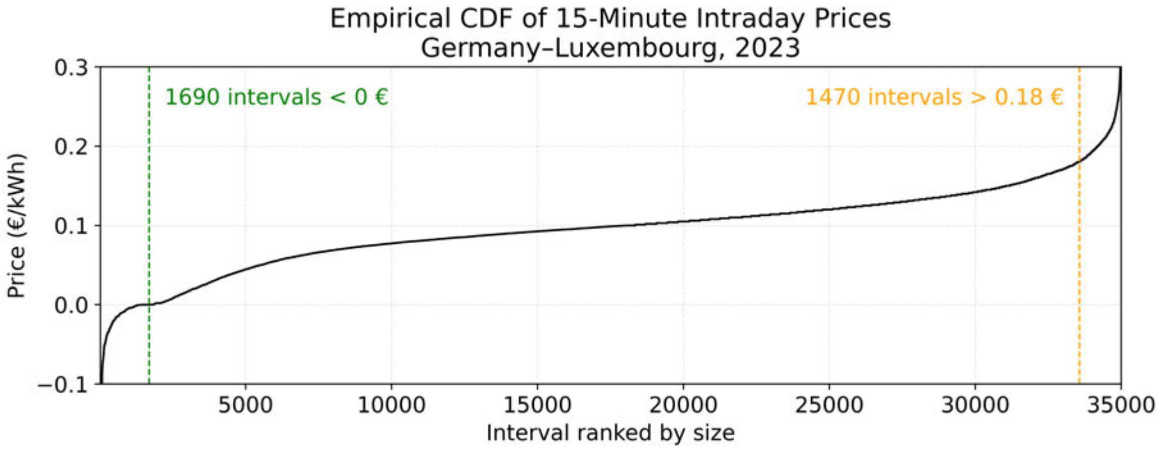

Figure 9.2: Empirical CDF of 15-Minute Intraday Prices Germany–Luxembourg, 2023

For smaller plant sizes (e.g., $P_{\text{BiogasPlant}} = 75$ kW), total costs exceed revenues, whereas for larger capacities (500 kW and 2,000 kW), revenues surpass costs—again reflecting economies of scale.

In summary, these findings confirm that the flexibility bonus is necessary and justified. Increased flexibility through overbuilding does not significantly increase (and can even slightly reduce) electricity and heat revenues. Without the bonus, flexibilization would not be economically attractive. The results therefore underscore the central role of policy incentives in promoting operational flexibility in biogas-based CHPUs.

BGtL Single-Operation

The results for the BGtL plant operated in single-operation (see Figure 8.2) show that total annual costs rise with increasing overbuilding. This is mainly due to the additional investments in biogas and SGS units, as well as the higher CAPEX and OPEX associated with the larger PCU. While electricity costs decrease under higher overbuilding—since the flexible operation allows the plant to run during periods of lower spot-market prices (as illustrated in Figure 9.3)—this saving is outweighed by the rising capital and storage costs.

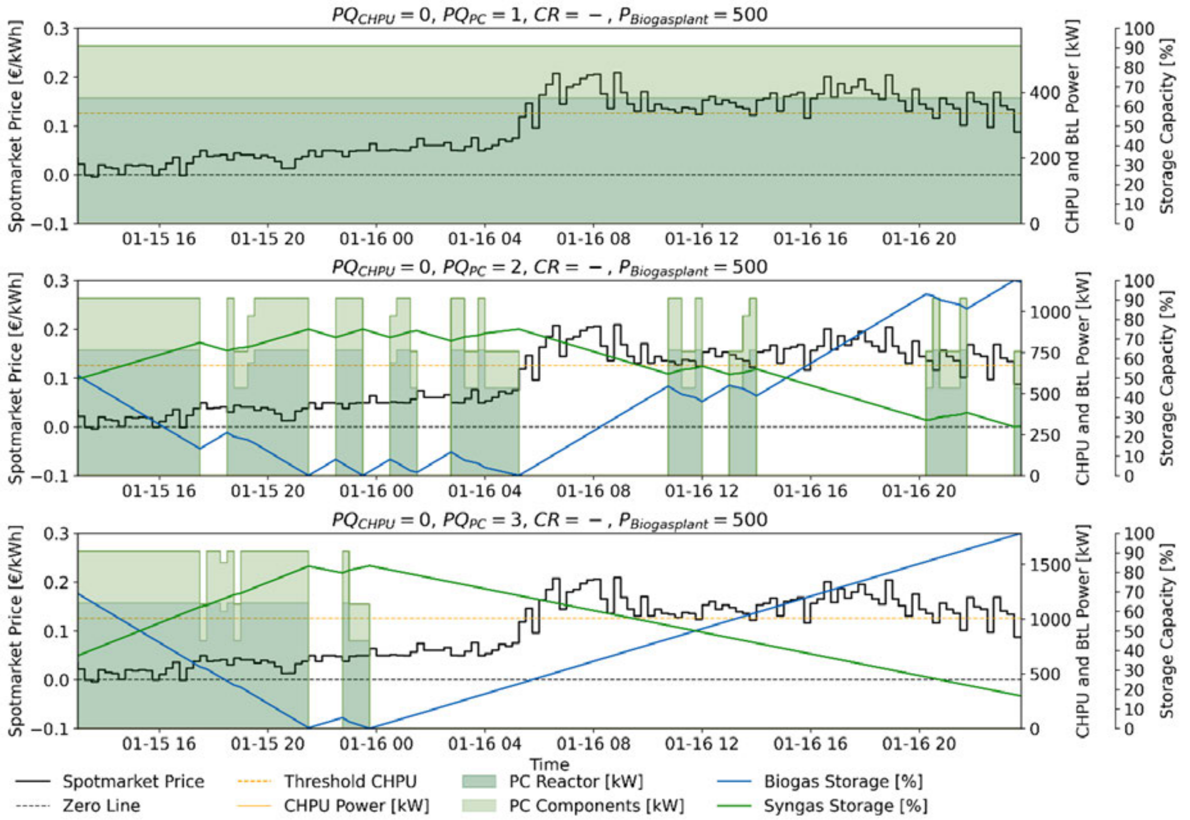

Figure 9.3: Influence of overbuilding on the operation of the PCU in BGtL single-operation.

The revenue remains nearly constant as the overbuilding stage increases. This is because only the PCU is overbuilt, whereas the FTS unit is not, so the total Syncrude output is essentially unchanged. A slight decrease in revenue is observed with higher overbuilding, as the flexible operation leads to some biogas and syngas not being fully converted within the simulation horizon (i.e., storage levels are not emptied by the final timestep, see Figure 9.4), resulting in slightly lower product output.

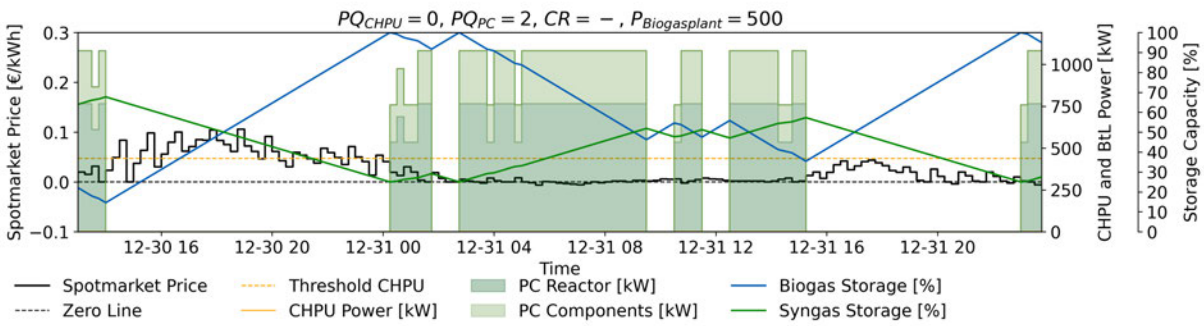

Figure 9.4: Plot of the last optimized day for BtL Single-Operation.

With increasing biogas plant capacity ($P_{\mathrm{BiogasPlant}}$), both the total profit and the absolute revenues increase, as Syncrude production scales linearly with plant size. At the same time, the share of CAPEX and OPEX in total costs declines due to economies of scale, while variable costs—particularly for electricity and biogas—become increasingly dominant for larger plants.

For the smallest plant size (75 kW), the results indicate that overbuilding is not economically viable: total costs exceed revenues for both double and triple overbuilding, and profit is only marginally positive in the standard scenario ($PQ_{PC} = 1$). This shows that overbuilding the BGtL plant has a detrimental effect on profitability at small scales, since the cost increase cannot be compensated by higher revenues.

Influence of overbuilding both systems

The decrease in Syncrude and electricity revenue is primarily due to the presence of biogas storage: not all produced biogas is utilized within the simulation horizon, leading to unconverted feedstock at the end of the period, as visible in Figure 9.5, which shows the final optimization window for the 3:3 scenario. Here, the BGS is filled to its maximum, reducing the amount of Syncrude or Electricity and Heat generated and thus revenue.

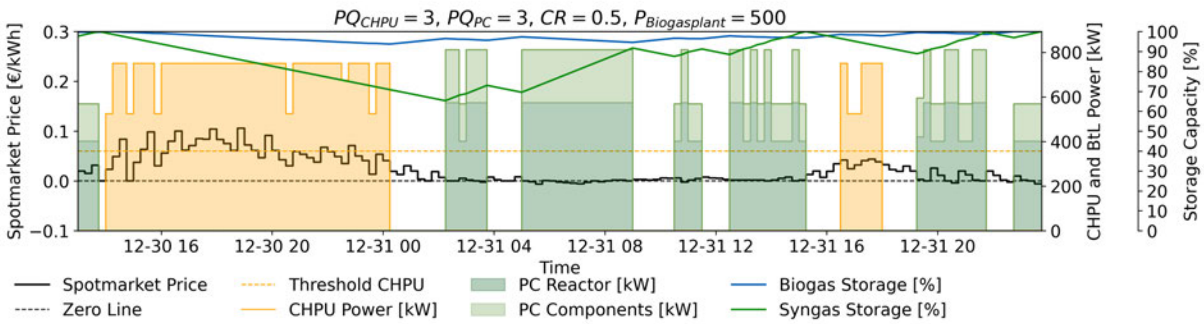

Figure 9.5: Plot of the last optimized day for BGtL and CHPU in combination with $PQ_{CHPU} : PQ_{PC} = 3 : 3$.

As biogas plant capacity increases, profit rises more strongly than in the CHPU single-operation case but less than in the BGtL single-operation case. This trend is explained by lower specific investment costs for all plant units at larger capacities, since storage investment costs scale linearly with size, and by a positive correlation between revenue and biogas plant capacity. The declining shares of CAPEX and OPEX in total costs also reflect the improved scaling behavior for larger plants.

Comparing the combined scenario to the single-operation cases reveals that total CAPEX and OPEX are substantially higher than in CHPU single-operation, but slightly lower than in BGtL single-operation. This is a result of splitting the produced biogas equally between both plant types ($CR = 0.5$), leading to each plant being dimensioned at half the size of its single-operation counterpart and combining the relatively low-cost CHPU unit with the overall more capital-intensive BGtL system.

The operational synergy between both plant types leads to lower electricity costs for the BGtL plant compared to single-operation. As shown in Figure 9.6, the PCU can run during periods of low electricity prices, while the CHPU can take over during high price periods, thus optimizing the dispatch between the two systems. Unlike in the single-operation scenario, the PCU is no longer forced to operate during peak price periods solely to prevent storage overflow, as the

CHPU can intervene when necessary. This operational flexibility is constrained by the model assumptions: biogas production is constant, and storage capacity limits must be respected.

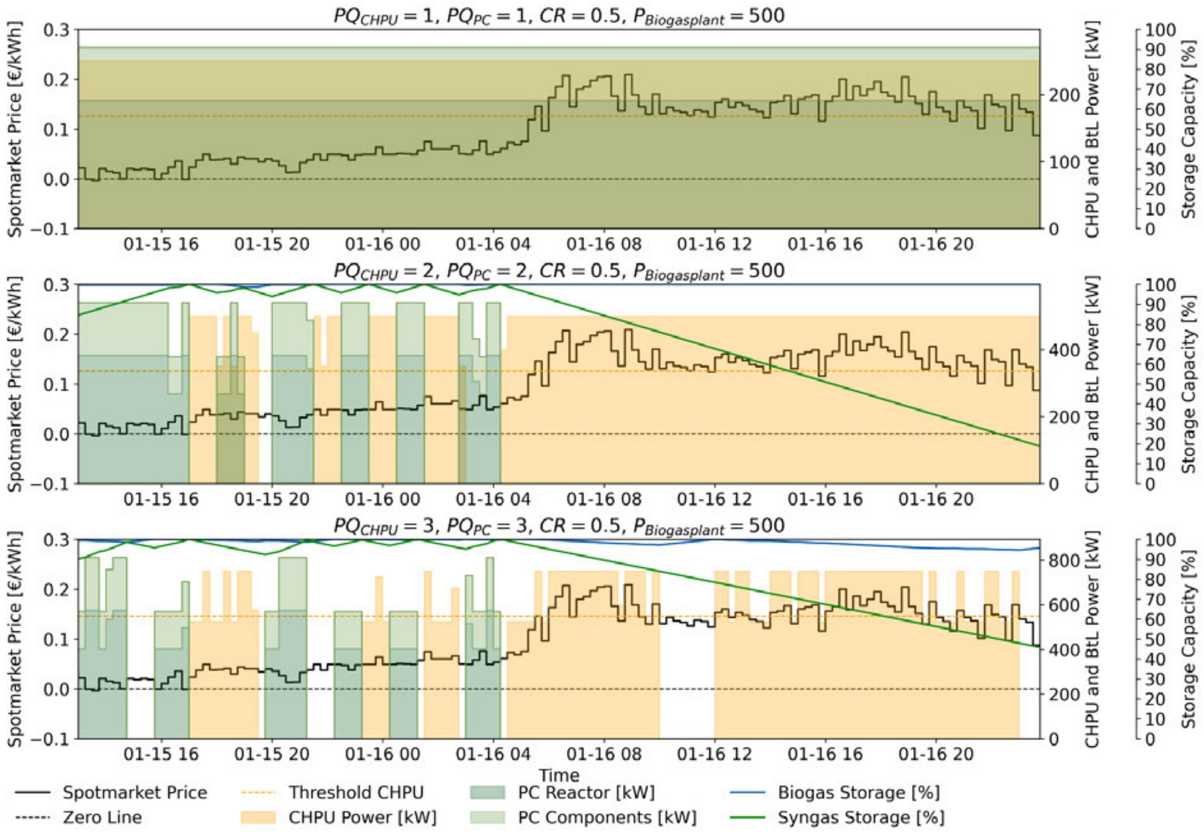

Figure 9.6: Influence of overbuilding on the operation of both plants in combination at the same overbuilding stages.

Despite this cost-optimizing interaction, the combined investment costs for both plant types remain higher than those of the single-operation cases, so overall profitability is lower than in the BGtL single-operation scenario. The Syncrude revenue is based on the fixed sales price of 3.325 €/kg$_{\text{Syncrude}}$, which leads to a relatively favorable profitability for the BGtL system in general.

Influence of overbuilding just one system

When overbuilding is applied to only one of the two systems in the combined configuration (CHPU and BGtL), distinct effects on cost, revenue, and operational behavior emerge.

Overbuilding the PCU leads to an increase in total costs, primarily due to higher investment and operating costs for the PCU itself and the associated SGS and BGS. The additional flexibility allows for a reduction in electricity costs, as the unit can operate more frequently during periods of low spot-market prices. However, these savings are outweighed by the increased capital costs, resulting in a slight overall decline in profit compared to the reference scenario with no overbuilding. Nevertheless, this decrease in profit is not as pronounced as in the BGtL single-operation case, since in the combined operation, the PCU is only dimensioned for half of the biogas output (CR = 0.5), which limits the scale of investment. Figure 9.7 illustrates that, under overbuilding, the PCU displays increased operational flexibility in response to electricity price fluctuations, while the CHPU continues to run at full load.

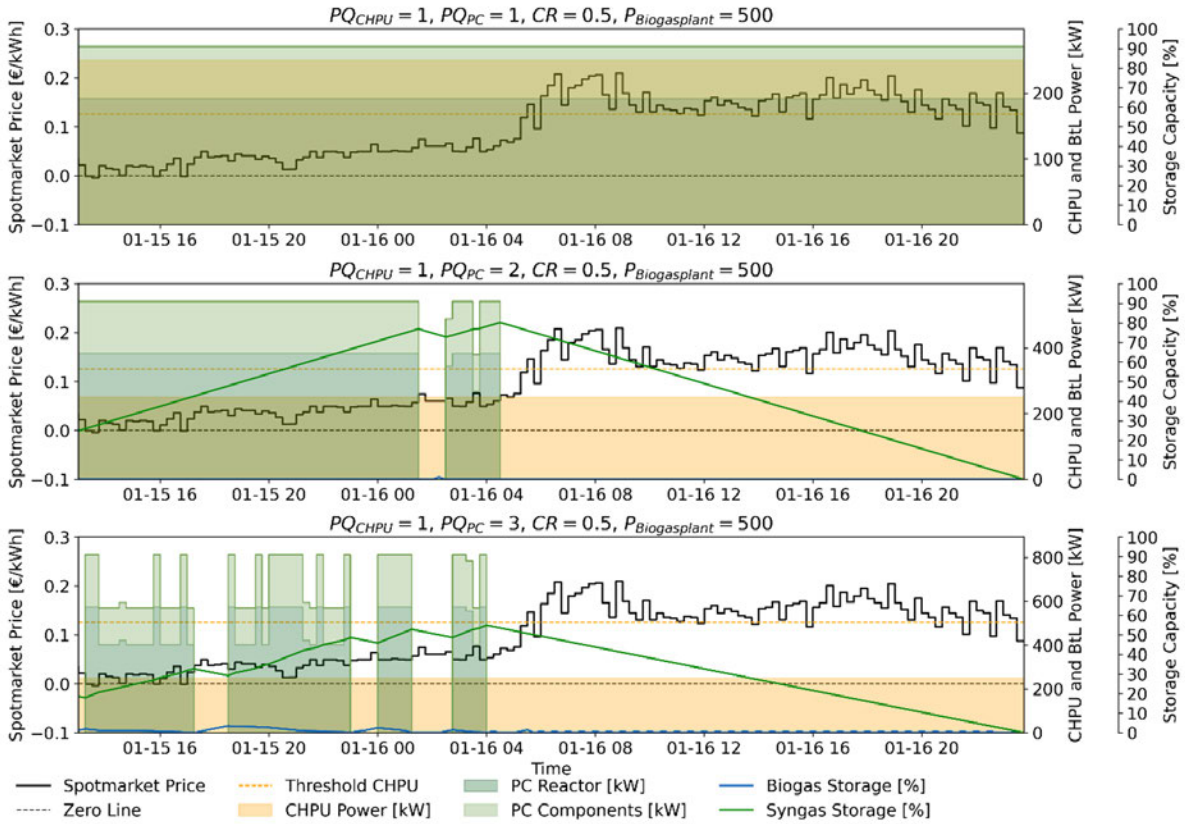

Figure 9.7: Influence of PCU overbuilding on the operation of both plants in combination.

In contrast, when only the CHPU is overbuilt, a different pattern emerges. Here, total costs decrease slightly, mainly due to the reduction in annualized CAPEX for the CHPU, while total revenues increase modestly. The flexibility bonus rises as a result of the increased installed capacity, and the CHPU becomes more responsive to high electricity price periods. The slight reduction in electricity revenue is more than compensated by the increase in the flexibility bonus. The positive effect on profit is slightly higher under CHPU overbuilding than under PCU overbuilding. This is also reflected operationally: as seen in Figure 9.8, the overbuilt CHPU discharges the BGS more effectively during periods of high prices, while the PCU continues to operate and refill storage during low-price periods.

Overall, the combined configuration softens the cost and revenue effects of overbuilding compared to the respective single-operation cases. The operational synergy between the two plants enables more efficient use of biogas and improved flexibility in responding to market signals, but the economic outcome depends strongly on which system is overbuilt.

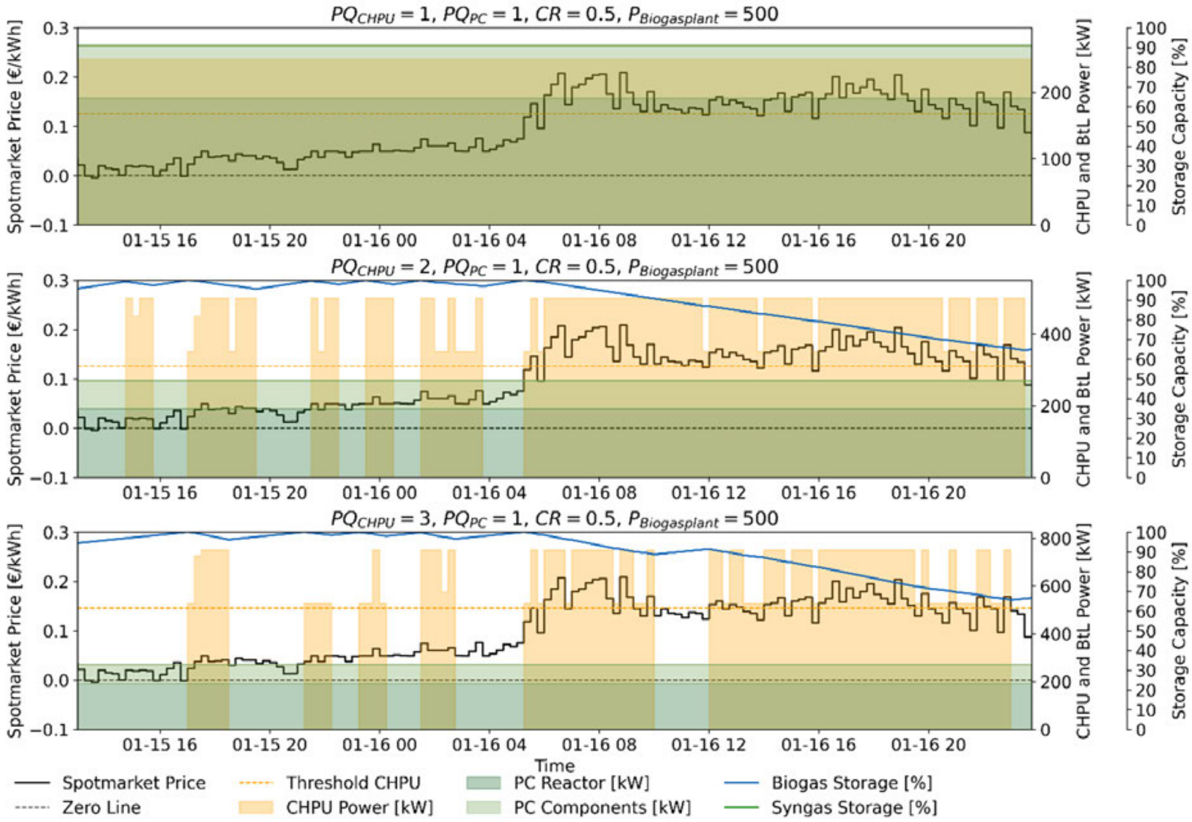

Figure 9.8: Influence of CHPU overbuilding on the operation of both plants in combination.

Influence of the biogas consumption ratio

The evaluation of different biogas CRs for the combined operation of CHPU and BGtL plants shows that a higher allocation of biogas to the BGtL system (CR = 0.75) leads to a higher profit than the other configurations. This result can be explained mainly with the higher revenue from Syncrude sales in the BGtL pathway, which compensates the increased costs for investment and operation when this plant is bigger.

If the biogas consumption ratio is lower for the BGtL plant (CR = 0.25), the costs are also lower, but at the same time the revenue drops more strongly, so that the total profit is reduced. The proportional change of the Syncrude and electricity revenue with the biogas allocation shows that the economic result depends strongly on how the biogas is distributed between both plants.

This behavior fits well with the results of the single-operation simulations. There, the BGtL plant achieves a better performance than the CHPU, especially because of the higher syncrude price in this work. Therefore, by changing the biogas CR, it is possible to influence the economic performance of the combined system, and a higher share for the BGtL pathway is generally more advantageous under the assumptions of this study.

Discussion of the results of the main simulation

The main simulation combines all parameter variations and provides a comprehensive overview of the profitability landscape for the analyzed system concepts. The discussion here summarizes and contextualizes the effects already observed for the individual parameters.

It can be seen that the highest ROI values are achieved for large-scale BGtL plants in single-operation. This is mainly due to two factors: First, the syncrude sales price (3.325 €/$kg_{Syncrude}$) was kept constant for all plant sizes. Second, increasing the biogas plant size leads to a reduction in specific capital costs for all units (CHPU, PC reactor, and FTS), while the revenue from syncrude production does not decrease. Therefore, for a small 75 kW biogas plant, the chosen syncrude price is too low and results in negative ROIs; for a 500 kW plant, the ROI is only slightly positive, and for a 2,000 kW plant, the ROI becomes very high. This underlines that the plant scale has a significant effect on profitability and that, in reality, the syncrude price would probably decrease with increasing plant size.

Overbuilding of the BGtL plant itself is not profitable in the examined cases. The additional investment costs from overbuilding are not compensated by the reduction of electricity costs under the considered electricity price conditions. If the spot market prices are more volatil, overbuilding could become profitable, but under the present assumptions, this is not the case.

Combined operation, in which both the CHPU and the BGtL are operated together, is also less profitable than the single-operation of the BGtL. This is because the combined approach splits the available biogas between the two plants, so that both units are dimensioned smaller, leading to higher specific investment costs. Moreover, with the chosen syncrude price, the revenue from FT-syncrude is much higher than from electricity and heat, so a higher biogas CR for the BGtL plant further increases the ROI. Thus, the highest combined-plant ROIs are also reached when the BGtL is dimensioned as large as possible (high biogas CR), although these values still remain below the best single-operation values of the BGtL plant.

The heatmap visualization in Figure 8.6 clearly reflects these findings. Negative ROIs occur mainly for small plant sizes and for configurations where the syncrude share is low. The best ROI is always found at the largest plant size, with single-operation of the BGtL and no overbuilding. The effect of varying the overbuilding stages, biogas CR, and plant scale is clearly visible.

Overall, the results highlight that profitability is strongly dependent on the chosen syncrude price, the scale of the plant, and the biogas distribution between the units. Under the current assumptions, the combination of both plants does not bring an advantage over the single-operation of a large BGtL plant. The underlying economic drivers are the scaling behavior of specific investment costs and the FT-Syncrude price.

Discussion of the optimal FT-Syncrude price

The simulation results show a clear relationship between Syncrude sales price, overbuilding level, and plant size regarding the economic viability of the BGtL plant in single-operation. As expected, the ROI increases linearly with higher Syncrude price for all plant sizes. At the same time, the influence of overbuilding on ROI is not linear: especially for the 2,000 kW plant, it can be observed that at low Syncrude prices, overbuilding even leads to an increase of ROI, although ROI remains negative in this region. This effect occurs because, at low Syncrude prices, the reduction in electricity costs due to flexible operation has a stronger impact on profit than the Syncrude revenue itself. However, when the Syncrude price rises, the positive effect of higher revenue outweighs the cost reduction from overbuilding, and the additional investment costs of overbuilding cause the ROI to decrease again, confirming the trend from the main simulation.

The results further demonstrate that the required Syncrude price to reach a positive ROI is strongly dependent on the plant size: larger biogas plants achieve a positive ROI already at lower Syncrude prices, while small plants require a significantly higher price. For example, the ROI for the 2,000 kW plant becomes positive at about 2.00 $€/\,kg_{Syncrude}$, for the 500 kW plant at approximately 2.50 $€/\,kg_{Syncrude}$, and for the 75 kW plant only at around 3.50 $€/\,kg_{Syncrude}$. The span of necessary Syncrude prices narrows for larger plants, indicating improved scaling effects with increasing capacity.

When the Syncrude price required to achieve a target ROI of 10 % is considered, it is clear that this target is most easily reached for large plants and without overbuilding. Overbuilding generally raises the minimum Syncrude price needed to reach economic viability. For instance, in the 2,000 kW scenario, the required Syncrude price for 10 % ROI ranges from 2.25 $€/\,kg_{Syncrude}$ (no overbuilding) to 2.44 $€/\,kg_{Syncrude}$ (triple overbuilding), while for the 75 kW plant, the price ranges from 4.02 $€/\,kg_{Syncrude}$ to 4.79 $€/\,kg_{Syncrude}$.

These results emphasize that plant scale and the selected Syncrude sales price are the decisive factors for the economic operation of a BGtL system. Overbuilding the PCU is only beneficial for ROI at very low Syncrude prices, which are not relevant for profitable operation. In all practical scenarios, the best economic results are achieved without overbuilding.

Discussion of the Required BGtL Flexibility Bonus

The simulation results make it clear that the flexibility bonus required to achieve economic viability for the BGtL plant in single-operation is significantly higher than for a typical CHPU. The necessary flexibility bonus decreases as the biogas plant size increases, reflecting the scaling advantages for larger installations. For the 2,000 kW plant, a flexibility bonus between 164 and 187 $€/\,kW_{PC,\,overbuilt}$ is sufficient to reach the 10 % ROI, while the 500 kW plant needs a bonus in the range of 340 to 379 $€/\,kW_{PC,\,overbuilt}$. For the smallest plant size of 75 kW, the required bonus rises to between 777 and 963 $€/\,kW_{PC,\,overbuilt}$.

In all cases, higher overbuilding factors result in a higher required flexibility bonus. This is because, with increased overbuilding, the additional investment and operational costs can no longer be compensated by electricity cost savings alone, especially at the Syncrude prices chosen for each plant size. The difference to the flexibility bonus for CHPUs, which is currently set at only 65 $€/\,kW_{CHPU,\,overbuilt}$, becomes clear: the values for the BGtL plant are considerably higher in every scenario. The reason for this is that overbuilding the BGtL plant involves not only the

PCU but also additional components such as a BGS and SGS, making the total investment more expensive.

In summary, the results show that the flexibility bonus which would be necessary to make overbuilding and therefore flexibilization of the PCU attractive, needs to be higher than the flexibility bonus currently paid for a CHPU. Furthermore, the required bonus depends strongly on the plant size and could be set lower for larger plants.

Discussion of the simulation with optimal Syncrude price and Flexibility Bonus

The results of this final simulation make it clear that, even when the Syncrude price and the flexibility bonus are chosen specifically to create similar ROI levels for both BGtL and CHP units in single operation, the combined operation of both units does not lead to higher economic performance. The ROI values found for the combined operation are consistently below those for the respective single-operation cases. This effect is visible for all combinations of overbuilding factors that were tested.

One main reason for this observation is the division of the available biogas between the two plants. When the total biogas is split equally (Biogas CR = 0.5), both the BGtL and CHP units are dimensioned smaller than in the single-operation scenarios. This reduced size leads to higher specific investment costs. At the same time, the potential benefits from increased operational flexibility and the additional revenue from electricity sales do not compensate for the additional capital expenditure.

In summary, these results confirm the findings of the main simulation: under the assumptions and market conditions used for this work, the single-operation of a BGtL plant or a CHPU is more economically attractive than a combination of both, even when the parameters are chosen so that both plants achieve approximately the same ROI in single-operation.

Summary of the results

The main objective of this work was to evaluate whether the combination of a BGtL plant and a CHPU could improve overall profitability. The initial hypothesis was that the flexible electricity production from the CHPU would increase revenues during periods of high electricity prices, while the BGtL plant could benefit from lower electricity costs during periods with low or negative prices, resulting in a higher overall ROI, then in the single-operation. To test this, all configurations were simulated for the calendar year 2023.

However, the results clearly contradict this hypothesis: in every scenario—regardless of biogas plant size or biogas CR—the combined operation yields a lower ROI than the respective single-operation of either unit, provided that each single-operation case is designed for comparable ROI levels (see Figure 8.10). Two main reasons explain this outcome:

First, total investment costs increase under the combined configuration. Although each individual system is downsized (for example, to half capacity when $\text{Biogas}_{\text{CR}} = 0.5$), the specific investment cost per kilowatt (€/kW) for the CHPU, PCU, and FTS rises, leading to higher overall investment costs.

Second, the electricity price volatility in 2023 was not high enough and negative prices were observed only for about 420 hours (see Figure 9.2). While the combined system does manage to lower part of the BGtL plant's electricity costs, the high fixed remuneration for the CHPU (0.18 €/kWh) was exceeded in only 370 hours. As a result, additional revenues from flexibilization remain marginal. The reduction in electricity costs and only slightly increased electricity revenues could not compensate for the higher investment costs.

Under the market conditions of 2023, combined operation is therefore less economical than single-operation. Nevertheless, both historical and projected data suggest that electricity price volatility will continue to rise in the future due to further expansion of renewable energy (see Figure 1.2 and [4–6]). At the same time, investment costs for FTS plants are expected to decrease [132].

In conclusion, a follow-up study using future electricity market data could investigate whether, under higher price volatility and lower capital costs, the combined BGtL–CHPU configuration might become financially attractive.

9.2 Comparison of the results with literature values

In this chapter, the results are compared with values from the literature. The single-operation CHPU results are benchmarked against literature data to assess their plausibility. Since the BGtL plant employing PC is a novel technology, a direct comparison with literature values is not possible. Instead, the evaluated FT-syncrude prices are compared with prices of other BtL-derived FT products, as well as with the current and projected future costs of conventional jet fuel.

Comparison of the CHPU Single-Operation Results

Schröer and Latacz-Lohmann also found that flexibilizing / overbuilding a CHPU only increases profit through the flexibility bonus; higher electricity market prices have negligible impact on profitability [133]. Haensel et al. concluded that a fourfold overbuild of the CHPU in single-operation yields the highest profit, primarily due to the larger flexibility bonus and decreasing specific capital costs [134]. These findings support the result that the flexibility bonus is the main driver of higher ROI under overbuilding.

Comparison of the FT-Syncrude prices with literature values

To compare the calculated syncrude price with current and projected jet fuel prices, the syncrude price must be adjusted by adding upgrading costs to obtain the jet fuel cost. It is assumed that upgrading would add an additional 5% to the base syncrude cost [26, 114]. Consequently, for the large biogas plant (2,000 kW) in single-operation mode, the resulting jet fuel price is approximately 2.36 €/kg; for the medium plant (500 kW), 2.90 €/kg; and for the small plant (75 kW), 4.22 €/kg.

Literature shows that synthetic FT-fuel prices fluctuate widely, ranging from 1.40 to 5.80 €/kg [25–27]. Thus, 2.36 €/kg for the large plant and 2.90 €/kg for the medium plant lie in the lower end of the spectrum, while 4.22 €/kg for the small plant is at the upper end.

Conventional jet fuel currently trades at about 0.50 €/L [135–137]. With a density of approximately 0.82 kg/L [138], this equals 0.61 €/kg. The CO_2 price is currently around 70 €/t [139] and is expected to rise by 2050, though the exact level is uncertain. Many projections assume an increase to 250 USD/tCO_2 [140]. However, recent studies indicate that the CO_2 removal rate in 2050 will determine the required price: if 7 GtCO_2/yr can be removed, 250 USD/tCO_2 suffices; if only 2 GtCO_2/yr, prices must exceed 600 USD/tCO_2 to achieve net zero [141].

Combustion of 1 kg jet fuel emits 3.16 kg CO_2 [142]. Thus, at 70 USD/tCO_2, the CO_2 surcharge is 0.22 USD/kg jet fuel; at 250 USD/tCO_2, 0.79 USD/kg; and at 600 USD/tCO_2, 1.90 USD/kg. With an average €/USD exchange rate of 0.895 over the past decade [143], and the base jet fuel price of 0.61 €/kg, the total cost (with a CO_2 price of 70 USD/tCO_2) is about 0.80 €/kg. If CO_2 costs 250 USD/tCO_2, the price rises to 1.32 €/kg; at 600 USD/tCO_2, 2.31 €/kg.

Compared with today's jet fuel price of 0.80 €/kg, even the lowest syncrude-based price (2.36 €/kg for the large plant) is nearly three times higher. With a CO_2 price of 250 USD/tCO_2, the total of 1.32 €/kg remains roughly half of 2.36 €/kg. Only under a CO_2 price of 600 USD/tCO_2 would the two costs converge.

As noted earlier, the syncrude production cost strongly depends on spot market volatility. With increasing renewable capacity and more negative price periods, electricity costs for BtL and BGtL operations are expected to decline, and capital costs are likely to fall as technologies mature—both reducing syncrude prices. Therefore, further simulations under alternative future electricity market scenarios are recommended to quantify their impact on syncrude production costs.

9.3 Critical Discussion of the Model's Key Assumptions

In this chapter, the critical assumptions of the thesis are discussed.

Assumptions Regarding the PC Reactor

The PC technology is novel and sparsely documented in the literature. Moreover, the planned pilot plant of the Plasma2X project was still under design at the time of this thesis, so no operational data were available. Consequently, several assumptions were made for the reactor that should be validated once the pilot plant is commissioned. A key assumption is that the PC reactor can be operated flexibly, with startup and shutdown times so short as to be negligible—an assumption made both because no literature values exist and to simplify the model and reduce simulation time. A PC reactor lifetime of 20 years were also assumed, which cannot yet be confirmed due to the technology's novelty. Finally, the reactor's capital costs were estimated via an experience curve and cost-scaling function, since only approximate investment figures for the Plasma2X pilot plant were available.

Simulation Period Limited to One Year

All simulations cover only the calendar year 2023. A forecast of future electricity markets was omitted to keep the scope manageable for a master's thesis. However, the electricity market is rapidly evolving, and volatility is expected to increase further with additional renewable capacity. Therefore, re-running the simulations using projected future market data would be valuable to determine whether higher volatility and more frequent negative prices could make combined operation more profitable than single-operation, and whether FT-syncrude costs in single-operation could decrease.

Biomass Substrate Costs

The results show that substrate costs account for a large share of total costs and become the dominant cost factor for large plants. This work used the German national average substrate mix; alternative feedstock compositions may be cheaper or more expensive, affecting gas composition and costs. Exploring such variations using the existing program code would be a good extension.

Specific Investment Costs CHPU

For the investment costs of the CHPUs, only two sources were available, resulting in a limited data set for curve fitting. Furthermore, the data from these sources varied significantly, leading to a fitted curve that in some cases deviates considerably from the actual values (see Figure 5.2). However, the focus of this thesis was not on the CHPUs but rather on the BGtL plant. Nevertheless, the curve fitting could be repeated with a larger data set in future work.

Specific Investment Costs FTS

Although the fitted curve for the FTS investment cost correlates well with the available data, it should be noted that the reference FTS plants identified in the literature have significantly higher capacities than those considered in this thesis. Unfortunately, no cost data could be found for smaller-scale FTS units. Due to the strong correlation of the fit and the lack of relevant data for small-scale FTS, the resulting formula was nevertheless applied in this study. However, if cost data for smaller-scale plants become available in the future, the curve fitting should be updated accordingly.

Assumptions Regarding Membrane Separation

For the membrane separation step it is assumed, for simplicity, that the membranes operate with 100 % separation efficiency. In reality such perfect performance is not achievable: a small share of the target components will not permeate completely and must be recycled to the compressor upstream of the membrane unit. This recycle stream increases the volumetric flow rate and thus the electric power demand of the compressor, meaning that the PCU total energy use will be somewhat higher than the model predicts. However, the additional load is expected to remain modest, so the idealised assumption was considered acceptable for the present study. Once the Plasma2X pilot plant is in operation, real data should replace this simplification to quantify the true impact on the energy balance.

9.4 Critical Discussion of Biogas Use for Synthetic Fuel Production

This chapter critically examines the use of biogas for synthetic fuel production. The simulations indicate that synthetic fuel production via the novel BGtL route is promising and, depending on the FT-syncrude price, can compete with the CHPU. However, combining both units currently yields lower profits than running each in single-operation. If not combined, the units compete for finite biogas feedstock, which otherwise helps stabilize the electricity grid as one of the few flexible renewable sources. Therefore, it is crucial to assess whether diverting large shares of biogas to fuel production would compromise grid stability.

Finally, synthetic fuels should be reserved for applications requiring high energy density—such as aviation and certain maritime uses—until battery technology matures. Batteries currently offer better overall energy efficiency [144], and research is underway to improve battery energy density for aviation [145–149]. Thus, synthetic fuels serve as a transitional technology.

Finally, the model's boundaries must be clearly defined to highlight opportunities for future research. This thesis built the model on the current state of knowledge and confined all simulations to the completed calendar year 2023, using actual market data from that period. The code, however, is fully parameterized and can be adapted to any other year or scenario of different parameters.

In future work, it would be valuable to run the model with projected electricity-market data reflecting higher renewable electricity share and increased price volatility, in order to assess how more extreme price swings and negative price events might affect BGtL plant operation and FT-syncrude production costs. Similarly, it could investigate whether, under such market conditions, combined CHPU–BGtL operation could outperform single-operation by exploiting dynamic arbitrage. Once the Plasma2X pilot plant is commissioned, its actual operational flexibility (startup and shutdown times) should be validated, and scenario analyses exploring a range of reactor lifetimes and capital cost levels should be performed to quantify their impact on ROI. Varying the biomass feedstock mix (for example, increasing or decreasing shares of manure, energy crops, or residues) would reveal how changes in gas composition influence biogas composition and price. Finally, extending the synthesis module to include methanol (or other e-fuel) pathways alongside Fischer–Tropsch would allow a direct techno-economic comparison of alternative BGtL products and help identify the most promising route.

A further promising direction for future research is to expand the model in order to optimize not only for profit, but also for system-supportiveness or grid-friendliness. In this thesis, nationwide spot market prices for Germany were used. However, a system-friendly optimization would need a more regional approach. For example, with high-resolution residual load data (ideally with 15-minute resolution) from a specific location, it would be possible to design an optimization that considers both economic performance and the positive impact on local grid stability and renewable integration. Including such regional and system-level objectives in the model could give a deeper understanding of how flexible BGtL and CHPU operation can support the energy transition beyond just profitability. This topic, which was not yet considered in the present thesis, is a valuable idea for future academic work.

10 Summary

The main objective of this thesis was to systematically analyze the technical and economic potential of a flexible biogas plant system that combines a Biogas-to-Liquid (BGtL) plant—using a flexible microwave plasma cracking (PC) and Fischer-Tropsch synthesis (FTS)—with a flexible Combined Heat-and-Power Unit (CHPU). This topic is highly relevant for the energy transition, as sectors like aviation and heavy transport need sustainable fuels. The idea is to use the carbon in biogas more efficiently and to create a system that can produce electricity and heat when electricity spot market prices are high, or convert biogas into FT-syncrude when electricity spot market prices are low or negative, thus increasing profitability through arbitrage.

A gap in current research is that, although flexible CHPU operation is common and even mandatory for large systems in Germany, and extensive literature exists on Biomass-to-Liquid (BtL) technologies and plant optimization, the combination of these two systems has not been studied in detail. Furthermore, there is currently no BGtL technology that converts biogas into syngas in a single process step, which the novel PC technology can achieve.

In this thesis, a deterministic multi-period Mixed-Integer Linear Programming (MILP) model was developed in Python using the Pyomo package. The model simulates plant operation for one year with a time resolution of 15 minutes, based on real electricity prices from the German market in 2023. It includes all significant technical, economic, and market constraints, such as plant sizes, storage management, unit commitment logic, and investment and operational costs. Special attention was given to realistically representing the new PC technology through thermodynamic calculations for all process steps. The model allows simulation of different scenarios by varying system parameters, such as biogas plant size, overbuilding factors for CHPU and BGtL, and the biogas consumption ratio between the two routes.

The thesis begins with an overview of biogas production and utilization in Germany, followed by a description of the reference system with the BGtL plant in more detail. After outlining the basics, the methodology is described. An essential part of the methodology involved researching simulation parameters. All relevant technical and economic parameters were derived from literature, current market data, and own thermodynamic calculations when necessary. Additionally, the MILP model, program code, and simulation procedure are explained.

It was found that both standalone CHPU and BGtL operations can be profitable, but for different reasons. The CHPU achieves higher ROIs through overbuilding because of the flexibility bonus, making flexible operation advantageous. In contrast, BGtL achieves the highest ROI when not overbuilt, thus not operated flexibly. This is mainly because BGtL plants consist of more individual units, significantly increasing investment costs with overbuilding, outweighing any reduction in electricity costs through flexible operation.

The combined operation results were simulated extensively across various expansion scenarios. In all tested configurations and market conditions for 2023, combined operation yielded lower returns compared to single operations. This was primarily due to two reasons: combining both plant types resulted in smaller-sized plants, increasing specific investment costs compared to single operations, and electricity price volatility in 2023 was insufficient to compensate for this. Although the electricity costs of the BGtL plant decrease when the plants are combined, this is mainly because, in combined operation, the CHPU takes over production during long periods of high electricity market prices. In contrast, in single operation, the BGtL must run during these times due to storage dynamics. However, the combination has hardly any positive effect on the revenue from electricity sold by the CHPU, because the chosen remuneration value is so high that there are very few periods when the market price actually exceeds this value. As a result, the increase in investment costs due to combining the plants is greater than the reduction in BGtL electricity costs or any increase in CHPU electricity revenue.

Further simulations determined optimal FT-syncrude prices and flexibility bonuses for the BGtL plant to achieve profitable overbuilding of the BGtL plant. Results indicated lower FT-syncrude prices could be viable for larger plants, with production costs ranging from 2.25 $€/kg_{\text{Syncrude}}$ for a 2,000 kW biogas plant, 2.76 $€/kg_{\text{Syncrude}}$ for a 500 kW biogas plant, and 4.02 $€/kg_{\text{Syncrude}}$ for a 75 kW biogas plant without overbuilding and in single-operation. The costs of large-scale plants are therefore competitive compared to values reported in the literature for sustainable FT-syncrudes. Considering increasing electricity market volatility and declining FTS investment costs, future production costs may decrease further. The flexibility bonus needed for profitable flexible operation is much higher than the current bonus for standard CHPU units, highlighting the need for specific incentives to support flexible BGtL operation.

Overall, the thesis finds that the current rules and market conditions in Germany usually support either flexible electricity production or synthetic fuel production as separate business models. However, this could change in the future. If electricity prices become more volatile, the share of renewable energy keeps rising, BGtL technologies are scaled up, and investment costs—especially for FTS—continue to fall, then using biogas flexibly for both electricity and fuel production could become a real competitive advantage. This work gives a solid quantitative basis and a transparent model that can be used for further technical and economic studies, as well as for optimizing future hybrid biogas plants.

Outlook

Building on the findings and methodological foundations of this thesis, future research offers possibilities for deepening both the scientific understanding and the practical deployment of hybrid biogas systems. One important next step is to adapt the optimization framework developed in this thesis to future electricity market scenarios. As the share of volatile renewable energies increases, forecasts up to 2045 predict substantially higher price volatility and more frequent periods of negative or extremely low electricity prices. Integrating such market data into the optimization model could reveal new threshold values and operational windows in which the combined operation of BGtL and CHPU units becomes not only technically, but also economically advantageous.

A second important topic is the use of real operational data from the PC Reactor. As soon as the

Plasma2X pilot plant provides operational data, it will be crucial to revise model assumptions regarding start-up and ramp times, efficiencies and operational lifetimes. This will help to make future simulations more realistic.

A further important research area concerns the expansion of the modeled product portfolio and system boundaries. Future modeling work should not be limited to Fischer–Tropsch products, but should also encompass alternative synthetic fuel pathways such as methanol.

Another interesting direction for future research is to further develop the model so that it optimizes not only for profit, but also for grid support and system integration. In this thesis, the focus was on nationwide spot market prices for Germany. For a more system-oriented approach, a regional perspective would be necessary. Using high-resolution residual load data from a specific area (ideally with 15-minute intervals), it would be possible to design an optimization that takes into account both economic results and positive effects on local grid stability and renewable energy integration. By including these grid support targets, the model could provide deeper insights into how flexible BGtL and CHPU operations can contribute to the energy transition—not just in terms of profitability. This aspect was not yet covered in the present thesis, but it offers valuable potential for future academic work.

A additional important point for future research is to look at changing biomass prices and different feedstock mixes. The simulations showed that, especially for large plants, the cost of biogas feedstock is often the biggest expense. If the type or mix of biomass changes, both the cost and the composition of the biogas will change as well. Studying such scenarios would therefore be very interesting and should be explored in future work.

In summary, the findings of this thesis show that, with the current electricity market, running BGtL or CHPU units in single operation is more profitable than the combination of both systems. But reducing investment costs and a changing spot market could make combined systems more attractive in the future. Therefore, future research should focus on the interaction of these factors to support the role of flexible, sustainable biogas plants in the energy transition for both flexible electricity and synthetic fuel production.

References

[1] I. T. Forum. The Potential of E-fuels to Decarbonise Ships and Aircraft. Tech. rep. Paris: OECD, 2023-01. DOI: 10.1787/3d96e0d9-en.

[2] R. Rajasegar, C. Mitsingas, E. Mayhew, Q. Liu, T. Lee, and J. Yoo. Development and Characterization of Additive-Manufactured Mesoscale Combustor Array. In: *Journal of Energy Engineering*, vol. 144. DOI: 10.1061/(ASCE)EY.1943-7897.0000527.

[3] E. Billig, M. Decker, W. Benzinger, F. Ketelsen, P. Pfeifer, R. Peters, D. Stolten, and D. Thrän. Non-Fossil CO2 Recycling—The Technical Potential for the Present and Future Utilization for Fuels in Germany. In: *Journal of CO2 Utilization*, vol. 30, pp. 130–141. ISSN: 2212-9820. DOI: 10.1016/j.jcou.2019.01.012.

[4] vbw and Prognos. Strompreisprognose bis 2045. 2024-09. [Online]. Available: https://www.vbw-bayern.de/vbw/Themen-und-Services/Energie-Klima/Energie/Neue-Strompreisprognose-bis-2040.jsp. (visited on 2025-06-13).

[5] V. Grimm, A. Ockenfels, L. Hirth, and K. Müller. Strommarkt – Balance zwischen Wettbewerbsfähigkeit, Nachhaltigkeit und Bezahlbarkeit | Aufsatz in Zeitschrift | ifo Institut. In: *ifo Schnelldienst*, no. 03/2025.

[6] BDEW. Ein langfristiges Marktdesign für Deutschland. In: Berlin, 2023-03.

[7] D. Chiaramonti and L. Testa. Deploying EU Biomethane Potential for Transports: Centralized/Decentralized Biogasrefinery Schemes to SAF and Maritime Fuels. In: *Applied Energy*, vol. 366, p. 123306. ISSN: 0306-2619. DOI: 10.1016/j.apenergy.2024.123306.

[8] D. Moodley. *On the Deactivation of Cobalt-Based Fischer-Tropsch Synthesis Catalysts.* Eindhoven, 2008-11. ISBN: 978-90-386-1399-4.

[9] M. Senden, F. Martens, W. Steenge, and R. Klein Nagelvoort. Shell's GTL: Its Technology and Design, Its Operation and Products. In: *International Petroleum Technology Conference*. OnePetro, 2005-11. DOI: 10.2523/IPTC-10683-MS.

[10] R. A. Fiato and P. W. Sibal. ExxonMobil's Advanced Gas-to-Liquids Technology–AGC-21. In: *SPE Middle East Oil and Gas Show and Conference*. OnePetro, 2005-03. DOI: 10.2118/93653-MS.

[11] R. Carapellucci and L. Giordano. Steam, Dry and Autothermal Methane Reforming for Hydrogen Production: A Thermodynamic Equilibrium Analysis. In: *Journal of Power Sources*, vol. 469, p. 228391. ISSN: 0378-7753. DOI: 10.1016/j.jpowsour.2020.228391.

[12] L. Testa. "Towards Sustainable Biofuels Production for Aviation and Maritime". PhD thesis. Turin: Politecnico di Torino, 2024.

[13] T. K. Poddar, G. G. Zaimes, S. Kar, D. M. Walker, and T. R. Hawkins. Life Cycle Analysis of Fischer-Tropsch Diesel Produced by Tri-Reforming and Fischer-Tropsch Synthesis (TriFTS) of Landfill Gas. In: *Environmental Science & Technology*, vol. 57, no. 48, pp. 19602–19611. ISSN: 1520-5851. DOI: 10.1021/acs.est.3c02162.

[14] S. T. Wismann et al. Electrified Methane Reforming: A Compact Approach to Greener Industrial Hydrogen Production. In: *Science*, vol. 364, no. 6442, pp. 756–759. DOI: 10.1126/science.aaw8775.

[15] J. Baltrusaitis and W. L. Luyben. Methane Conversion to Syngas for Gas-to-Liquids (GTL): Is Sustainable CO2 Reuse via Dry Methane Reforming (DMR) Cost Competitive with SMR and ATR Processes? In: *ACS Sustainable Chemistry & Engineering*, vol. 3, no. 9, pp. 2100–2111. DOI: 10.1021/acssuschemeng.5b00368.

[16] A. M. Ranjekar and G. D. Yadav. Dry Reforming of Methane for Syngas Production: A Review and Assessment of Catalyst Development and Efficacy. In: *Journal of the Indian Chemical Society*, vol. 98, no. 1, p. 100002. ISSN: 0019-4522. DOI: 10.1016/j.jics.2021.100002.

[17] X. Zhao, A. Naqi, D. M. Walker, T. Roberge, M. Kastelic, B. Joseph, and J. N. Kuhn. Conversion of Landfill Gas to Liquid Fuels through a TriFTS (Tri-Reforming and Fischer–Tropsch Synthesis) Process: A Feasibility Study. In: *Sustainable Energy & Fuels*, vol. 3, no. 2, pp. 539–549. ISSN: 2398-4902. DOI: 10.1039/C8SE00344K.

[18] S. Soleimani and M. Lehner. Tri-Reforming of Methane: Thermodynamics, Operating Conditions, Reactor Technology and Efficiency Evaluation—A Review. In: *Energies*, vol. 15, no. 19, p. 7159. ISSN: 1996-1073. DOI: 10.3390/en15197159.

[19] N. Posdziech. Research into Sustainable PtL Fuel Production in the Face of Electricity Fluctuations at Industriepark Höchst Frankfurt/Main. 2022. [Online]. Available: https://www.now-gmbh.de/en/news/pressreleases/3-4-million-euro-funding-commitment-for-repose-e-fuel-project/ (visited on 2025-07-01).

[20] T. U. Hamburg. PowerFuel – Demonstration Und Potentialanalyse Neuer Technologien Zur Sektorkopplung Für Die Erzeugung von Synthesekraftstoff Aus Kohlenstoffdioxid. 2021. [Online]. Available: https://www.tuhh.de/iue/forschung/projekte/powerfuel.

[21] Production of Sustainable Aircraft Grade Kerosene from Water and Air Powered by Renewable Electricity, through the Splitting of CO2, Syngas Formation and Fischer-Tropsch Synthesis | KEROGREEN | Projekt | Fact Sheet | H2020. 2022. [Online]. Available: https://cordis.europa.eu/project/id/763909.

[22] KIT. Klimaneutralität: Schiffstreibstoff aus Abwasser. 2025-03. [Online]. Available: https://www.kit.edu/kit/pi%5C_2025%5C_023%5C_klimaneutralitat-schiffstreibstoff-aus-abwasser.php (visited on 2025-06-19).

[23] atmosfair. Deutschland: Grünes E-Kerosin. [Online]. Available: https://www.atmosfair.de/de/klimaschutzprojekte/ptl-e-kerosin/ptl-anlage/ (visited on 2025-06-19).

[24] HAW Hamburg. Skalierbare Erzeugung Regenerativer Flüssiger Kraftstoffe Mit Niedertemperatur-Mikrowellen-Plasma – Plasma2X. 2023. [Online]. Available: https://www.haw-hamburg.de/forschung/forschungsprojekte-detail/project/project/show/plasma2x/ (visited on 2025-07-13).

[25] D. Huber. "Multi-Objective Heat Exchanger Network Synthesis: Simultaneous Optimization of Heat Integration and Process Design". Thesis. Technische Universität Wien, 2024. DOI: 10.34726/hss.2024.104883.

[26] A. Soler et al. *E-Fuels: A Techno-Economic Assessment of European Domestic Production and Imports towards 2050 – Update*. Brussels, 2024-03. ISBN: 978-2-87567-184-4.

[27] dena. E-Kerosene for Commercial Aviation. 2022. [Online]. Available: https://www.dena.de/infocenter/e-kerosene-for-commercial-aviation/ (visited on 2025-05-06).

[28] N. Nadja, V. Denysenko, and J. Daniel-Gromke. Biogaserzeugung und -nutzung in Deutschland: Report zum Anlagenbestand Biogas und Biomethan. In: vol. DBFZ Report, no. 50, VII, 9–122 pages. DOI: 10.48480/ZPTB-YY32.

[29] FNR. Flexibilisierung von Biogasanlagen. [Online]. Available: https://biogas.fnr.de/biogas-nutzung/stromerzeugung/flexibilisierung-von-biogasanlagen.

[30] FNR. Speicherkraftwerk im Hochschwarzwald versorgt 250 Haushalte mit Wärme. 2022-11. [Online]. Available: https://www.fnr.de/presse/pressemitteilungen/archiv/archiv-nachricht/speicherkraftwerk-im-hochschwarzwald-versorgt-250-haushalte-mit-waerme (visited on 2025-06-25).

[31] FNR. Biogas-Speicherkraftwerke: flexibler Strom und kommunale Wärme aus heimischen Rohstoffen. 2023-07. [Online]. Available: https://biogas.fnr.de/service/presse/presse/aktuelle-nachricht/biogas-speicherkraftwerke-flexibler-strom-und-kommunale-waerme-aus-heimischen-rohstoffen (visited on 2025-06-25).

[32] G. Chen, O. Lugovoy, P. Piris-Cabezas, and A. Stratton. *Intermittent Production of Electricity-Based Synthetic Jet Fuel as a Demand-Side Management Strategy for Grid Decarbonization*. SSRN Scholarly Paper. Rochester, NY, 2024-11. DOI: 10.2139/ssrn.5029916.

[33] L. Collins. World's First Large-Scale Green Methanol Plant Officially Inaugurated. 2025-5. [Online]. Available: https://www.hydrogeninsight.com/innovation/worlds-first-large-scale-green-methanol-plant-officially-inaugurated/2-1-1818687 (visited on 2025-06-24).

[34] M. S. Taslimi, A. Khosravi, Y. K. Nugroho, and N. G. M. Rytter. Optimization and Analysis of Methanol Production from CO2 and Solar-Driven Hydrogen Production: A Danish Case Study. In: *International Journal of Hydrogen Energy*, vol. 69, pp. 466–476. ISSN: 0360-3199. DOI: 10.1016/j.ijhydene.2024.05.033.

[35] M. Dotzauer. Determining Optimal Component Configurations for Flexible Biogas Plants Based on Power Prices of 2020–2022 and the Legislation Framework in Germany. In: *Renewable Energy*, vol. 236, p. 121252. ISSN: 0960-1481. DOI: 10.1016/j.renene.2024.121252.

[36] J. Güsewell, L. Eltrop, and K. Hufendiek. Seasonal Flexibilisation: A Solution for Biogas Plants to Improve Profitability. In: *Advances in Applied Energy*, vol. 2, p. 100034. ISSN: 2666-7924. DOI: 10.1016/j.adapen.2021.100034.

[37] FNR. Substrateinsatz in Biogasanlagen. 2024. [Online]. Available: `https://mediathek.fnr.de/grafiken/bioenergie/biogas/substrateinsatz-in-biogasanlagen.html` (visited on 2024-12-10).

[38] S. Majer, P. Kornatz, J. Daniel-Gromke, N. Rensburg, A. Brosowski, K. Oehmichen, and J. Liebetrau. *Stand Und Perspektiven Der Biogaserzeugung Aus Gülle*. Leipzig: DBFZ, 2019. ISBN: 978-3-946629-48-1.

[39] Y. Li et al. Composition and Toxicity of Biogas Produced from Different Feedstocks in California. In: *Environmental Science & Technology*, vol. 53, no. 19, pp. 11569–11579. ISSN: 1520-5851. DOI: `10.1021/acs.est.9b03003`.

[40] A. Lallement, C. Peyrelasse, C. Lagnet, A. Barakat, B. Schraauwers, S. Maunas, and F. Monlau. A Detailed Database of the Chemical Properties and Methane Potential of Biomasses Covering a Large Range of Common Agricultural Biogas Plant Feedstocks. In: *Waste*, vol. 1, no. 1, pp. 195–227. ISSN: 2813-0391. DOI: `10.3390/waste1010014`.

[41] *The Biofuels Handbook*. The Royal Society of Chemistry, 2011-07. ISBN: 978-1-84973-026-6. DOI: `10.1039/9781849731027`.

[42] W. Hermeling, K. Nachtmann, and F. Scholwin. *Biogas – ein Taschenbuch für die Erzeugerpraxis: Erzeugerwissen, Aufbereitung und Vermarktung*. Wiesbaden: Springer Fachmedien, 2023. ISBN: 978-3-658-39604-6 978-3-658-39605-3. DOI: `10.1007/978-3-658-39605-3`.

[43] L. Ackermann, N. Gabrek, B. Zachmann, A. Neitz-Regett, and S. Seifermann. Cost-Benefit Analysis and Comparison of Grid-Stabilizing Energy Flexibility Options and Their Applications in Relation to the German Energy System. In: *Renewable Energy Focus*, vol. 49, p. 100570. ISSN: 1755-0084. DOI: `10.1016/j.ref.2024.100570`.

[44] Fachagentur Nachwachsende Rohstoffe, Deutsches Biomasseforschungszentrum, Kuratorium für Technik und Bauwesen in der Landwirtschaft, and Institut für Agrartechnologie und Biosystemtechnik, eds. *Leitfaden Biogas: von der Gewinnung zur Nutzung*. 7. Auflage. Bioenergie. Rostock: Druckerei Weidner, 2016. ISBN: 978-3-00-014333-5.

[45] J.-M. Kapust. "Modellierung Einer Power to Liquid-Anlage Mit Einer Mikrowellen-Plasmalyse Als Gaswandlungstechnologie Und Anschließender Fischer-Tropsch-Synthese". PhD thesis. Hamburg: HAW Hamburg, 2023-04.

[46] F. Grzegorzewski. Influence of Non-Thermal Plasma Species on the Structure and Functionality of Isolated and Plant-based 1,4-Benzopyrone Derivatives and Phenolic Acids. In: DOI: `10.14279/depositonce-2778`.

[47] C. Tendero, C. Tixier, P. Tristant, J. Desmaison, and P. Leprince. Atmospheric Pressure Plasmas: A Review. In: *Spectrochimica Acta Part B: Atomic Spectroscopy*, vol. 61, no. 1, pp. 2–30. ISSN: 0584-8547. DOI: `10.1016/j.sab.2005.10.003`.

[48] M. Sterner and I. Stadler, eds. *Energiespeicher - Bedarf, Technologien, Integration*. Berlin, Heidelberg: Springer, 2017. ISBN: 978-3-662-48892-8. DOI: `10.1007/978-3-662-48893-5`.

[49] S. S. Ail and S. Dasappa. Biomass to Liquid Transportation Fuel via Fischer Tropsch Synthesis – Technology Review and Current Scenario. In: *Renewable and Sustainable Energy Reviews*, vol. 58, pp. 267–286. ISSN: 1364-0321. DOI: 10.1016/j.rser.2015.12.143.

[50] D. Schröder. "Herstellung kurz- und mittelkettiger Olefine durch Fischer-Tropsch-Synthese". PhD thesis. Bayreuth, 2022.

[51] M. Grüner. "Experimental Studies on Fischer-Tropsch Synthesis in a Millistructured Reactor". Thesis. Technische Universität Wien, 2022. DOI: 10.34726/hss.2022.91286.

[52] L. Guo, J. Sun, Q. Ge, and N. Tsubaki. Recent Advances in Direct Catalytic Hydrogenation of Carbon Dioxide to Valuable C2+ Hydrocarbons. In: *Journal of Materials Chemistry A*, vol. 6, no. 46, pp. 23244–23262. ISSN: 2050-7496. DOI: 10.1039/C8TA05377D.

[53] Y. H. Choi, Y. J. Jang, H. Park, W. Y. Kim, Y. H. Lee, S. H. Choi, and J. S. Lee. Carbon Dioxide Fischer-Tropsch Synthesis: A New Path to Carbon-Neutral Fuels. In: *Applied Catalysis B: Environmental*, vol. 202, pp. 605–610. ISSN: 0926-3373. DOI: 10.1016/j.apcatb.2016.09.072.

[54] H. Zachariassen and J.-M. Kapust. *Plasma2X Anlagenbeschreibung*. 2024.

[55] G. Schaumann and K. W. Schmitz. Investitionsrechnungen – Betriebswirtschaftliche Grundlagen. In: *Kraft-Wärme-Kopplung*. Ed. by G. Schaumann and K. W. Schmitz. Berlin, Heidelberg: Springer, 2010, pp. 245–285. ISBN: 978-3-642-01425-3. DOI: 10.1007/978-3-642-01425-3_6.

[56] U. Lassen. Fundamente und Finanzierungsbeziehungen. In: *Immobilienfinanzierung und -investition: Eine Einführung in Praxis und Theorie*. Ed. by U. Lassen. Berlin: Erich Schmidt Verlag GmbH & Co. KG, 2024, pp. 23–132. ISBN: 978-3-503-21266-8. DOI: 10.37307/b.978-3-503-21266-8.01.

[57] FNR. Faustzahlen. [Online]. Available: https://biogas.fnr.de/daten-und-fakten/faustzahlen (visited on 2024-10-01).

[58] FNR. Wirtschaftsdünger als Substrat in Biogasanlagen. 2024. [Online]. Available: https://mediathek.fnr.de/wirtschaftsdunger-als-substrat-in-biogasanlagen.html (visited on 2024-12-10).

[59] FNR. Energiepflanzenanbau für Biogas. 2023. [Online]. Available: https://mediathek.fnr.de/energiepflanzenanbau-fur-biogas.html (visited on 2024-12-10).

[60] N. Elhaus, P. Treiber, and J. Karl. Biogas im künftigen Energiesystem. In: *Lehrstuhl für Energieverfahrenstechnik*.

[61] W. Hermeling, K. Nachtmann, and F. Scholwin. Aufbau und Betrieb von Biogasanlagen. In: *Biogas – ein Taschenbuch für die Erzeugerpraxis: Erzeugerwissen, Aufbereitung und Vermarktung*. Ed. by W. Hermeling, K. Nachtmann, and F. Scholwin. Wiesbaden: Springer Fachmedien, 2023, pp. 31–66. ISBN: 978-3-658-39605-3. DOI: 10.1007/978-3-658-39605-3_2.

[62] P. P. Argalis and K. Veģere. (PDF) Perspective Biomethane Potential and Its Utilization in the Transport Sector in the Current Situation of Latvia. In: *ResearchGate*. DOI: 10.3390/su13147827.

[63] W. Nowak and J. Arthkamp. *BHKW-Grundlagen*. 2010-06.

[64] N. Elhaus, P. Treiber, and J. Karl. Studie Biogas im Energiesystem 2024. 2024-9. [Online]. Available: https://www.evt.tf.fau.de/faustudie%5C_biogasimenergiesystem2024/ (visited on 2024-12-10).

[65] F. Scholwin and J. Grope. Durchführbarkeitsstudie - Biogas als Kraftstoff aus landwirtschaftlichen und kommunalen Reststoffen in Neukirch/Lausitz. In.

[66] M. Heiermann. Biogas in der Landwirtschaft - Wirtschaftlichkeit von Biogasanlagen. In: *Ministerium für Ländliche Entwicklung, Umwelt und Verbraucherschutz des Landes Brandenburg*.

[67] D. M. Riley, J. Tian, G. Güngör-Demirci, P. Phelan, J. R. Villalobos, and R. J. Milcarek. Techno-Economic Assessment of CHP Systems in Wastewater Treatment Plants. In: *Environments*, vol. 7, no. 10, p. 74. ISSN: 2076-3298. DOI: 10.3390/environments7100074.

[68] P. Kaparaju and J. Rintala. Generation of Heat and Power from Biogas for Stationary Applications: Boilers, Gas Engines and Turbines, Combined Heat and Power (CHP) Plants and Fuel Cells. In: *The Biogas Handbook*. Ed. by A. Wellinger, J. Murphy, and D. Baxter. Woodhead Publishing Series in Energy. Woodhead Publishing, 2013-01, pp. 404–427. ISBN: 978-0-85709-498-8. DOI: 10.1533/9780857097415.3.404.

[69] T. Plankenbühler, S. Kolb, K. Herkendell, and J. Karl. *Screening Wasserstoff Technik*. Nürnberg, 2021-04.

[70] M. R. Atelge et al. A Critical Overview of the State-of-the-Art Methods for Biogas Purification and Utilization Processes. In: *Sustainability*, vol. 13, no. 20, p. 11515. ISSN: 2071-1050. DOI: 10.3390/su132011515.

[71] D. Deublein and A. Steinhauser. *Biogas from Waste and Renewable Resources: An Introduction, 2nd, Revised and Expanded Edition | Wiley*. 2011. ISBN: 978-3-527-64371-4. [Online]. Available: https://www.wiley.com/en-us/Biogas+from+Waste+and+Renewable+Resources%3A+An+Introduction%2C+2nd%2C+Revised+and+Expanded+Edition-p-9783527643714 (visited on 2024-09-16).

[72] E. Hoffmann. Machbarkeitsstudie für neue Umweltzeichen für die Produktgruppe: Kleine Blockheizkraftwerk-Module. In: Berlin: Umweltbundesamt, 2001.

[73] M. Dehli. Energieeinsparung durch die gekoppelte Erzeugung von Strom und Wärme mit Blockheizkraftwerken. In: *Energieeffizienz in Industrie, Dienstleistung und Gewerbe: Energietechnische Optimierungskonzepte für Unternehmen*. Ed. by M. Dehli. Wiesbaden: Springer Fachmedien, 2020, pp. 203–249. ISBN: 978-3-658-23204-7. DOI: 10.1007/978-3-658-23204-7_8.

[74] K. Rohrig, P. Hochloff, U. Holzhammer, F. Schlögl, W. Lehnert, K. Rehfeldt, J. Dieckmann, and L. Hofmann. Flexible Stromproduktion aus Biogas und Biomethan. In: DOI: 10.24406/publica-fhg-297987.

[75] energas. Zuverlässiges Blockheizkraftwerk - Energas. 2018-02. [Online]. Available: https://energas-gmbh.de/flexibilisierung/.

[76] Flexperten. Handlungsempfehlungen - kompakt. [Online]. Available: https://www.kwk-flexperten.net/handlungsempfehlungen-%5C%E2%5C%80%5C%93-kompakt (visited on 2025-05-07).

[77] S. Ishikawa, N. O. Connell, R. Lechner, R. Hara, H. Kita, and M. Brautsch. Load Response of Biogas CHP Systems in a Power Grid. In: *Renewable Energy*, vol. 170, pp. 12–26. ISSN: 0960-1481. DOI: 10.1016/j.renene.2021.01.120.

[78] EnBW. Direktvermarktung Strom: zuverlässig & transparent | interconnector.de. [Online]. Available: https://www.interconnector.de/direktvermarktung-strom/ (visited on 2024-12-04).

[79] EnBW. Umsatzsteuer in der Direktvermarktung: Wer muss diese ausweisen? - interconnector.de. 2019-10. [Online]. Available: https://www.interconnector.de/energieblog/direktvermarktung/umsatzsteuer-in-der-direktvermarktung-wer-muss-diese-ausweisen/ (visited on 2024-12-04).

[80] L. Energy. Maximieren Sie Ihre Erlöse mit der Strom Direktvermarktung. [Online]. Available: https://www.luox-energy.de/gewerbe/direktvermarktung (visited on 2025-01-27).

[81] Capital PV SAS. 10 häufige Fragen & Antworten zur Direktvermarktung Strom. 2024. [Online]. Available: https://www.direktvermarktungstrom.de/post/10-haufige-fragen-and-antworten (visited on 2025-01-27).

[82] Bundesnetzagentur. Ausschreibungsverfahren. [Online]. Available: https://www.bundesnetzagentur.de/DE/Fachthemen/ElektrizitaetundGas/Ausschreibungen/Biomasse/Ausschreibungsverfahren/start.html (visited on 2025-01-27).

[83] Bundesnetzagentur. Gebotstermin 1. November 2019. 2019. [Online]. Available: https://www.bundesnetzagentur.de/DE/Fachthemen/ElektrizitaetundGas/Ausschreibungen/Biomasse/BeendeteAusschreibungen/Gebotstermin%5C_01%5C_11%5C_2019/gebotstermin%5C_0111%5C_2019%5C_node.html?r=1.

[84] Bundesnetzagentur. Biomasse / Gebotstermin 1. April 2020. 2020. [Online]. Available: https://www.bundesnetzagentur.de/DE/Fachthemen/ElektrizitaetundGas/Ausschreibungen/Biomasse/BeendeteAusschreibungen/Gebotstermin%5C_01%5C_04%5C_2020/gebotstermin%5C_0104%5C_2020.html (visited on 2025-01-27).

[85] Bundesnetzagentur. Biomasse / Gebotstermin 1. November 2020. 2020. [Online]. Available: https://www.bundesnetzagentur.de/DE/Fachthemen/ElektrizitaetundGas/Ausschreibungen/Biomasse/BeendeteAusschreibungen/Gebotstermin%5C_01%5C_11%5C_2020/gebotstermin%5C_0111%5C_2020%5C_node.html.

[86] Bundesnetzagentur. Biomasse / Gebotstermin 1. März 2021. 2021. [Online]. Available: https://www.bundesnetzagentur.de/DE/Fachthemen/ElektrizitaetundGas/Ausschreibungen/Biomasse/BeendeteAusschreibungen/Gebotstermin%5C_01%5C_03%5C_2021/gebotstermin%5C_0103%5C_2021.html?r=1.

[87] Bundesnetzagentur. Biomasse / Gebotstermin 1. September 2021. 2021. [Online]. Available: https://www.bundesnetzagentur.de/DE/Fachthemen/ElektrizitaetundGas/Ausschreibungen/Biomasse/BeendeteAusschreibungen/Gebotstermin%5C_01%5C_09%5C_2021/gebotstermin%5C_0109%5C_2021.html (visited on 2025-01-27).

[88] Bundesnetzagentur. Biomasse / Gebotstermin 1. März 2022. 2022. [Online]. Available: https://www.bundesnetzagentur.de/DE/Fachthemen/ElektrizitaetundGas/Ausschreibungen/Biomasse/BeendeteAusschreibungen/Gebotstermin%5C_01%5C_03%5C_2022/artikel.html (visited on 2025-01-27).

[89] Clearingstelle EEG. *Ergebnisse Der Zweiten Ausschreibungsrunde 2022 Für Biomasseanlagen.* 2022. [Online]. Available: https://www.clearingstelle-eeg-kwkg.de/ausschreibung/6516 (visited on 2025-01-27).

[90] Bundesnetzagentur. Gebotstermin 1. April 2023. 2023. [Online]. Available: https://www.bundesnetzagentur.de/DE/Fachthemen/ElektrizitaetundGas/Ausschreibungen/Biomasse/BeendeteAusschreibungen/Gebotstermin01042023/start.html.

[91] Bundesnetzagentur. Biomasse: Gebotstermin 1. Oktober 2023. 2023. [Online]. Available: https://www.bundesnetzagentur.de/DE/Fachthemen/ElektrizitaetundGas/Ausschreibungen/Biomasse/BeendeteAusschreibungen/Gebotstermin01102023/artikel.html (visited on 2025-01-27).

[92] Bundesnetzagentur. Biomasse: Gebotstermin 1. April 2024. 2024. [Online]. Available: https://www.bundesnetzagentur.de/DE/Fachthemen/ElektrizitaetundGas/Ausschreibungen/Biomasse/BeendeteAusschreibungen/GtApril2024/artikel.html (visited on 2025-01-27).

[93] Bundesnetzagentur. *Ausschreibung Biomasse: Gebotstermin 1. Oktober 2024.* 2024. [Online]. Available: https://www.bundesnetzagentur.de/DE/Fachthemen/ElektrizitaetundGas/Ausschreibungen/Biomasse/GtOkt2024/start.html (visited on 2025-01-27).

[94] K. Scherzinger. Folgekonzepte für landwirtschaftliche Biogasanlagen. In: *Folgekonzepte für den Weiterbetrieb von landwirtschaftlichen Biogasanlagen: Investitionsrechnungsverfahren für die Modellbewertung.* Ed. by K. Scherzinger. Wiesbaden: Springer Fachmedien, 2023, pp. 33–69. ISBN: 978-3-658-43812-8. DOI: 10.1007/978-3-658-43812-8_4.

[95] C. Herbes, V. Halbherr, and L. Braun. Factors Influencing Prices for Heat from Biogas Plants. In: *Applied Energy*, vol. 221, pp. 308–318. ISSN: 0306-2619. DOI: 10.1016/j.apenergy.2018.03.188.

[96] K. Scherzinger. Entwicklungen der Biogaserzeugung in Deutschland. In: *Folgekonzepte für den Weiterbetrieb von landwirtschaftlichen Biogasanlagen: Investitionsrechnungsverfahren für die Modellbewertung.* Ed. by K. Scherzinger. Wiesbaden: Springer Fachmedien, 2023, pp. 11–22. ISBN: 978-3-658-43812-8. DOI: 10.1007/978-3-658-43812-8_2.

[97] A. Louwen and J. S. Lacerda. Chapter 2 - The Experience Curve: Concept, History, Methods, and Issues. In: *Technological Learning in the Transition to a Low-Carbon Energy System.* Ed. by M. Junginger and A. Louwen. Academic Press, 2020-01, pp. 9–31. ISBN: 978-0-12-818762-3. DOI: 10.1016/B978-0-12-818762-3.00002-9.

[98] G. Faber et al. Adapting Technology Learning Curves for Prospective Techno-Economic and Life Cycle Assessments of Emerging Carbon Capture and Utilization Pathways. In: *Frontiers in Climate*, vol. 4. ISSN: 2624-9553. DOI: 10.3389/fclim.2022.820261.

[99] H. Böhm, A. Zauner, D. C. Rosenfeld, and R. Tichler. Projecting Cost Development for Future Large-Scale Power-to-Gas Implementations by Scaling Effects. In: *Applied Energy*, vol. 264, p. 114780. ISSN: 0306-2619. DOI: 10.1016/j.apenergy.2020.114780.

[100] M. Linnemann. Teil 2 Marktrollen der deutschen Energiewirtschaft – Unterschiedliche Marktrollen und Ihre Bedeutung. In: *Energiewirtschaft für (Quer-)Einsteiger: Einmaleins der Stromwirtschaft*. Ed. by M. Linnemann. Wiesbaden: Springer Fachmedien, 2024, pp. 15–333. ISBN: 978-3-658-43555-4. DOI: 10.1007/978-3-658-43555-4_2.

[101] BDEW. *BDEW-Strompreisanalyse Juli 2024*. [Online]. Available: https://www.bdew.de/service/daten-und-grafiken/bdew-strompreisanalyse/(visited on2024-09-16)

[102] V. Pawlik. Netzentgelt für Strom nach Kundengruppe in Deutschland bis 2023. 2024-11. [Online]. Available: https://de.statista.com/statistik/daten/studie/168548/umfrage/entwicklung-der-netzentgelte-nach-kundengruppe-seit-2006/ (visited on 2024-11-25).

[103] Hamburg Wasser. Tarife und Gebühren von Hamburg Wasser. 2024. [Online]. Available: https://www.hamburgwasser.de/service/preise-und-informationen/tarife-und-gebuehren (visited on 2024-12-22).

[104] Statistisches Bundesamt. Wasserwirtschaft. 2024. [Online]. Available: https://www.destatis.de/DE/Themen/Gesellschaft-Umwelt/Umwelt/Wasserwirtschaft/%5C_inhalt.html (visited on 2024-12-22).

[105] Q. Smejkal, U. Rodemerck, E. Wagner, and M. Baerns. Economic Assessment of the Hydrogenation of CO2 to Liquid Fuels and Petrochemical Feedstock. In: *Chemie Ingenieur Technik*, vol. 86, no. 5, pp. 679–686. ISSN: 1522-2640. DOI: 10.1002/cite.201300180.

[106] S. Brynolf, M. Taljegard, M. Grahn, and J. Hansson. Electrofuels for the Transport Sector: A Review of Production Costs. In: *Renewable and Sustainable Energy Reviews*, vol. 81, pp. 1887–1905. ISSN: 1364-0321. DOI: 10.1016/j.rser.2017.05.288.

[107] R. C. Boehm, Z. Yang, D. C. Bell, J. Feldhausen, and J. S. Heyne. Lower Heating Value of Jet Fuel from Hydrocarbon Class Concentration Data and Thermo-Chemical Reference Data: An Uncertainty Quantification. In: *Fuel*, vol. 311, p. 122542. ISSN: 0016-2361. DOI: 10.1016/j.fuel.2021.122542.

[108] R. Peters, N. Wegener, R. Samsun, F. Schorn, J. Riese, M. Grünewald, and D. Stolten. A Techno-Economic Assessment of Fischer–Tropsch Fuels Based on Syngas from Co-Electrolysis. In: *Processes*, vol. 10, p. 699. DOI: 10.3390/pr10040699.

[109] V. Eyberg, V. Dieterich, S. Bastek, M. Dossow, H. Spliethoff, and S. Fendt. Techno-Economic Assessment and Comparison of Fischer–Tropsch and Methanol-to-Jet Processes to Produce Sustainable Aviation Fuel via Power-to-Liquid. In: *Energy Conversion and Management*, vol. 315, p. 118728. ISSN: 0196-8904. DOI: 10.1016/j.enconman.2024.118728.

[110] R. Baliban, J. Elia, and C. Floudas. Toward Novel Hybrid Biomass, Coal, and Natural Gas Processes for Satisfying Current Transportation Fuel Demands, 1: Process Alternatives, Gasification Modeling, Process Simulation, and Economic Analysis. In: *ResearchGate*. DOI: 10.1021/ie100063y.

[111] F. Trippe, M. Fröhling, F. Schultmann, R. Stahl, E. Henrich, and A. Dalai. Comprehensive Techno-Economic Assessment of Dimethyl Ether (DME) Synthesis and Fischer–Tropsch Synthesis as Alternative Process Steps within Biomass-to-Liquid Production. In: *Fuel Processing Technology*, vol. 106, pp. 577–586. ISSN: 0378-3820. DOI: 10.1016/j.fuproc.2012.09.029.

[112] P. Runge, C. Sölch, J. Albert, and V. Grimm. Economic Comparison of Different Electric Fuels for Energy Scenarios in 2035. In: *ResearchGate*. DOI: 10.1016/j.apenergy.2018.10.023.

[113] P. Buchenberg et al. Global Potentials and Costs of Synfuels via Fischer–Tropsch Process. In: *Energies*, vol. 16, no. 4, p. 1976. ISSN: 1996-1073. DOI: 10.3390/en16041976.

[114] J. Hobohm et al. *Status Und Perspektiven Flüssiger Energieträger in Der Energiewende*. 2018-05.

[115] Zorg Biogas GmbH. Doppelmembrangasspeicher Kuppelform 1/3 D. [Online]. Available: https://zorg-biogas.com/de/equipment/gasspeicher/doppelmembrangasspeicher-kuppelform-1%5C_3d (visited on 2024-12-09).

[116] SKVE. Das neue Biomassepaket und seine Auswirkungen auf die Anlagengestaltung. 2025. [Online]. Available: https://www.skve.de/aktuelles/das-neue-biomassepaket (visited on 2025-05-09).

[117] C. van Leeuwen and M. Mulder. Power-to-Gas in Electricity Markets Dominated by Renewables. In: *Applied Energy*, vol. 232, pp. 258–272. ISSN: 0306-2619. DOI: 10.1016/j.apenergy.2018.09.217.

[118] J. Gorre, F. Ruoss, H. Karjunen, J. Schaffert, and T. Tynjälä. Cost Benefits of Optimizing Hydrogen Storage and Methanation Capacities for Power-to-Gas Plants in Dynamic Operation. In: *Applied Energy*, vol. 257, p. 113967. ISSN: 0306-2619. DOI: 10.1016/j.apenergy.2019.113967.

[119] FCH. Srudy on Early Business Cases for H2 in Energy Storage and More Broadly Power to H2 Applications. Tech. rep. 2017-06.

[120] S. Drünert, U. Neuling, S. Timmerberg, and M. Kaltschmitt. Power-to-X (PtX) aus „Überschussstrom“ in Deutschland – Ökonomische Analyse. In: *Zeitschrift für Energiewirtschaft*, vol. 43, no. 3, pp. 173–191. ISSN: 1866-2765. DOI: 10.1007/s12398-019-00256-7.

[121] D. Bionaz, P. Marocco, D. Ferrero, K. Sundseth, and M. Santarelli. Life Cycle Environmental Analysis of a Hydrogen-Based Energy Storage System for Remote Applications. In: *Energy Reports*, vol. 8, pp. 5080–5092. ISSN: 2352-4847. DOI: 10.1016/j.egyr.2022.03.181.

[122] Wasserstofftank H2 Speicher 324 kg | SW10021. [Online]. Available: https://www.ladeengel.de/Wasserstofftank-H2-Speicher-324-kg/SW10021.

[123] epexspot. Market Data Services | EPEX SPOT. [Online]. Available: https://www.epexspot.com/en/marketdataservices (visited on 2025-07-04).

[124] IBM. What Is Optimization Modeling? 2023-08. [Online]. Available: https://www.ibm.com/think/topics/optimization-model (visited on 2025-05-16).

[125] B. Saravanan, S. Das, S. Sikri, and D. P. Kothari. A Solution to the Unit Commitment Problem—a Review. In: *Frontiers in Energy*, vol. 7, no. 2, pp. 223–236. ISSN: 2095-1698. DOI: 10.1007/s11708-013-0240-3.

[126] S. Y. Abujarad, M. W. Mustafa, and J. J. Jamian. Recent Approaches of Unit Commitment in the Presence of Intermittent Renewable Energy Resources: A Review. In: *Renewable and Sustainable Energy Reviews*, vol. 70, pp. 215–223. ISSN: 1364-0321. DOI: 10.1016/j.rser.2016.11.246.

[127] I. Abdou and M. Tkiouat. Unit Commitment Problem in Electrical Power System: A Literature Review. In: *ResearchGate*. DOI: 10.11591/ijece.v8i3.pp1357-1372.

[128] N. Zendehdel, A. Karimpour, and M. Oloomi. Optimal Unit Commitment Using Equivalent Linear Minimum up and down Time Constraints. In: *2008 IEEE 2nd International Power and Energy Conference*. 2008-12, pp. 1021–1026. DOI: 10.1109/PECON.2008.4762625.

[129] R. Bailey. *The Economics of Financial Markets*. New York: Cambridge University Press, 2005-01. ISBN: 978-0-521-84827-5.

[130] Z. Shen, W. Wei, D. Wu, T. Ding, and S. Mei. Modeling Arbitrage of an Energy Storage Unit without Binary Variables. In: *CSEE Journal of Power and Energy Systems*, vol. 7, no. 1, pp. 156–161. ISSN: 2096-0042. DOI: 10.17775/CSEEJPES.2019.03340.

[131] Directorate-General for Climate Action (European Commission) et al. *EU Reference Scenario 2020: Energy, Transport and GHG Emissions : Trends to 2050*. Publications Office of the European Union, 2021. ISBN: 978-92-76-39356-6.

[132] A. Energiewende, A. Verkehrswende, and F. Economics. Die zukünftigen Kosten strombasierter synthetischer Brennstoffe. Tech. rep. 2018-02.

[133] D. Schröer and U. Latacz-Lohmann. Betriebswirtschaftlicher Vergleich der Flexibilisierung und rohgasseitigen Bündelung von Biogasbestandsanlagen anhand eines Fallbeispieles. In: *Berichte über Landwirtschaft - Zeitschrift für Agrarpolitik und Landwirtschaft*. ISSN: 2196-5099. DOI: 10.12767/buel.v100i1.376.

[134] K. Haensel, T. Barchmann, M. Dotzauer, E. Fischer, and J. Liebetrau. Further Operation of Flexible Biogas Plants – Realisable Bid Prices in the EEG 2017. In: *agricultural engineering.eu*, vol. 75, no. 2. ISSN: 2943-5641. DOI: 10.15150/lt.2020.3235.

[135] IEA. Renewables 2021. Tech. rep. Paris, 2021-12.

[136] Jet A1 Price Germany. 2025. [Online]. Available: https://jet-a1-fuel.com/price/germany (visited on 2025-06-14).

[137] IATA. *Fuel Fact Sheet*. 2025.

[138] T. Edwards. "Kerosene" Fuels for Aerospace Propulsion - Composition and Properties. In: *38th AIAA/ASME/SAE/ASEE Joint Propulsion Conference & Exhibit*. American Institute of Aeronautics and Astronautics. DOI: 10.2514/6.2002-3874.

[139] statista. EU-Emissionshandel: Entwicklung der Preise 2025. 2025. [Online]. Available: https://de.statista.com/statistik/daten/studie/1454492/umfrage/co2-preise-im-emissionshandelssystem-der-eu/ (visited on 2025-06-24).

[140] IEA. Net Zero by 2050. Tech. rep. 2021-05.

[141] A. Merfort et al. Separating CO2 Emission from Removal Targets Comes with Limited Cost Impacts. In: *Nature Communications*, vol. 16, no. 1, p. 5298. ISSN: 2041-1723. DOI: 10.1038/s41467-025-60606-7.

[142] IATA. *IATA Carbon Offset Program - Frequently Asked Questions*. 2022.

[143] E. C. Bank. Euro exchange rates charts. In.

[144] J. Kersey, N. D. Popovich, and A. A. Phadke. Rapid Battery Cost Declines Accelerate the Prospects of All-Electric Interregional Container Shipping. In: *Nature Energy*, vol. 7, no. 7, pp. 664–674. ISSN: 2058-7546. DOI: 10.1038/s41560-022-01065-y.

[145] B. A. Adu-Gyamfi and C. Good. Electric Aviation: A Review of Concepts and Enabling Technologies. In: *Transportation Engineering*, vol. 9, p. 100134. ISSN: 2666-691X. DOI: 10.1016/j.treng.2022.100134.

[146] V. Viswanathan, A. H. Epstein, Y.-M. Chiang, E. Takeuchi, M. Bradley, J. Langford, and M. Winter. The Challenges and Opportunities of Battery-Powered Flight. In: *Nature*, vol. 601, no. 7894, pp. 519–525. ISSN: 1476-4687. DOI: 10.1038/s41586-021-04139-1.

[147] Y. Tang, W. Guo, and R. Zou. Nickel-Based Bimetallic Battery-Type Materials for Asymmetric Supercapacitors. In: *Coordination Chemistry Reviews*, vol. 451, p. 214242. ISSN: 0010-8545. DOI: 10.1016/j.ccr.2021.214242.

[148] J. Verma and D. Kumar. Retracted Article: Recent Developments in Energy Storage Systems for Marine Environment. In: *Materials Advances*, vol. 2, no. 21, pp. 6800–6815. ISSN: 2633-5409. DOI: 10.1039/D1MA00746G.

[149] M. Perčić, L. Frković, T. Pukšec, B. Ćosić, O. L. Li, and N. Vladimir. Life-Cycle Assessment and Life-Cycle Cost Assessment of Power Batteries for All-Electric Vessels for Short-Sea Navigation. In: *Energy*, vol. 251, p. 123895. ISSN: 0360-5442. DOI: 10.1016/j.energy.2022.123895.

[150] I. Barin. *Thermochemical Data of Pure Substances*. Vol. 3. VCH Weinheim, 1995. ISBN: 978-3-527-28745-1.

[151] NIST Office of Data and Informatics. NIST Database. [Online]. Available: https://webbook.nist.gov/chemistry/ (visited on 2025-04-03).

[152] D. L. Millar. On the Determination of Efficiency of a Gas Compressor. In: *Energies*, vol. 17, no. 13, p. 3260. ISSN: 1996-1073. DOI: 10.3390/en17133260.

[153] J. F. Messerly, G. B. J. Guthrie, S. S. Todd, and H. L. Finke. Low-Temperature Thermal Data for Pentane, n-Heptadecane, and n-Octadecane. Revised Thermodynamic Functions for the n-Alkanes, C5-C18. In: *Journal of Chemical & Engineering Data*, vol. 12, no. 3, pp. 338–346. ISSN: 0021-9568. DOI: 10.1021/je60034a014.

A Appendices

Appendices Table of Contents

A.1 Thermodynamic Calculations

A.1.1 Data Tables

H2[g] HYDROGEN (GAS) 2.016

Phase	T	C_p	S	-(G-H298)/T	H	H-H298	G	ΔH_f	ΔG_f	log K_f
	[K]	[J / (K mol)		]	[kJ / mol				]	[-]
GAS	298.15	28.836	130.680	130.680	0.000	0.000	−38.962	0.000	0.000	0.000
	300.00	28.849	130.858	130.681	0.053	0.053	−39.204	0.000	0.000	0.000
	400.00	29.182	139.216	131.818	2.959	2.959	−52.727	0.000	0.000	0.000
	500.00	29.260	145.737	133.974	5.882	5.882	−66.987	0.000	0.000	0.000

Figure A.1: Thermodynamic data of H_2 [150].

28.010 CARBON MONOXIDE (GAS) **CO[g]**

Phase	T	C_p	S	-(G-H298)/T	H	H-H298	G	ΔH_f	log K_f
	[K]	[J / (K mol)		]	[kJ / mol				[-]
GAS	298.15	29.140	197.661	197.661	−110.541	0.000	−169.474	−110.541	24.033
	300.00	29.144	197.841	197.662	−110.487	0.054	−169.840	−110.530	23.914
	400.00	29.342	206.250	198.807	−107.564	2.977	−190.064	−110.129	19.112
	500.00	29.794	212.841	200.977	−104.609	5.932	−211.030	−110.035	16.237

Figure A.2: Thermodynamic data of CO [150].

CO2[g] CARBON DIOXIDE (GAS) 44.010

Phase	T	C_p	S	-(G-H298)/T	H	H-H298	G	ΔH_f	log K_f
	[K]	[J / (K mol)		]	[kJ / mol				[-]
GAS	298.15	37.132	213.770	213.770	−393.505	0.000	−457.240	−393.505	69.091
	300.00	37.217	214.000	213.770	−393.436	0.069	−457.636	−393.506	68.666
	400.00	41.326	225.291	215.282	−389.501	4.004	−479.618	−393.580	51.535
	500.00	44.625	234.880	218.266	−385.198	8.307	−502.638	−393.666	41.255

Figure A.3: Thermodynamic data of CO_2 [150].

H2O[g] WATER (GAS) 18.015

Phase	T	C_p	S	-(G-H298)/T	H	H-H298	G	ΔH_f	log K_f
	[K]	[J / (K mol)		]	[kJ / mol				[-]
GAS	298.15	33.590	188.959	188.959	−241.826	0.000	−298.164	−241.826	40.053
	300.00	33.596	189.167	188.960	−241.764	0.062	−298.514	−241.844	39.792
	400.00	34.261	198.910	190.284	−238.375	3.451	−317.939	−242.847	29.245
	500.00	35.230	206.656	192.809	−234.902	6.924	−338.230	−243.826	22.891

Figure A.4: Thermodynamic data of H_2O (gaseous) [150].

16.043				METHANE (GAS)					CH4[g]
Phase	T	C_p	S	−(G−H298)/T	H	H−H298	G	ΔH_f	log K_f
	[K]	[	J / (K mol)	]	[		kJ / mol		[−]
GAS	298.15	35.645	186.214	186.214	−74.873	0.000	−130.393	−74.873	8.892
	300.00	35.707	186.434	186.214	−74.807	0.066	−130.737	−74.930	8.811
	400.00	40.489	197.310	187.665	−71.015	3.858	−149.939	−77.986	5.489
	500.00	46.349	206.968	190.574	−66.676	8.197	−170.160	−80.824	3.418

Figure A.5: Thermodynamic data of CH_4 [150].

	Lower Heating Value		Higher Heating Value	
Biogas CH_4 Content, %	**MJ/m^3**	**kWh/m^3**	**MJ/m^3**	**kWh/m^3**
45	16.1	4.47	17.9	4.97
50	17.9	4.97	19.9	5.53
55	19.7	5.47	19.9	6.08
60	21.5	5.96	23.9	6.63
65	23.3	6.46	25.9	7.18
70	25.1	6.96	27.9	7.74
	Upgraded Biogas			
95	34.0	9.44	37.8	10.50
96	34.4	9.54	38.2	10.61
97	34.7	9.64	38.6	10.72
98	35.1	9.74	39.0	10.83
99	35.4	9.84	39.4	10.94

Figure A.6: LHV and HHV of Biogas based on different CH_4 Content [62].

Table A.1: Shomate Coefficients for Various Species [151]

Species	A	B	C	D	E
H_2	33.07	-11.36	11.43	-2.77	-0.16
O_2	31.32	-20.24	57.87	-36.51	-0.01
CH_4	-0.70	108.48	-42.52	5.86	0.68
CO_2	25.00	55.19	-33.69	7.95	-0.14
CO	25.57	6.10	4.06	-2.67	0.13
$H_2O_{(l)}$	-203.61	1523.29	-3196.41	2474.46	3.86
$H_2O_{(g)}$	30.09	6.83	6.79	-2.53	0.08
C1	-0.70	108.48	-42.52	5.86	0.68

A.1.2 Used Thermodynamic Formulas

Each process unit is modeled under specific assumptions regarding pressure, temperature, and flow. Only the essential aspects are summarized below.

Heat Capacity Calculation via the Shomate Equation

The molar specific heat capacity C_p (in J/(mol · K)) is calculated according to the Shomate equation:

$$C_p = A + B\left(\frac{T}{1,000}\right) + C\left(\frac{T}{1,000}\right)^2 + D\left(\frac{T}{1,000}\right)^3 + \frac{E}{\left(\frac{T}{1,000}\right)^2}, \tag{A.1}$$

where T is the temperature in Kelvin and A, B, C, D, E are the Shomate coefficients. The mass-specific heat capacity c_p (in J/(kg · K)) is then obtained by dividing C_p by the molar mass M:

$$c_p = \frac{C_p}{M}. \tag{A.2}$$

Mixture Properties

The effective molar mass M of a gas mixture is calculated from the mass flow rate $\dot{m}$ and the molar flow rate $\dot{n}$ as follows:

$$M = \frac{\dot{m}}{\dot{n}} = \sum_i \xi_i\, M_i = \sum_i \psi_i\, M_i, \tag{A.3}$$

where ξ_i and ψ_i denote the mass and mole fractions of component i, respectively, and M_i is the molar mass of component i.

For a gas mixture, the specific gas constant R is computed as a mass-fraction weighted sum of the individual gas constants:

$$R = \sum_i \xi_i\, R_i, \tag{A.4}$$

and the overall specific isobaric heat capacity is given by

$$c_p = \sum_i \xi_i \, c_{p,i}. \tag{A.5}$$

The specific isochoric heat capacity is then

$$c_v = c_p - R, \tag{A.6}$$

and the isentropic exponent κ is calculated as

$$\kappa = \frac{c_p}{c_v} = \frac{c_p}{c_p - R}. \tag{A.7}$$

Heat Transfer

The heat transfer rate $\dot{Q}$ for a heat exchanger is determined by:

$$\dot{Q} = \dot{m} \, c_p \, (T_2 - T_1), \tag{A.8}$$

where $\dot{m}$ is the mass flow rate (in kg/s), T_1 the inlet temperature, and T_2 the outlet temperature. Conversely, for a given heat transfer rate, the outlet temperature is calculated as:

$$T_2 = \frac{\dot{Q}}{\dot{m} \, c_p} + T_1. \tag{A.9}$$

Polytropic Compressor Model

In the compressor model, a polytropic process is assumed, meaning that a portion of the heat generated during compression is removed in-process. Consequently, the polytropic exponent n is slightly lower than the isentropic exponent κ. For the compressors examined in this study, we adopt

$$n = 1 + 0.75 \, (\kappa - 1). \tag{A.10}$$

which corresponds to a moderate level of interstage cooling during compression [152]. The polytropic work per unit mass is given by

$$w_{\text{poly}} = \frac{R_{\text{mix}} \, T_1}{n - 1} \left[\left(\frac{p_2}{p_1} \right)^{\frac{n-1}{n}} - 1 \right], \tag{A.11}$$

so that the compressor power P_t is

$$P_t = \dot{m} \, w_{\text{poly}}, \tag{A.12}$$

and the outlet temperature after compression is

$$T_2 = T_1 \left(\frac{p_2}{p_1} \right)^{\frac{n-1}{n}}. \tag{A.13}$$

Mixture Heat Capacity Calculation

Finally, the overall specific heat capacity of a gas mixture is calculated by determining the individual $c_{p,i}$ using the Shomate equation and then computing the mass-fraction weighted sum:

$$c_{p,\text{mix}} = \sum_i \xi_i \, c_{p,i}. \tag{A.14}$$

A.1.3 Thermodynamic Calculations for the BGtL Plant

To improve the traceability of the calculations, the detailed process flow diagram showing individual components and streams is provided in Figure A.7 and in Tables A.2 and A.3.

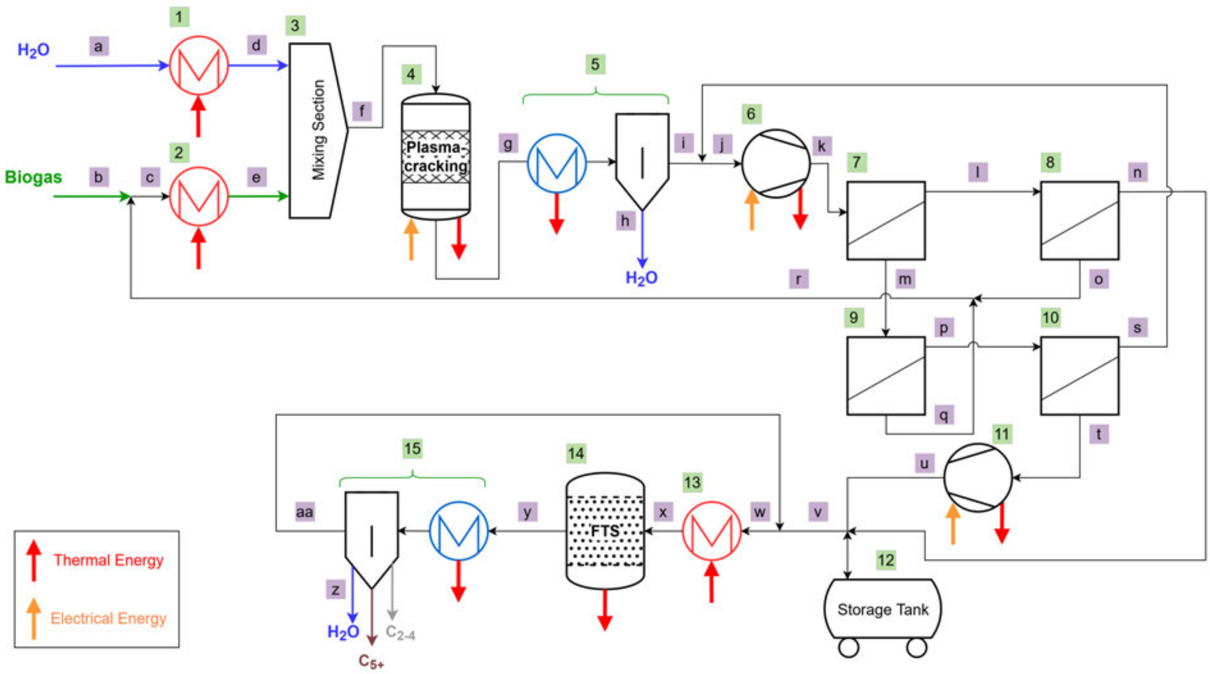

Figure A.7: Detailed Flowchart of the BGtL Plant with Component and Streamtags.

To enable the simulation of the BGtL system, the plant's energy demand represents a key input parameter. As a reference, the pilot plant developed within the "Plasma2X" project is considered. The energy demand was determined through thermodynamic evaluations of the process streams as well as of the individual components of the system. These calculations were primarily carried out using the Python script `thermodynamic_calculations.py`. For the sake of clarity and brevity, only the most relevant calculation steps are presented here.

Plasmacracking Plant

The basis for the thermodynamic assessment is the documented power input of the microwave unit in the PC Reactor of the Plasma2X Project, amounting to 10.00 kW, in combination with the reaction equation provided in Eq. A.15. Accounting for an estimated microwave loss of 1.00 kW, an effective input power of 9.00 kW is assumed. Furthermore, the synthesis gas composition is

Table A.2: Liste der Komponenten

Number	Component
1	Water Heater
2	Biogas Heater
3	Mixing Section
4	PC Reactor
5	Water Seperator
6	Compressor Gasmixture
7	H2/CO-Membrane Seperation
8	CO/CH4-Membrane Seperation
9	H2/CO2-Membrane Seperation
10	H2/Residual-Membrane Seperation
11	Compressor H2
12	Syngas Storage Tank
13	Heater Syngas
14	FTS Reactor
15	Seperator Hydrocarbons and Water

designed to achieve an H_2/CO ratio of 2.2.

The flow factor, defined as the ratio between the fraction of feed gas bypassing the reaction zone and the fraction subjected to cracking, is set to 4. Consequently, one quarter of the gas stream enters the microwave's reactive zone, while the remaining three quarters pass through the system unconverted. It is further assumed that the gas fraction entering the reactive zone is fully cracked under the given process conditions. For simplification, it is also assumed that no by-products, such as short-chain hydrocarbons (e.g., C_2–C_4), are formed during the PC process. Although such compounds may occur under real process conditions, their quantities are expected to be negligible, thereby justifying this simplification.

Based on these assumptions, the mass flow rates of the feed streams Biogas Feed, Water Feed and Gasmixture Feed and the resulting product gas Gasmixture Post Plasmacracking within the PC Reactor can be determined.

For the targeted H_2/CO ratio of 2.2, the following stoichiometric equation is obtained:

$$4\,CH_4 + CO_2 + 3\,H_2O \rightarrow 5\,CO + 11\,H_2 \tag{A.15}$$

Based on the standard formation enthalpies of the gas components and the molar amounts, the reaction enthalpy is calculated to be 879.2 kJ/mol (see **??**).

Using the effective microwave power of 9.00 kJ/s, the conversion rate can be determined as follows:

$$\dot{n} = \frac{9.00\,\text{kJ/s}}{879.2\,\text{kJ/mol}} \approx 0.010237\,\text{mol/s} \tag{A.16}$$

The thermophysical properties of the gas components involved in the reaction are summarized

Table A.3: Streams and mass flows (kg/h)

Stream	Name	T [°C]	p [bar]	$\dot{m}_{H_2O}$	$\dot{m}_{CO_2}$	$\dot{m}_{CH_4}$	$\dot{m}_{CO}$	$\dot{m}_{H_2}$	$\dot{m}_{C_{5+}}$
a	Water Feed	25	1	7.960	0	0	0	0	0
b	Biogas Feed	25	1	0	1.621	2.359	0	0	0
c	Biogas Feed Mixture	25	1	0	6.484	9.436	0	0	0
d	Water Feed Vaporized	105	1	7.960	0	0	0	0	0
e	Biogas Feed Mixture Heated	105	1	0	6.484	9.436	0	0	0
f	Gas Mixture Feed to Plasmacracking	105	1	7.960	6.484	9.436	0	0	0
g	Gas Mixture Post–Plasmacracking	105	1	5.970	4.863	7.077	5.159	0.811	0
h	Separated Water	25	1	5.970	0	0	0	0	0
i	Gas Post–Water Separator	25	1	0	4.863	7.077	5.159	0.811	0
j	Gas Pre–Compressor	25	1	0	4.863	7.077	5.159	0.811	0
k	Gas Post–Compressor	25	30	0	4.863	7.077	5.159	0.811	0
l	Gas Mixture (CO + CH_4)	25	30	0	0	7.077	5.159	0	0
m	Gas Mixture (H_2 + CO_2)	25	6	0	4.863	0	0	0.811	0
n	CO Membrane Separation	25	30	0	0	0	5.159	0	0
o	CH_4 Membrane Separation	25	1	0	0	7.077	0	0	0
p	Gas Mixture H_2 + Residual	25	6	0	0	0	0	0.811	0
q	CO_2 Membrane Separation	25	6	0	4.863	0	0	0	0
r	Biogas Recycling	25	1	0	4.863	7.077	0	0	0
s	Residual Recycling	25	6	0	0	0	0	0	0
t	H_2 Membrane Separation	25	1	0	0	0	0	0.811	0
u	H_2 Membrane Separation Compressed	25	30	0	0	0	0	0.811	0
v	Syngas	25	30	0	0	0	5.159	0.811	0
w	Syngas + Recycling	16.6	30	0	0	0	8.598	1.351	0
x	Heated Syngas + Recycling	250	30	0	0	0	8.598	1.351	0
y	FTS Product	250	30	3.283	0	0	3.439	0.540	2.328
z	Product Post–Separation	4	30	3.283	0	0	0	0	2.328
aa	Syngas Recycling	4	30	0	0	0	3.439	0.540	0

Table A.4: Assumptions for the BtL Reference Plant

Parameter	Value	Unit
Microwave Power	10.00	kW=kJ/s
Loss Power	1.00	kW=kJ/s
Effective Power	9.00	kW=kJ/s
H_2/CO Ratio	2.2	-
Flow Factor	4	-
Syngas Recycling Factor	40	%

in Table A.5. The standard formation enthalpy at 105 °C and ambient pressure has been calculated using literature values (see [150]). Based on the stoichiometric coefficients and the calculated conversion rate, the mass and volumetric flow rates of the individual components can be determined. The corresponding flow rates are shown in Table A.6.

Since the flow factor is 4, four times as much feed gas is required for the PC reaction. To achieve this, the CH_4 and CO_2 that pass through the PCU without being cracked are later recycled, so that an increase in the biogas feed is not necessary. However, the water feed must be increased by a factor of four, because the steam is filtered out by a Water Separator after the PC reactor to ensure that the gas mixture is dry for subsequent processes.

Thus, a mass flow of 7.96 kg/h of H_2O is obtained for the Water Feed, while the Biogas Feed comprises 1.621 kg/h of CO_2 and 2.359,kg/h of CH_4. A temperature of 25 °C and ambient pressure are assumed. Since the Biogas Recycling gas is also cooled down during the process to 25 °C, it

Table A.5: Properties of the Gas Components

Substance	Standard Formation Enthalpy (105 °C, 1.01325 bar) [kJ/mol]	Density (0 °C, 1.01325 bar) [kg/Nm^3]	Molar Mass [g/mol]
CO	-108.2	1.251	28
CO_2	-390.4	1.98	44
H_2O (g)	-239.1	0.88	18
CH_4	-71.8	0.717	16
H_2	2.3	0.08988	2

Table A.6: Flow Rates of the Plasmacracking Reaction Reactants and Products (Reference Plant: 10 kW)

Component	mol	mol/s	g/s	g/h	kg/h	Nm^3/h
CO_2	1	0.010	0.450	1621.5	1.621	0.819
H_2O (g)	3	0.031	0.553	1990.0	1.990	2.261
CH_4	4	0.041	0.655	2358.5	2.359	3.289
CO	5	0.051	1.433	5159.2	5.159	4.124
H_2	11	0.113	0.225	810.7	0.811	9.020

must be mixed with the Biogas Feed and then jointly heated to 105 °C by the Biogas Heater. As three quarters of the biogas pass through the PC Reactor, it is simplified by assuming that the mass flow of the recycled biogas is exactly three times that of the Biogas Feed. Consequently, the Biogas Recycling stream contains 4.863 kg/h of CO_2 and 7.077 kg/h of CH_4. This stream is mixed into the Biogas Feed, resulting in the combined mass flows of the Biogas Feed Mixture amounting to 6.484 kg/h of CO_2 and 9.436 kg/h of CH_4. In addition, the product gas stream Gasmixture Post Plasmacracking can be determined. It consists of the reaction products — 5.159 kg/h of CO and 0.811 kg/h of H_2 — as well as the uncracked biogas and steam, which amount to 5.970 kg/h of H_2O, 4.863 kg/h of CO_2, and 7.077 kg/h of CH_4.

Table A.7: Mass flows (kg/h) for water and biogas feeds

Stream	Name	T [°C]	p [bar]	$\dot{m}_{H_2O}$	$\dot{m}_{CO_2}$	$\dot{m}_{CH_4}$	$\dot{m}_{CO}$	$\dot{m}_{H_2}$	$\dot{m}_{C_5-C_{50}}$
a	Water Feed	25	1	7.960	0	0	0	0	0
b	Biogas Feed	25	1	0	1.621	2.359	0	0	0
c	Biogas Feed Mixture	25	1	0	6.484	9.436	0	0	0
d	Water Feed vaporized	105	1	7.960	0	0	0	0	0
e	Biogas Feed Mixture heated	105	1	0	6.484	9.436	0	0	0
f	Gasmixture Feed Plasmacracking	105	1	7.960	6.484	9.436	0	0	0
g	Gasmixture Post Plasmacracking	105	1	5.970	4.863	7.077	5.159	0.811	0
h	Seperated Water	25	1	5.970	0	0	0	0	0
i	Gas Post Water Seperator	25	1	0	4.863	7.077	5.159	0.811	0

Water Heater

The first component for which the required electrical power is to be determined is the Water Heater. Its function is to raise the temperature of the Water Feed to 105 °C and to fully vaporize the fluid. The calculations are based on the application of the heat capacity equations (A.1, A.2, A.5) in conjunction with the heat exchanger model described in Equation A.8. The relevant parameters used for this calculation are summarized in Table A.8. It is assumed for simplicity that no losses occur. Water has a specific heat capacity of 4,220.02 J/(kgK) in its liquid state

Table A.8: Thermodynamic properties of the Water Feed

Stream	Name	T_{start} [°C]	T_{boiling} [°C]	T_{end} [°C]	Δh_{vap} [kJ/kg]	$\dot{m}$ [kg/s]	$c_p^{(l)}$ [J/(kg K)]	$c_p^{(g)}$ [J/(kg K)]
a	Water Feed	25	100	105	2,242	2.21×10^{-3}	4,220.02	1892.01

and 1,892.01 J/(kgK) in its gaseous state. Consequently, the calculation is divided into two parts. Equation A.17 determines the power required to heat the water to 100 °C. Under the assumption of no heat losses, this process requires 699.82 W.

$$Q_{\text{water\_heating}} = 2.21 \times 10^{-3}\,\frac{\text{kg}}{\text{s}} \cdot 4,220.02\,\frac{\text{J}}{\text{kg K}} \cdot (373.15 - 297.15)\,\text{K} = \underline{699.82\,\text{W}} \tag{A.17}$$

It is then simplified by assuming that all of the water evaporates at 100 °C. The calculation employs a latent heat of vaporization of 2,242 kJ/kg (Equation A.18), resulting in a vaporization power of 4,957.31 W.

$$Q_{\text{vaporization}} = 2.21 \times 10^{-3}\,\frac{\text{kg}}{\text{s}} \cdot 2,242\,\frac{\text{J}}{\text{kg}} = \underline{4,957.31\,\text{W}} \tag{A.18}$$

Finally, Equation A.19 calculates the power required to raise the temperature of the vapor from 100 °C to 105 °C, which amounts to 20.92 W.

$$Q_{\text{steam\_heating}} = 2.21 \times 10^{-3}\,\frac{\text{kg}}{\text{s}} \cdot 1,892.01\,\frac{\text{J}}{\text{kg K}} \cdot (378.15 - 373.15)\,\text{K} = \underline{20.92\,\text{W}} \tag{A.19}$$

In summary, these contributions yield a total power demand of 5,678.05 W (Equation A.20) for the Water Heater.

$$Q_{\text{WaterHeater}} = 699.82\,\text{W} + 4,957.31\,\text{W} + 20.92\,\text{W} = \underline{\underline{5,678.05\,\text{W}}} \tag{A.20}$$

Biogas Heater

The Biogas Feed Mixture is also to be heated from 25 °C to 105 °C. For this purpose, the Biogas Heater is used, which is assumed to operate without heat losses, analogous to the Water Heater. As in the previous calculation, Equation A.8 is applied. Since the biogas remains in the gaseous phase throughout the process, only a single heat transfer step needs to be considered.

Table A.9: Thermodynamic properties of the Biogas Feed Mixture

Stream	Name	T_1 [°C]	T_2 [°C]	$\dot{m}$ [kg/s]	c_p [J/(kg K)]
c	Biogas Feed Mixture	25	105	4.42×10^{-3}	1661.08

Based on a mass flow rate of 4.42×10^{-3} kg/s and a specific heat capacity of $1,661.08$ J/(kg K), the resulting thermal power amounts to 587.65 W.

$$Q_{\text{BiogasHeater}} = 4.42 \times 10^{-3}\,\frac{\text{kg}}{\text{s}} \cdot 1,661.08\,\frac{\text{J}}{\text{kg K}} \cdot (373.15 - 297.15)\,\text{K} = \underline{\underline{587.65\,\text{W}}} \tag{A.21}$$

Water Seperator

After the PC process, the gas stream Gasmixture Post Plasmacracking passes through the Water Separator, which functions as a condensate separator. In this unit, the gas is cooled down to 25 °C in order to condense and separate the water content from the gas phase. The thermodynamic properties of the gas are summarized in Table A.10.

Table A.10: Thermodynamic properties of the Gasmixture Post Plasmacracking

Stream	Name	T_1 [°C]	T_2 [°C]	$\dot{m}$ [kg/s]	c_p [J/(kg K)]
g	Gasmixture Post Plasmacracking	105	25	6.63×10^{-3}	2184.26

To determine the amount of heat to be removed, Equation A.19 for the heat exchanger is applied again:

$$Q_{\text{WaterSeperator}} = 6.63 \times 10^{-3}\,\frac{\text{kg}}{\text{s}} \cdot 2,184.26\,\frac{\text{J}}{\text{kg K}} \cdot (297.15 - 378.15)\,\text{K} = \underline{\underline{-2,010.67\,\text{W}}} \tag{A.22}$$

Since heat is extracted from the gas, the thermal power is negative and amounts to $-2,010.67$ W. In this context, it is ideally assumed that the entire water content of 5.97 kg/h is removed from the gas stream.

Compressor Gasmixture

The dry gas stream Gasmixture Pre Compressor is compressed from 1 bar to 30 bar using a compressor. A polytropic compression process is assumed. The calculations are based on the polytropic compression equations (Eq.A.10 – A.13). The thermodynamic and flow properties of the gas mixture are summarized in TableA.11.

Table A.11: Thermodynamic and flow properties of the Gasmixture Pre Compressor

Stream	Name	T [°C]	p_{start} [bar]	p_{end} [bar]	$\dot{m}$ [kg/s]	R [J/(kg,K)]	κ [-]	n [-]
i	Gas Post Water Separator	25	1	30	$4.98 \cdot 10^{-3}$	528.31	1.346	1.260

$$w_{\text{poly,CompressorGasmixture}} = \frac{528.31, \text{J/(kg, K)} \cdot 297.15, \text{K}}{1.26 - 1} \cdot \left[\left(\frac{30, \text{bar}}{1, \text{bar}} \right)^{\frac{1.26-1}{1.26}} - 1 \right] = \underline{614,333.69, \text{J/kg}} \tag{A.23}$$

$$P_{\text{CompressorGasmixture}} = 4.98 \times 10^{-3}, \text{kg/s} \cdot 614,333.69, \text{J/kg} = \underline{\underline{3,059.66, \text{W}}} \tag{A.24}$$

$$T_{end} = 297.15, \text{K} \left(\frac{30, \text{bar}}{1, \text{bar}} \right)^{\frac{1.26-1}{1.26}} = \underline{599.38, \text{K}} \tag{A.25}$$

The results show that the Compressor Gasmixture requires a mechanical power input of 3,059.66 W and heats the gas mixture up to 599.38 K during the compression process. It is now assumed that the excess thermal energy of the gas can be utilized elsewhere in the system, for example in heating processes. To determine the amount of thermal power contained in the gas after compression, Equation A.19 is applied. The corresponding thermodynamic parameters for the post-compression state are summarized in Table A.12.

Table A.12: Thermodynamic properties of the Gasmixture Post Compressor during cooling

Stream	Name	T_{start} [°C]	T_{end} [°C]	$\dot{m}$ [kg/s]	c_p [J/(kg,K)]
j	Gasmixture Post Compressor	326.23	25	$4.98 \cdot 10^{-3}$	2,549.56

$$Q_{\text{CompressorGasmixture}} = 4.98 \cdot 10^{-3}\,\frac{\text{kg}}{\text{s}} \cdot 2,549.56\,\frac{\text{J}}{\text{kg K}} \cdot (297.15 - 599.38)\,\text{K} = \underline{\underline{-3,820.85\,\text{W}}} \tag{A.26}$$

The calculation indicates that the gas mixture contains a recoverable thermal power of -3,820.85 W.

Compressor H_2

Now the gas mixture passes through the membrane separation process, which does not require any additional energy input. For simplicity, it is assumed that the membrane separation achieves 100% separation efficiency. In practice, however, this is not realistic. This means that any unseparated excess would be recycled, resulting in a higher load on the Compressor Gasmixture. Since the pressure on the hydrogen side drops from 30 bar to ambient pressure during membrane separation, and the hydrogen is to be recombined with the carbon monoxide stream (which remains at 30 bar) after separation, the hydrogen must be recompressed to 30 bar. This is accomplished using the polytropic compressor Compressor H2.

Table A.13: Thermodynamic and flow properties of the H2 Membrane Seperation

Stream	Name	T [°C]	p_{start} [bar]	p_{end} [bar]	$\dot{m}$ [kg/s]	R [J/(kg,K)]	κ [-]	n [-]
i	Gas Post Water Separator	25	1	30	$0.23 \cdot 10^{-3}$	4,124.01	1.405	1.304

$$w_{\text{poly CompressorH}_2} = \frac{4,124.01\,\text{J/(kg, K)} \cdot 297.15\,\text{K}}{1.304 - 1} \cdot \left[\left(\frac{30\,\text{bar}}{1\,\text{bar}}\right)^{\frac{1.304-1}{1.304}} - 1\right] = \underline{4,871,955.56\,\text{J/kg}} \tag{A.27}$$

$$P_{\text{CompressorH}_2} = 0.23 \times 10^{-3}\,\text{kg/s} \cdot 4,871,955.56\,\text{J/kg} = \underline{\underline{1,096.19\,\text{W}}} \tag{A.28}$$

$$T_{end} = 297.15\,\text{K}\left(\frac{30\,\text{bar}}{1\,\text{bar}}\right)^{\frac{1.304-1}{1.304}} = \underline{656.84\,\text{K}} \tag{A.29}$$

The calculation shows that the required power input for the Compressor H_2 is 1,096.19 W, and the hydrogen heats up to 656.84 K during the compression process.

The formula for calculating a heat exchanger can now be used to calculate the thermal energy generated.

Table A.14: Thermodynamic properties of the H2 Membrane Seperation

Stream	Name	T_{start} [°C]	T_{end} [°C]	$\dot{m}$ [kg/s]	c_p [J/(kg,K)]
j	Gasmixture Post Compressor	383,69	25	$0.225 \cdot 10^{-3}$	14,298.48

$$Q_{\text{CompressorHydrogen}} = 0.225 \cdot 10^{-3}\,\frac{\text{kg}}{\text{s}} \cdot 14,298.48\,\frac{\text{J}}{\text{kg}\,\text{K}} \cdot (297.15 - 656.84)\,\text{K} = \underline{\underline{-1,155.38\,\text{W}}} \tag{A.30}$$

Heater Syngas

The H_2 is now mixed with CO to form the Syngas. This can then be either stored in the Syngas Storage Tank or sent directly to the FTS Reactor. Before entering the reactor, the Syngas Recycling stream is blended in and heated to 250 °C. The combined Syngas + Syngas Recycling stream consists of 8.598 kg/h CO and 1.351 kg/h H_2.

Table A.15: Thermodynamic properties of the Syngas + Syngas Recycling

Stream	Name	T_{start} [°C]	T_{end} [°C]	$\dot{m}$ [kg/s]	c_p [J/(kg,K)]
j	Gasmixture Post Compressor	25	250	$2.763 \cdot 10^{-3}$	2,840.74

$$Q_{\text{HeaterSyngas}} = 2.763 \cdot 10^{-3}\,\frac{\text{kg}}{\text{s}} \cdot 2,840.74\,\frac{\text{J}}{\text{kg}\,\text{K}} \cdot (523.15 - 297.15)\,\text{K} = \underline{\underline{1766.41\,\text{W}}} \tag{A.31}$$

FTS Reactor

After heating to 250 °C, the synthesis gas (8.598 kg/h CO and 1.351 kg/h H_2) enters the FTS Reactor. A CO conversion of 60 % is assumed, so that 40 % of the feed remains unreacted.

The overall stoichiometry for linear paraffin formation is

$$n\,\text{CO} + (2n+1)\,\text{H}_2 \;\longrightarrow\; \text{C}_\text{n}\text{H}_{\text{2n+2}} + n\,\text{H}_2\text{O} \tag{A.32}$$

The chain-length distribution is given by the ASF law

$$w_n = (1-\alpha)^2\, n\, \alpha^{n-1}, \qquad \alpha = 0.89,\; n = 1 \dots 50, \tag{A.33}$$

and the resulting wheigt fractions are shown in Figure A.8.

The mass flows of products and unconverted reactants are calculated as follows:

$$\dot{n}_{\text{CO,feed}} = \frac{8.598\,\text{kg/h}}{28.01\,\text{g/mol}} = \frac{8,598\,\text{g/h}}{28.01\,\text{g/mol}} = 307\,\text{mol/h} = 0.307\,\text{kmol/h},$$

$$\dot{n}_{\text{H}_2\text{,feed}} = \frac{1.351\,\text{kg/h}}{2.016\,\text{g/mol}} = \frac{1,351\,\text{g/h}}{2.016\,\text{g/mol}} = 670\,\text{mol/h} = 0.670\,\text{kmol/h}.$$

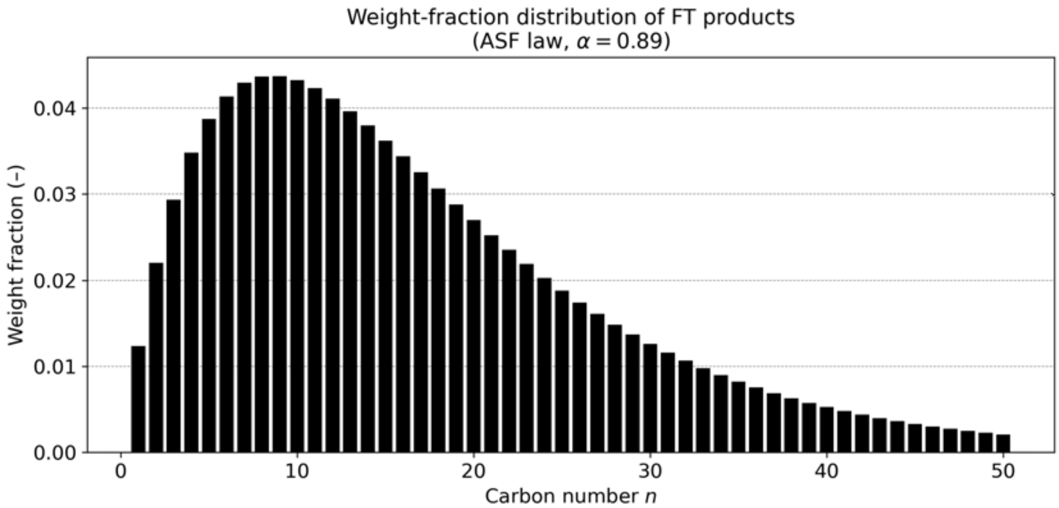

Figure A.8: Weight fraction distribution of FT products (ASF law, $\alpha = 0.89$).

With 60% CO conversion, the reacted molar flows become

$$\dot{n}_{\mathrm{CO,react}} = 0.60 \cdot 0.307\,\mathrm{kmol/h} = 0.184\,\mathrm{kmol/h}, \quad \dot{n}_{\mathrm{H_2,react}} = 2 \cdot 0.184\,\mathrm{kmol/h} = 0.368\,\mathrm{kmol/h}.$$

The paraffin mass flow (–CH_2– basis) follows by multiplying the reacted CO with the molar mass of CH_2 units:

$$m_{\mathrm{HC}} = 0.184\,\mathrm{kmol/h} \cdot 1,000\,\mathrm{mol/kmol} \cdot 14.027\,\mathrm{g/mol} = 2,580\,\mathrm{g/h} = 2.580\,\mathrm{kg/h}.$$

Applying the C_{5+} fraction $w_{C_{5+}} = 0.9016$ yields which are calculated with the ASF law before

$$m_{C_{5+}} = 0.9016 \cdot 2.580\,\mathrm{kg/h} = \underline{2.326\,\mathrm{kg/h}}.$$

The water mass flow is

$$m_{\mathrm{H_2O}} = 0.184\,\mathrm{kmol/h} \cdot 1,000\,\mathrm{mol/kmol} \cdot 18.015\,\mathrm{g/mol} = 3,315\,\mathrm{g/h} = \underline{3.315\,\mathrm{kg/h}}.$$

Finally, the unreacted feed species are:

$$m_{\mathrm{CO,unreact}} = 0.40 \cdot 8.598\,\mathrm{kg/h} = \underline{3.44\,\mathrm{kg/h}},$$

$$m_{\mathrm{H_2,consumed}} = 0.368\,\mathrm{kmol/h} \cdot 1,000\,\mathrm{mol/kmol} \cdot 2.016\,\mathrm{g/mol} = 742\,\mathrm{g/h} = \underline{0.742\,\mathrm{kg/h}},$$
$$m_{\mathrm{H_2,unreact}} = 1.351\,\mathrm{kg/h} - 0.742\,\mathrm{kg/h} = 0.609\,\mathrm{kg/h} \approx \underline{0.609\,\mathrm{kg/h}}.$$

The next step is to determine the reaction enthalpy of the FTS reaction. To do this, the enthalpy of formation of the hydrocarbons is determined first.

$$x_n \;=\; \frac{w_n/M_n}{\sum_{k=1}^{50}(w_k/M_k)}, \qquad M_n = 12.011\,n + 1.008\,(2n+2)\ \mathrm{g/mol}.$$

Using the linear rule-of-thumb

$$\Delta_f H^\circ(\mathrm{HC}) \approx -25.6\,n \;-\; 44.6 \quad [\mathrm{kJ/mol}],$$

the mixture's standard formation enthalpy becomes

$$\Delta_f H^\circ_{\mathrm{HC,mix}} = \sum_{n=1}^{50} x_n \, \Delta_f H^\circ(\mathrm{C_n H_{2n+2}}).$$

The calculation shows that the standard formation enthalpy of the hydrocarbons is -278.5 kJ/mol or -2.139 MJ/kg.

The previously determined mixture formation enthalpy $\Delta_f H^\circ_{\mathrm{HC,mix}}$ and the average chain length $\bar{n}$ are used to compute the reaction enthalpy per mole of hydrocarbon molecules, then multiply by the actual molar production rate.

The properties are:

$$\Delta_f H^\circ_{\mathrm{HC,mix}} = -278.510 \text{ kJ/mol}, \quad \bar{n} = 9.137, \quad M_{\mathrm{HC}} = 130.182 \text{ g/mol}.$$

And the calculation of the reaction enthalpy per mole of hydrocarbons:

$$\Delta_r H^\circ = \Big[\Delta_f H^\circ_{\mathrm{HC}} + \bar{n}\,\Delta_f H^\circ(\mathrm{H_2O})\Big] - \Big[\bar{n}\,\Delta_f H^\circ(\mathrm{CO}) + (2\,\bar{n}+1)\,\Delta_f H^\circ(\mathrm{H_2})\Big].$$

Using $\Delta_f H^\circ(\mathrm{H_2O}) = -241.826\,\mathrm{kJ/mol}$, $\Delta_f H^\circ(\mathrm{CO}) = -110.541\,\mathrm{kJ/mol}$, $\Delta_f H^\circ(\mathrm{H_2}) = 0$:

$$\Delta_r H^\circ = [-278.510 + 9.137 \cdot (-241.826)] - [9.137 \cdot (-110.541) + (2 \cdot 9.137 + 1) \cdot 0]$$

$$= -1\,479.831 \text{ kJ/mol hydrocarbons (HC)}.$$

With the production rate of the hydrocarbons, the heat loss can be determined:

$$\dot{n}_{\mathrm{HC}} = \frac{2.580\,\mathrm{kg/h}}{130.182\,\mathrm{g/mol}} = \frac{2,580.000\,\mathrm{g/h}}{130.182\,\mathrm{g/mol}} = 19.814\,\mathrm{mol/h} = 0.019814\,\mathrm{kmol/h}.$$

$$\dot{Q}_{\mathrm{FTS}} = \dot{n}_{\mathrm{HC}} \;\cdot\; \Delta_r H^\circ = 19.814\,\mathrm{mol/h} \;\cdot\; (-1,479.831\,\mathrm{kJ/mol})$$

$$= -29,307.4\,\mathrm{kJ/h} = \underline{\underline{-8.141\,\mathrm{kW}}}.$$

Seperator Hydrocarbons and Water

Finally, the FTS Product stream is separated in a single Separator. For simplicity, only one unit is considered, although in practice multiple separators are employed to fractionate the paraffins by chain length. The simplified Separator Hydrocarbons and Water splits all hydrocarbons (C5+ and C1–4) and water from the not reacted syngas. The Syngas Recycling stream exiting the FTS

Reactor is not separated but recycled directly. It is further assumed that any light hydrocarbons (C1–4) are removed from the system rather than returned to the Plasmacracking Reactor for additional cracking, which could also be possible. Inside the separator, the mixture is cooled in stages from 250 °C down to a final 4 °C. As the temperature decreases, hydrocarbons condense in order of decreasing chain length (long chains first). For simplicity, it is assumed that the entire hydrocarbon–water mixture separates at 4 °C. An average specific heat capacity is assumed based on the mean chain length of approximately 17, derived from the weight-fraction distribution. Heptadecane ($C_{17}H_{36}$) has a specific heat capacity of 534.34 J/mol·K at 297.15 K [153], which is rounded to 600 J/mol·K to reflect an average cooling temperature of approximately 400 K. The properties of the other components are calculated as before using the Shomate equation in the Python script.

The cooling duty is then calculated using the standard heat-exchanger equation.

Table A.16: Thermodynamic properties of the FTS Product

Stream	**Name**	T_{start} [°C]	T_{end} [°C]	$\dot{m}$ [kg/s]	c_p [J/(kg,K)]
j	Gasmixture Post Compressor	250	4	$2.763 \cdot 10^{-3}$	2,270.85

$$Q_{\text{HeaterSyngas}} = 2.763 \cdot 10^{-3}\,\frac{\text{kg}}{\text{s}} \cdot 2,270.85\,\frac{\text{J}}{\text{kg K}} \cdot (277.15 - 523.15)\,\text{K} = \underline{\underline{-1,543.49\,\text{W}}} \tag{A.34}$$

A.1.4 Calculation of the reaction enthalpy of the PC process

The thermodynamic data is only available at a resolution of 100K [150]. The temperature of the PC process will be 378K. A linear behavior is assumed for simplicity. Thus, the following formula can be applied:

$$\Delta H(T) = \Delta H_{300K} + (\Delta H_{400K} - \Delta H_{300K}) \cdot \frac{T - 300K}{100\,\text{K}} \tag{A.35}$$

This results in the following reaction enthalpies for the components:

$$\begin{aligned}\Delta H_{CO_2}(378\,\text{K}) = -393.4\,\text{kJ/mol} &\quad + \left[-389.5\,\text{kJ/mol} - \left(-393.4\,\text{kJ/mol}\right)\right] \cdot \frac{378\,\text{K} - 300\,\text{K}}{100\,\text{K}} \\ \approx \underline{\underline{-390.4\,\text{kJ/mol}}} &\end{aligned} \tag{A.36}$$

$$\begin{aligned}\Delta H_{CH_4}(378\,\text{K}) = -74.8\,\text{kJ/mol} &\quad + \left[-71.0\,\text{kJ/mol} - \left(-74.8\,\text{kJ/mol}\right)\right] \cdot \frac{378\,\text{K} - 300\,\text{K}}{100\,\text{K}} \\ \approx \underline{\underline{-71.8\,\text{kJ/mol}}} &\end{aligned} \tag{A.37}$$

$$\Delta H_{\mathrm{H_2O_{(g)}}}(378\,\mathrm{K}) = -241.8\,\mathrm{kJ/mol} \quad + \Big[-238.4\,\mathrm{kJ/mol} - \Big(-241.8\,\mathrm{kJ/mol}\Big)\Big] \cdot \frac{378\,\mathrm{K} - 300\,\mathrm{K}}{100\,\mathrm{K}}$$
$$\approx \underline{\underline{-239.1\,\mathrm{kJ/mol}}} \tag{A.38}$$

$$\Delta H_{\mathrm{CO}}(378\,\mathrm{K}) = -110.5\,\mathrm{kJ/mol} \quad + \Big[-107.6\,\mathrm{kJ/mol} - \Big(-110.5\,\mathrm{kJ/mol}\Big)\Big] \cdot \frac{378\,\mathrm{K} - 300\,\mathrm{K}}{100\,\mathrm{K}}$$
$$\approx \underline{\underline{-108.2\,\mathrm{kJ/mol}}} \tag{A.39}$$

$$\Delta H_{\mathrm{H_2}}(378\,\mathrm{K}) = 0.053\,\mathrm{kJ/mol} \quad + \Big[2.959\,\mathrm{kJ/mol} - \Big(0.053\,\mathrm{kJ/mol}\Big)\Big] \cdot \frac{378\,\mathrm{K} - 300\,\mathrm{K}}{100\,\mathrm{K}}$$
$$\approx \underline{\underline{2.3\,\mathrm{kJ/mol}}} \tag{A.40}$$

Using the molar quantities, the reaction enthalpy of the process can now be calculated:

$$\Delta H_R = \sum_{i \in \text{products}} n_i\, \Delta H_f(i) - \sum_{j \in \text{reactants}} n_j\, \Delta H_f(j) \tag{A.41}$$

$$\begin{aligned}
\Delta H_R &= \Big[11 \cdot \Delta H_{\mathrm{H_2}} + 5 \cdot \Delta H_{\mathrm{CO}}\Big] - \Big[4 \cdot \Delta H_{\mathrm{CH_4}} + \Delta H_{\mathrm{CO_2}} + 3 \cdot \Delta H_{\mathrm{H_2O}}\Big] \\
&= \Big[11 \cdot 2.3 + 5 \cdot (-108.2)\Big]\,\mathrm{kJ/mol} - \Big[4 \cdot (-71.8) + (-390.4) + 3 \cdot (-239.1)\Big]\,\mathrm{kJ/mol} \\
&= \Big[25.3 - 541\Big]\,\mathrm{kJ/mol} - \Big[-287.2 - 390.4 - 717.3\Big]\,\mathrm{kJ/mol} \\
&= -515.7\,\mathrm{kJ/mol} - \Big(-1394.9\,\mathrm{kJ/mol}\Big) \\
&= \underline{\underline{+879.2\,\mathrm{kJ/mol}}}
\end{aligned} \tag{A.42}$$

A.1.5 Calculation of the Biogas Substrate Costs

$$w_{\text{slurry}} = 0.55, \quad w_{\text{silage}} = 0.45 \tag{A.43}$$

$$
\begin{aligned}
\text{oDS}_{\text{slurry}} &= w_{\text{slurry}} \cdot \text{TS}_{\text{slurry}} \cdot \frac{\text{oDS}}{\text{DS}}_{\text{slurry}} \\
&= 0.55\ \text{t} \cdot 0.10 \cdot 0.80 = 0.044\ \text{t oDS} \\
\text{oDS}_{\text{silage}} &= w_{\text{silage}} \cdot \text{TS}_{\text{silage}} \cdot \frac{\text{oDS}}{\text{DS}}_{\text{silage}} \\
&= 0.45\ \text{t} \cdot 0.35 \cdot 0.95 = 0.1496\ \text{t oDS}
\end{aligned}
\tag{A.44}
$$

$$
\text{oDS}_{\text{total}} = 0.044 + 0.1496 = 0.1936\ \text{t oDS per t fresh substrate} \tag{A.45}
$$

$$
\begin{aligned}
V_{\text{biogas}} &= \text{oDS}_{\text{slurry}} \cdot 380 + \text{oDS}_{\text{silage}} \cdot 650 \\
&= 0.044 \cdot 380 + 0.1496 \cdot 650 \\
&= 16.72 + 97.24 = 113.96\ \text{Nm}^3_{\text{biogas}}
\end{aligned}
\tag{A.46}
$$

$$
K_{\text{substrate}} = w_{\text{slurry}} \cdot 40\,\frac{€}{\text{t oDS}} = 0.45\ \text{t} \cdot 40\,\frac{€}{\text{t}} = 18.00\,€ \tag{A.47}
$$

$$
\begin{aligned}
C_{\text{substrate}} &= \frac{K_{\text{substrate}}}{V_{\text{biogas}}} = \frac{18\,€}{113.96\ \text{Nm}^3} \\
&\approx \underline{\underline{0.158\ €/\text{Nm}^3_{\text{biogas}}}}
\end{aligned}
\tag{A.48}
$$

A.2 Simulation Results and ROI Calculation Example

A.2.1 Simulation Results Tables

Table A.17: CHPU Single-Operation: Cost and revenue components (k€, rounded to 0.1; Deviations from PQ 1 in brackets)

P_{rated}	PQ	$\text{CAPEX}_{\text{BGP}}$	OPEX_{BGP}	$\text{CAPEX}_{\text{BGstor}}$	$\text{OPEX}_{\text{BGstor}}$	$\text{CAPEX}_{\text{CHPU}}$	$\text{OPEX}_{\text{CHPU}}$	$C_{\text{biogas,CHP}}$
75	1	527.0	21.1	0.0	0.0	238.1	7.1	59.4
	2	527.0	21.1	18.4	1.3	314.2 (+32.0%)	9.4 (+32.0%)	59.4
	3	527.0	21.1	21.3	1.5	369.5 (+55.2%)	11.1 (+55.2%)	59.4
500	1	1,774.6	71.0	0.0	0.0	508.5	15.3	396.1
	2	1,774.6	71.0	34.6	2.4	671.0 (+32.0%)	20.1 (+32.0%)	396.1
	3	1,774.6	71.0	53.7	3.8	789.1 (+55.2%)	23.7 (+55.2%)	396.1
2,000	1	4,309.3	172.4	0.0	0.0	885.4	26.6	1,584.4
	2	4,309.3	172.4	91.8	6.4	1,168.3 (+32.0%)	35.0 (+32.0%)	1 584.4
	3	4,309.3	172.4	168.0	11.8	1,374.0 (+55.2%)	41.2 (+55.2%)	1 584.4

P_{rated}	PQ	$R_{\text{el,CHP}}$	$R_{\text{heat,CHP}}$	Flexibility Bonus
75	1	105.4	9.6	0.0
	2	103.6 (−1.8%)	9.7 (+0.7%)	4.9
	3	102.9 (−2.3%)	9.7 (+0.7%)	9.8
500	1	702.8	64.1	0.0
	2	690.4 (−1.8%)	64.5 (+0.7%)	32.5
	3	686.3 (−2.3%)	64.5 (+0.7%)	65.0
2,000	1	2 811.0	256.2	0.0
	2	2 761.6 (−1.8%)	258.1 (+0.7%)	130.0
	3	2 745.1 (−2.3%)	258.1 (+0.7%)	260.0

Table A.18: BGtL single-operation: Cost and revenue components (k€, rounded to 0.1; deviations from PQ 1 in brackets)

P_{rated}	PQ	$\text{CAPEX}_{\text{BGP}}$	OPEX_{BGP}	$\text{CAPEX}_{\text{BGstor}}$	$\text{OPEX}_{\text{BGstor}}$	CAPEX_{PC}	OPEX_{PC}
75	1	526.98	21.08	0.0	0.0	541.79	21.67
	2	526.98	21.08	18.4	1.3	821.19 (+51.7%)	32.85 (+51.7%)
	3	526.98	21.08	21.3	1.5	1,047.37 (+93.3%)	41.89 (+93.3%)
500	1	1,774.6	70.98	0.0	0.0	1,691.1	67.64
	2	1,774.6	70.98	34.6	2.4	2,563.3 (+51.6%)	102.53 (+51.6%)
	3	1,774.6	70.98	53.7	3.8	3,269.2 (+93.3%)	130.77 (+93.3%)
2,000	1	4,309.3	172.37	0.0	0.0	3,885.2	155.41
	2	4,309.3	172.37	91.8	6.4	5,888.8 (+51.7%)	235.55 (+51.7%)
	3	4,309.3	172.37	168.0	11.8	7,510.7 (+93.3%)	300.43 (+93.3%)

P_{rated}	PQ	OPEX_{FTS}	$\text{CAPEX}_{\text{SGstor}}$	$\text{OPEX}_{\text{SGstor}}$	$C_{\text{el,BtL}}$	$C_{\text{biogas,BtL}}$	$C_{\text{water,BtL}}$
75	1	28.75	0.0	0.0	112.21	59.41	1.6
	2	28.75	90.4	1.4	93.46 (−16.7%)	59.41	1.6
	3	28.75	135.7	2.0	87.10 (−22.4%)	59.41	1.6
500	1	100.56	0.0	0.0	748.08	396.10	10.7
	2	100.56	602.9	9.0	622.96 (−16.7%)	396.10	10.7
	3	100.56	904.4	13.6	580.65 (−22.4%)	396.10	10.7
2,000	1	251.07	0.0	0.0	2,992.3	1,584.4	42.6
	2	251.07	2,411.8	36.2	2,491.9 (−16.7%)	1,584.4	42.6
	3	251.07	3,617.7	54.3	2,322.6 (−22.4%)	1,584.4	42.6

P_{rated}	PQ	R_{Fuel}
75	1	388.5
	2	386.1 (−0.6%)
	3	384.8 (−0.9%)
500	1	2,589.8
	2	2,574.0 (−0.6%)
	3	2,565.5 (−0.9%)
2,000	1	10,359.3
	2	10 296.2 (−0.6%)
	3	10 261.9 (−0.9%)

Table A.19: Combined BGtL-CHPU system: Cost and revenue components (k€, rounded to 0.1; deviations from PQs 1:1 in brackets)

P_{rated}	PQs	$\text{CAPEX}_{\text{BGP}}$	OPEX_{BGP}	$\text{CAPEX}_{\text{BGstor}}$	$\text{OPEX}_{\text{BGstor}}$	CAPEX_{PC}	OPEX_{PC}
75	1:1	527.0	21.1	0.0	0.0	357.4	14.3
	2:2	527.0	21.1	27.0	1.9	541.8 (+51.6%)	21.7 (+51.6%)
	3:3	527.0	21.1	32.7	2.3	691.0 (+93.3%)	27.6 (+93.3%)
500	1:1	1,774.6	71.0	0.0	0.0	1,115.7	44.6
	2:2	1,774.6	71.0	91.8	6.4	1,691.1 (+51.6%)	67.6 (+51.6%)
	3:3	1,774.6	71.0	129.9	9.1	2,156.9 (+93.3%)	86.3 (+93.3%)
2,000	1:1	4,309.3	172.4	0.0	0.0	2,563.3	102.5
	2:2	4,309.3	172.4	320.4	22.4	3,885.2 (+51.6%)	155.4 (+51.6%)
	3:3	4,309.3	172.4	472.8	33.1	4,955.2 (+93.3%)	198.2 (+93.3%)

P_{rated}	PQs	$\text{CAPEX}_{\text{CHPU}}$	$\text{OPEX}_{\text{CHPU}}$	OPEX_{FTS}	$\text{CAPEX}_{\text{SGstor}}$	$\text{OPEX}_{\text{SGstor}}$	$C_{\text{el,BtL}}$
75	1:1	180.4	5.4	18.2	0.0	0.0	56.1
	2:2	238.1 (+32.0%)	7.1 (+31.9%)	18.2	45.2	0.7	46.2 (–17.6%)
	3:3	280.0 (+55.2%)	8.4 (+55.2%)	18.2	67.8	1.0	42.7 (–23.9%)
500	1:1	385.4	11.6	63.6	0.0	0.0	374.0
	2:2	508.5 (+32.0%)	15.3 (+31.9%)	63.6	301.5	4.5	308.3 (–17.6%)
	3:3	598.1 (+55.2%)	17.9 (+55.2%)	63.6	452.2	6.8	284.5 (–23.9%)
2,000	1:1	670.9	20.1	158.9	0.0	0.0	1 496.2
	2:2	885.4 (+32.0%)	26.6 (+32.0%)	158.9	1 205.9	18.1	1 233.1 (–17.6%)
	3:3	1 041.3 (+55.2%)	31.2 (+55.2%)	158.9	1 808.8	27.1	1 137.9 (–23.9%)

P_{rated}	PQs	$C_{\text{biogas,BtL}}$	$C_{\text{water,BtL}}$	$C_{\text{biogas,CHP}}$	$R_{\text{Fuel,BtL}}$	$R_{\text{el,CHP}}$	$R_{\text{heat,CHP}}$
75	1:1	29.7	0.8	29.7	194.2	52.7	4.8
	2:2	29.7	0.8	29.7	193.4 (–0.4%)	51.2 (–2.8%)	4.8
	3:3	29.7	0.8	29.7	192.7 (–0.8%)	50.8 (–3.6%)	4.8 (–0.2%)
500	1:1	198.0	5.3	198.0	1,294.9	351.4	32.0
	2:2	198.0	5.3	198.0	1,289.1 (–0.4%)	341.4 (–2.9%)	32.0
	3:3	198.0	5.3	198.0	1,284.8 (–0.8%)	338.7 (–3.6%)	32.0 (–0.2%)
2,000	1:1	792.2	21.3	792.2	5,179.7	1,405.5	128.1
	2:2	792.2	21.3	792.2	5,156.3 (–0.5%)	1,365.5 (–2.8%)	128.1
	3:3	792.2	21.3	792.2	5,139.1 (–0.8%)	1,354.7 (–3.6%)	127.8 (–0.2%)

P_{rated}	PQs	Flexibility Bonus
75	1:1	0.0
	2:2	2.4
	3:3	4.9
500	1:1	0.0
	2:2	16.3
	3:3	32.5
2,000	1:1	0.0
	2:2	65.0
	3:3	130.0

Table A.20: Combined BGtL-CHPU system: Cost and revenue components for the (k€, rounded to 0.1; deviations from PQs 1:1 in brackets)

P_{rated}	PQs	$\text{CAPEX}_{\text{BGP}}$	OPEX_{BGP}	$\text{CAPEX}_{\text{BGstor}}$	$\text{OPEX}_{\text{BGstor}}$	CAPEX_{PC}	OPEX_{PC}
500	1:1	1 774.6	70.98	0.00	0.00	1,115.7	44.63
	2:2	1 774.6	70.98	91.78	6.42	1,691.1 (+51.6%)	67.64 (+51.6%)
	3:3	1,774.6	70.98	129.88	9.09	2,156.9 (+93.3%)	86.28 (+93.3%)
500	1:2	1,774.6	70.98	53.67	3.76	1,691.1 (–0.0%)	67.64 (–0.0%)
	1:3	1,774.6	70.98	72.73	5.09	1,691.1 (–0.0%)	67.64 (–0.0%)
500	2:1	1,774.6	67.45	53.67	3.76	1,115.7 (–0.0%)	44.63 (–0.0%)
	3:1	1,774.6	64.26	72.73	5.09	1,115.7 (–0.0%)	44.63 (–0.0%)

P_{rated}	PQs	$\text{CAPEX}_{\text{CHPU}}$	$\text{OPEX}_{\text{CHPU}}$	OPEX_{FTS}	$\text{CAPEX}_{\text{SGstor}}$	$\text{OPEX}_{\text{SGstor}}$	$C_{\text{el,BtL}}$
500	1:1	385.4	11.56	63.64	0.0	0.0	374.04
	2:2	508.5 (+31.9%)	15.26 (+32.0%)	63.64	301.47	4.52	308.29 (–17.6%)
	3:3	598.1 (+55.2%)	17.94 (+55.2%)	63.64	452.21	6.78	284.49 (–23.9%)
500	1:2	385.4	11.56	63.64	301.47	4.52	308.29 (–17.6%)
	1:3	385.4	11.56	63.64	452.21	6.78	284.49 (–23.9%)
500	2:1	508.5 (+31.9%)	15.26 (+32.0%)	63.64	0.0	0.0	374.04 (–0.0%)
	3:1	598.1 (+55.2%)	17.94 (+55.2%)	63.64	0.0	0.0	374.04 (–0.0%)

P_{rated}	PQs	$C_{\text{biogas,PC}}$	$C_{\text{water,PC}}$	$C_{\text{biogas,CHP}}$	$R_{\text{Fuel,BtL}}$	$R_{\text{el,CHP}}$	$R_{\text{heat,CHP}}$
500	1:1	198.05	5.33	198.05	1,294.9	351.4	32.03
	2:2	198.05	5.33	198.05	1,289.1 (–0.4%)	341.36 (–2.9%)	32.02 (–0.0%)
	3:3	198.05	5.33	198.05	1,284.8 (–0.8%)	338.66 (–3.6%)	31.96 (–0.2%)
500	1:2	198.05	5.33	198.05	1,286.8 (–0.6%)	351.38 (–0.0%)	32.03 (–0.0%)
	1:3	198.05	5.33	198.05	1,281.8 (–1.0%)	351.38 (–0.0%)	32.03 (–0.0%)
500	2:1	198.05	5.33	198.05	1,294.9 (–0.0%)	344.35 (–2.0%)	32.20 (+0.5%)
	3:1	198.05	5.33	198.05	1,294.9 (–0.0%)	342.16 (–2.6%)	32.14 (+0.4%)

P_{rated}	PQs	Flexibility Bonus
500	1:1	0.0
	2:2	16.25
	3:3	32.50
500	1:2	0.0
	1:3	0.0
500	2:1	16.25
	3:1	32.50

Table A.21: Combined BGtL-CHPU system: Cost and revenue components (k€, rounded to 0.1; deviations from CR = 0.50 of the respective PQ group in brackets)

PQs	CR	$CAPEX_{BGP}$	$OPEX_{BGP}$	$CAPEX_{BGstor}$	$OPEX_{BGstor}$	$CAPEX_{PC}$	$OPEX_{PC}$
1:1	0.50	1,774.6	71.0	0.0	0.0	1,115.7	44.6
	0.25	1,774.6	71.0	0.0	0.0	736.1 (–34.0 %)	29.4 (–34.0 %)
	0.75	1,774.6	71.0	0.0	0.0	1,423.0 (+27.5 %)	56.9 (+27.5 %)
2:2	0.50	1,774.6	71.0	91.8	6.4	1,691.1	67.6
	0.25	1,774.6	71.0	91.8	6.4	1,115.7 (–34.0 %)	44.6 (–34.0 %)
	0.75	1,774.6	71.0	91.8	6.4	2,156.9 (+27.5 %)	86.3 (+27.5 %)
3:3	0.50	1,774.6	71.0	129.9	9.1	2 156.9	86.3
	0.25	1,774.6	71.0	129.9	9.1	1,423.0 (–34.0 %)	56.9 (–34.0 %)
	0.75	1,774.6	71.0	129.9	9.1	2,890.9 (+27.5 %)	115.1 (+27.5 %)

PQs	CR	$CAPEX_{CHPU}$	$OPEX_{CHPU}$	$OPEX_{FTS}$	$CAPEX_{SGstor}$	$OPEX_{SGstor}$	$C_{el,BtL}$
1:1	0.50	385.4	11.6	63.6	0.0	0.0	374.0
	0.25	453.2 (+17.6 %)	13.6 (+17.6 %)	40.3 (–36.7 %)	0.0	0.0	187.0 (–50.0 %)
	0.75	292.1 (–24.2 %)	8.8 (–24.2 %)	83.2 (+30.7 %)	0.0	0.0	561.1 (+50.0 %)
2:2	0.50	508.5	15.3	63.6	301.5	4.5	308.3
	0.25	598.1 (+17.6 %)	17.9 (+17.6 %)	40.3 (–36.7 %)	150.7 (–50.0 %)	2.3 (–50.0 %)	154.2 (–50.0 %)
	0.75	385.4 (–24.2 %)	11.6 (–24.2 %)	83.2 (+30.7 %)	452.2 (+50.0 %)	6.8 (+50.0 %)	463.7 (+50.4 %)
3:3	0.50	598.1	17.9	63.6	452.2	6.8	284.5
	0.25	703.4 (+17.6 %)	21.1 (+17.6 %)	40.3 (–36.7 %)	226.1 (–50.0 %)	3.4 (–50.0 %)	142.1 (–50.1 %)
	0.75	453.2 (–24.2 %)	13.6 (–24.2 %)	83.2 (+30.7 %)	678.3 (+50.0 %)	10.2 (+50.0 %)	431.2 (+51.6 %)

PQs	CR	$C_{biogas,PC}$	$C_{water,PC}$	$C_{biogas,CHP}$	$R_{Fuel,BtL}$	$R_{el,CHP}$	$R_{heat,CHP}$
1:1	0.50	198.0	5.3	198.0	1,294.9	351.4	32.0
	0.25	99.0 (–50.0 %)	2.7 (–49.6 %)	297.1 (+50.0 %)	647.5 (–50.0 %)	527.1 (+50.0 %)	48.0 (+50.0 %)
	0.75	297.1 (+50.0 %)	8.0 (+49.4 %)	99.0 (–50.0 %)	1,942.4 (+50.0 %)	175.7 (–50.0 %)	16.0 (–50.0 %)
2:2	0.50	198.0	5.3	198.0	1,289.1	341.4	32.0
	0.25	99.0 (–50.0 %)	2.7 (–49.6 %)	297.1 (+50.0 %)	644.7 (–50.0 %)	514.9 (+50.9 %)	48.2 (+50.6 %)
	0.75	297.1 (+50.0 %)	8.0 (+49.4 %)	99.0 (–50.0 %)	1,933.6 (+50.0 %)	169.0 (–50.5 %)	15.9 (–50.4 %)
3:3	0.50	198.0	5.3	198.0	1,284.8	338.7	32.0
	0.25	99.0 (–50.0 %)	2.7 (–49.6 %)	297.1 (+50.0 %)	642.5 (–50.0 %)	511.2 (+50.9 %)	48.2 (+50.7 %)
	0.75	297.1 (+50.0 %)	8.0 (+49.4 %)	99.0 (–50.0 %)	1,927.5 (+50.0 %)	167.0 (–50.7 %)	15.8 (–50.6 %)

PQs	CR	Flexibility Bonus
1:1	0.50	0.0
	0.25	0.0
	0.75	0.0
2:2	0.50	16.3
	0.25	24.4 (+50.0 %)
	0.75	8.1 (-50.0 %)
3:3	0.50	32.5
	0.25	48.8 (+50.0 %)
	0.75	16.3 (-50.0 %)

A.2.2 Example ROI Calculation

As an illustrative example, the calculations are presented for the CHPU in single-operation ($\mathrm{PQ}_{\mathrm{CHPU}} = 1$) with a biogas plant capacity of 500 kW. The corresponding cost and revenue data are provided in Table A.17 in the appendix.

1. CHPU lifetime N_{CHPU}. The CHPU is designed for 60,000 FLH and operates 8,760 h/year in the reference case:

$$N_{\mathrm{CHPU}} = \frac{60,000\ \mathrm{h}}{8,760\ \mathrm{h\,a^{-1}}} \approx 6.85\ \mathrm{a}. \tag{A.49}$$

2. Total annual costs C. Below is the sum of annualised capital costs, fixed OPEX and variable costs:

$$\begin{aligned} C &= \frac{C_{0,\mathrm{BGP}}}{20} + \frac{C_{0,\mathrm{CHPU}}}{N_{\mathrm{CHPU}}} + \frac{C_{0,\mathrm{BGP}} + C_{0,\mathrm{CHPU}}}{2} i + \mathrm{OPEX}_{\mathrm{BGP}} + \mathrm{OPEX}_{\mathrm{CHPU}} + C_{\mathrm{biogas,\,CHP}} \\ &= \frac{1,774,600}{20} + \frac{508,500}{6.85} + \frac{1,774,600 + 508,500}{2} \cdot 0.06 + 71,000 + 15,300 + 396,100 \\ &= 713,900\ \text{€}\,\mathrm{a^{-1}}. \end{aligned} \tag{A.50}$$

3. Total annual revenue R. Revenue from electricity and heat generation:

$$R = R_{\mathrm{el,\,CHP}} + R_{\mathrm{heat,\,CHP}} = 702,800 + 64,100 = 766,900\ \text{€}\,\mathrm{a^{-1}}. \tag{A.51}$$

4. Annual profit Π_{year}. Difference between revenue and total costs:

$$\Pi_{\mathrm{year}} = R - C = 766,900 - 713,900 = 53,000\ \text{€}\,\mathrm{a^{-1}}. \tag{A.52}$$

5. Return on investment (ROI). Profit divided by average invested capital:

$$\mathrm{ROI} = \frac{\Pi_{\mathrm{year}}}{(C_{0,\mathrm{BGP}} + C_{0,\mathrm{CHPU}})/2} = \frac{53,000}{(1,774,600 + 508,500)/2} \approx 4.6\%. \tag{A.53}$$

B Digital Appendices

The following additional content is provided on the accompanying digital storage medium:

B.1 Source Code MILP Model

This folder contains all Python scripts required for the MILP optimization, including `main.py`, `Optimization.py`, and `cost_calculations.py`. Furthermore, the datasets `spotmarket_data.txt` (for the arbitrage optimization) and `spotmarket_data_threshold.txt` (for the threshold calculation for the CHPU) are included. All files are required to reproduce the optimization results presented in this thesis.

B.2 Thermodynamic Calculations

This folder contains the Python script `thermodynamic_calculations.py`, which was used for the thermodynamic calculations of the BGtL plant described in Chapter 5.3. The script allows the user to reproduce all calculations and figures related to the thermodynamic evaluation.

Erklärung zur selbstständigen Bearbeitung einer Abschlussarbeit

Hiermit versichere ich, dass ich die vorliegende Arbeit ohne fremde Hilfe selbständig verfasst und nur die angegebenen Hilfsmittel benutzt habe. Wörtlich oder dem Sinn nach aus anderen Werken entnommene Stellen sind unter Angabe der Quellen kenntlich gemacht.

Ort	Datum	Unterschrift im Original